

UNIVERSITY OF EDUCATION, WINNEBA

**DEPARTMENT OF MECHANICAL AND AUTOMOTIVE TECHNOLOGY
EDUCATION**

**ANALYSIS OF THE EFFECT OF DUAL INJECTION ON COMBUSTION
CHARACTERISTICS OF GASOLINE DIRECT INJECTION (GDI) ENGINE**



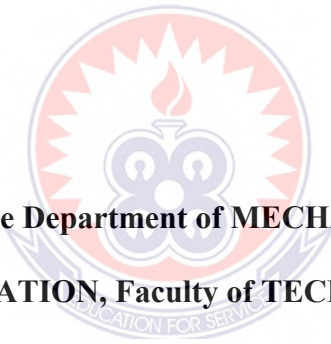
2021

UNIVERSITY OF EDUCATION, WINNEBA

**ANALYSIS OF THE EFFECT OF DUAL INJECTION ON COMBUSTION
CHARACTERISTICS OF GASOLINE DIRECT INJECTION (GDI) ENGINE**

FELIX ZATOR TEMBILE

(200030480)



**A Thesis Submitted to the Department of MECHANICAL AND AUTOMOTIVE
TECHNOLOGY EDUCATION, Faculty of TECHNICAL EDUCATION, School
of Graduate Studies, COLLEGE OF TECHNOLOGY EDUCATION, Kumasi in
Partial Fulfillment of The Requirement for The Award of Master of Philosophy
in Automotive Engineering Technology Degree.**

SEPTEMBER, 2021

DECLARATION

Student's Declaration

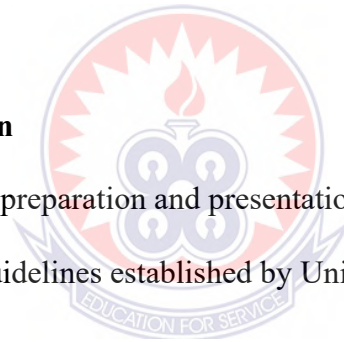
I, FELIX ZATOR TEMBILE, declare that this thesis, except quotation and references in the published works that have been identified and duly acknowledged is entirely my original work, and it has not been submitted either in part or whole for another degree elsewhere.

SIGNATURE.....

DATE:.....

Supervisor's Declaration

I hereby declare that the preparation and presentation of this thesis was supervised in accordance with the guidelines established by University of Education, Winneba.



NAME: DR. SHERRY K. AMEDORME

SIGNATURE:.....

DATE:.....

DEDICATION

This research is dedicated to the LORD God Almighty, El-Elohe-Yisrael. The research is also dedicated to my parents; Yaw Tembile and Hannah Banyaware and my beloved Dr. Gifty Sintim.



ACKNOWLEDGEMENT

This research would not be complete if I show no appreciation towards the many services others provided. First of all, I wish to express my utmost gratitude to EL-ELOHE-YISRAEL, The God of the house of Yisrael for how far He has brought me. I am most grateful to my father Engr. S.N. Nsoh for his advice and unwavering support. You have my love and gratitude, Sir. I acknowledge the great support and guidance of my supervisor, Dr. Sherry K. Amedorme, God bless you Sir. I am grateful to my pastor Mr. Abraham Commey and his wife Dr. (Mrs) Vida Commey for their support and prayers. God bless you. I am also thankful to my father Mr. Yaw Tembile and my dear mama Hannah Banyaware for their prayers and support. Finally, I am very grateful to my dearly beloved Dr. Gifty Sintim for the prayers, encouragement and support. I say the Lord God Almighty bless you.



ABSTRACT

The production of hydrocarbons (HC), carbon dioxides (CO₂) and nitrogen oxides (NO_x) are the serious issues of Gasoline Direct Injection (GDI) during stratified lean operation. In attempt to solve these setbacks, this research explores the effect of dual direct injection on air-fuel mixture characteristics, combustion and species transport characteristics after combustion at both early and late fuel injection modes. The researcher used the 2021 ANSYS design modeler for geometry designs and meshing and used the ANSYS Fluent for simulation and numerical analysis. The results revealed that during mixture preparation phase dual injection at early injection results in higher TKE, velocity magnitude, turbulent intensity, dissipation rate but lower turbulent viscosity than when the fuel was injected late. The combustion and species transport results also revealed that at late injection, specific heat capacity (C_p) and its equivalent flame temperature was high enough to initiate dissociation of combustion products into O₂, N₂, HC and CO as compared to when the fuel was injected early. The turbulent burning velocity of the flame was 2290m/s at late injection while that during the early injection mode was 397m/s. Post combustion mass fraction results showed the presence of O₂ and N₂ in the combustion chamber in the late injection as against zero O₂ and N₂ in the early injection mode. Mass fractions of NO_x and CO₂ production were also high during late injection than in the early injection. The mass fraction of H₂O vapour produced in the early injection was higher than that of the late injection mode. The study reveals that dual direct injection engine operated at early injection mode is more efficient in mixture preparation and dissipation, engine cooling effect and reduced exhaust NO_x and CO₂. It is therefore recommended that automotive companies in Ghana should consider the efficiency of dual direct GDI engine for emission control and fuel economy for incorporation into the Ghana-made vehicles to support Ghana's industrialization drive.

TABLE OF CONTENTS

CONTENTS	PAGE
DECLARATION	ii
DEDICATION	iii
ACKNOWLEDGEMENT	iv
ABSTRACT.....	v
TABLE OF CONTENTS.....	vi
LIST OF TABLES	xii
LIST OF FIGURES	xiii
CHAPTER ONE	1
INTRODUCTION	1
1.1 Background to The Study	1
1.2 Statement of The Problem	3
1.3 Purpose of The Study.....	4
1.4 Significance of The Study.....	6
1.5 Organization of The Study.....	5
CHAPTER TWO	6
LITERATURE REVIEW	6
2.1 Introduction.....	6
2.2 Emission Standards.....	6
2.3 Technologies of Fuel Injection	12
2.3.1 Port Fuel Injection (PFI)	12
2.3.2 Direct Injection (DI)	13
2.3.3 Gasoline Direct Injection (GDI)	15

2.3.4 Dual Injection.....	18
2.4 Advantages of Dual Injection	20
2.4.1 Control flexibility.....	20
2.4.2 Enhanced Cooling Effect	21
2.4.3 Knock Mitigation	24
2.4.4 Engine Downsizing.....	24
2.4.5 Fast Combustion Speed	25
2.4.6 Extended Lean Burn Limit.....	26
CHAPTER THREE.....	28
METHODS AND MATERIALS	28
3.1 Introduction.....	28
3.2 Numerical Methods.....	28
3.3 Geometry of the Combustion Chamber	29
3.4 Meshing.....	33
3.5 Procedural Approach	36
3.6 Species Transport Model	38
CHAPTER FOUR.....	41
RESULTS AND DISCUSSIONS	41
4.1 Introduction.....	41
4.2 Comparison of dual GDI and Single GDI engines at late and early injection modes	41
4.2.1 Turbulent Kinetic Energy	41
4.2.2 Velocity Magnitude	43

4.2.3 Turbulent Dissipation Rate	45
4.2.4 Turbulent Intensity	46
4.2.5 Turbulent Viscosity	47
4.3 Species transport	49
4.3.1 Flame Temperature at Late injection mode	50
4.3.2 Flame temperature at Early injection mode	51
4.3.3 Comparison of flame temperatures of single direct injection engine at different injection modes	53
4.3.4 Comparison of flame temperatures of dual direct injection (DI) engine at different injection modes	54
4.3.5 Temperature and Composition Dependent Heat Capacity at Late injection mode	55
4.3.6 Temperature and Composition Dependent Heat Capacity at Early injection mode	56
4.3.7 Mixture specific heat (C_p) at Late injection mode (Piston at BDC).....	58
4.3.8 Mixture specific heat (C_p) at Early injection mode (Piston at TDC)	59
4.3.9 Comparison between mixture specific heat of single DI engines at early and late injection modes.	61
4.3.10 Comparison between mixture specific heat of dual DI engines at early and late injection modes.	62
4.3.11 Turbulent burning velocity at late injection mode (Piston at BDC)	63
4.3.12 Turbulent burning velocity at early injection mode (Piston at TDC)	65
4.3.13 Comparison of Turbulent burning velocities of single DI engine at early and late injection modes	67

4.3.14 Comparison of Turbulent burning velocities of Dual DI engine at early and late injection modes	68
4.3.14 Mass fraction of Octane at Late injection mode (Piston at BDC)	69
4.3.15 Mass fraction of Octane at Early injection mode (Piston at TDC).....	70
4.3.16 Comparison of mass fractions of octane(C ₁₆ H ₂₉) in single DI engine at early and late injection modes.....	71
4.3.17 Comparison of mass fractions of octane (C ₁₆ H ₂₉) in Dual DI engine at early and late injection modes.....	72
4.3.18 Mass fraction of Oxygen (O ₂) at Late injection mode (Piston at BDC)	73
4.3.19 Mass fraction of Oxygen (O ₂) at Early injection mode (Piston at TDC).....	75
4.3.20 Comparison of mass fractions of oxygen (O ₂) in single DI engine at early and late injection modes.	77
4.3.21 Comparison of mass fractions of oxygen (O ₂) in Dual DI engine at early and late injection modes.	78
4.3.22 Mass fraction of Nitrogen (N ₂) at Late injection mode (Piston at BDC).....	79
4.3.23 Mass fraction of Nitrogen (N ₂) at Early injection mode (Piston at TDC)	81
4.3.24 Comparison of mass fractions of Nitrogen (N ₂) in Single DI engine at early and late injection modes.....	82
4.3.25 Comparison of mass fractions of Nitrogen(O ₂) in Dual DI engine at early and late injection modes.	83
4.3.26 Mass fraction of Carbon dioxide (CO ₂) at Late injection mode (Piston at BDC)	84
4.3.27 Mass fraction of Carbon dioxide (CO ₂) at Early injection mode (Piston at TDC).....	86

4.3.28 Comparison of mass fractions of Carbon dioxide (CO ₂) in single DI engine at early and late injection modes.....	88
4.3.29 Comparison of mass fractions of Carbon dioxide (CO ₂) in Dual DI engine at early and late injection modes.....	89
4.3.30 Mass fraction of Water Vapour (H ₂ O) at Late injection mode (Piston at BDC)	90
4.3.31 Mass fraction of Water Vapour (H ₂ O) at Early injection mode (Piston at TDC)	91
4.3.32 Comparison of mass fractions of Water vapour (H ₂ O) in single DI engine at early and late injection modes.....	93
4.3.32 Comparison of mass fractions of Water vapour (H ₂ O) in Dual DI engine at early and late injection modes.....	94
4.3.33 NO _x Production at Late injection mode (piston at BDC).....	95
4.3.34 NO _x Production at Early injection mode (piston at TDC)	97
4.3.35 Comparison of NO _x mass fractions of single DI engines at early and late injection modes	99
4.3.36 Comparison of NO _x mass fractions of dual DI engines at early and late injection modes	100
 CHAPTER FIVE	91
CONCLUSIONS AND RECOMMENDATIONS	91
5.1 Introduction.....	91
5.2 Summary of findings.....	91
5.3 Conclusion.....	96
5.4 Recommendation	97

5.5 Suggestions for Further Research	98
REFERENCES	99
APPENDIX	112



LIST OF TABLES

Table 2.1: Limit of Sulphur and engine features about European standards.....	10
Table 2.2: Engine specifications of the top 20 most famous gasoline vehicle models in Australia in 2019.....	13
Table 2.3: Comparison between advantages and disadvantages PFI and DI technologies	17
Table 3.1: Main technical parameters of the engine	32



LIST OF FIGURES

Figure 3.1: Dimension of cylinder	31
Figure 3.2: Dimension of cylinder bore and stroke	31
Figure 3.3: 3D geometry of a computational domain with piston at BDC.....	32
Figure 3.4: Dimensions of the dual direct injection model.....	32
Figure 3.5: 3D geometry of the computational domain with piston at TDC	33
Figure 3.6: Mesh of cylinder with single direct injector at BDC.....	34
Figure 3.8: Mesh of cylinder with single direct injector at TDC.....	35
Figure 3.9: Mesh of cylinder with dual direct injector at TDC	35
Figure 4.1: Turbulent Kinetic Energy against Injection velocity at (a)TDC, (b)BDC.....	42
Figure 4.2: Velocity Magnitude against Injection Velocity at (a) BDC, (b)TDC	44
Figure 4.3: Turbulent Dissipation Rate against Injection velocity at (a) BDC, (b)TDC	45
Figure 4.4: Turbulent Intensity against Injection velocity at (a) BDC, (b)TDC.....	47
Figure 4.5: Turbulent Viscosity against Injection velocity at (a)TDC, (b)BDC	48
Figure 4.6: Contour plot of temperature distribution at constant heat capacity of 1000 J/kg – K of (a) single GDI and (b) dual GDI	50
Figure 4.7: Contour plot of temperature distribution at constant heat capacity of 1000 J/kg – K of (a) single GDI and (b) dual GDI	52
Figure 4.8: Peak flame temperature of single DI engine at TDC and BDC	53
Figure 4.9: Peak flame temperature of Dual DI engine at TDC and BDC	54
Figure 4.10: Contours diagram of Temperature distribution for Variable Cp of single GDI	55
Figure 4.11: Diagram of Temperature distribution for Variable Cp of dual GDI	56

Figure 4.12: Contours plot of Temperature distribution for Variable Cp of single GDI	57
Figure 4.13: Contours plot of Temperature distribution for Variable Cp of dual GDI	57
Figure 4.14: Contours plot of Temperature distribution for Specific Heat of single GDI	58
Figure 4.15: Contours plot of Temperature distribution for Specific Heat of dual GDI	59
Figure 4.16: Contours plot of Temperature distribution for Specific Heat of single GDI	60
Figure 4.17: Contours plot of Temperature distribution for Specific Heat of dual GDI	61
Figure 4.18: Mixture specific heat (Cp) of single GDI Engine operating modes.....	61
Figure 4.19: Mixture specific heat (Cp) of dual GDI Engine operating modes	62
Figure 4.20: Velocity Vectors contour plot for Variable Cp of single GDI	63
Figure 4.21: Velocity Vectors contour plot for Variable Cp of dual GDI.....	64
Figure 4.22: Velocity Vectors contour plot for Variable Cp of single GDI).....	65
Figure 4.23: Velocity Vectors contour plot for Variable Cp of dual GDI.....	66
Figure 4.24: Turbulent burning velocities of single GDI Engine operating modes.....	67
Figure 4.25: Turbulent burning velocities of dual GDI Engine operating modes.	68
Figure 4.25: Contours plot of Octane Mass Fraction of single GDI.....	69
Figure 4.26: Contours plot of Octane Mass Fraction of dual GDI	69
Figure 4.27: Contours plot of Octane Mass Fraction of single GDI.....	70
Figure 4.28: Contours plot of Octane Mass Fraction of dual GDI	71
Figure 4.29: Mass fraction of Octane of single GDI Engine operating modes.....	72
Figure 4.30: Mass fraction of Octane of dual GDI Engine operating modes	72

Figure 4.31: Contours plot of Oxygen Mass Fraction of single GDI	73
Figure 4.32: Contours plot of Oxygen Mass Fraction of dual GDI.....	74
Figure 4.33: Contours plot of Oxygen Mass Fraction of single GDI	75
Figure 4.34: Contours plot of Oxygen Mass Fraction of dual GDI.....	76
Figure 4.36: Mass fraction of Oxygen of dual GDI Engine operating modes.....	78
Figure 4.37: Contours plot of Nitrogen Mass Fraction of Single GDI	79
Figure 4.38: Contours plot of Nitrogen Mass Fraction of dual GDI	80
Figure 4.39: Contours plot of Nitrogen Mass Fraction of Single GDI	81
Figure 4.40: Contours plot of Nitrogen Mass Fraction of dual GDI	81
Figure 4.41: Mass fraction of Nitrogen of single GDI Engine operating modes.....	82
Figure 4.42: Mass fraction of Nitrogen of dual GDI Engine operating modes	83
Figure 4.43: Contours plot of Carbon dioxide Mass Fraction of single GDI	84
Figure 4.44: Contours plot of Carbon dioxide Mass Fraction of dual GDI.....	85
Figure 4.45: Contours plot of Carbon dioxide Mass Fraction of single GDI	86
Figure 4.46: Contours plot of Carbon dioxide Mass Fraction of dual GDI.....	87
Figure 4.47: Mass fraction of Carbon dioxide of single GDI Engine operating modes	88
Figure 4.48: Mass fraction of Carbon dioxide of single GDI Engine operating modes	89
Figure 4.50: Contours plot of Water Mass Fraction of dual GDI.....	90
Figure 4.51: Contours plot of Water Mass Fraction of single GDI	91
Figure 4.51: Contours plot of Water Mass Fraction of dual GDI.....	92
Figure 4.52: Mass fraction of water of single GDI Engine operating modes	93
Figure 4.53: Mass fraction of water of dual GDI Engine injection modes.....	94

Figure 4.54: Contours plot of NO_x Mass Fraction—Prompt and Thermal NO_x Formation of single GDI.....95

Figure 4.55: Contours plot of NO_x Mass Fraction—Prompt and Thermal NO_x Formation of dual GDI.....96

Figure 4.56: Contours plot of NO_x Mass Fraction—Prompt and Thermal NO_x Formation of single GDI.....97

Figure 4.57: Contours plot of NO_x Mass Fraction—Prompt and Thermal NO_x Formation of dual GDI.....98

Figure 4.58: Mass fraction of NO_x of single GDI Engine injection modes99

Figure 4.59: Mass fraction of NO_x of dual GDI Engine injection modes..... 100



CHAPTER ONE INTRODUCTION

1.1 Background to the Study

Internal combustion engines are widely preferred as power sources for vehicles because of their high thermal efficiency, smaller heat loss and power output. Up to now, most internal combustion engines operate on fossil fuels and this possess serious pollution problems to mankind and other living things. (Prockop & Chichkova, 2007; Wang et al., 2007).

Engineers are attempting to build engines with improved brake-specific fuel consumption (BSFC) in order to improve combustion technology and increase fuel economy. Increase in crude oil consumption, emission regulations, and the challenge of depletion have moved automotive engineers to strive for better fuel efficiency (Park et al., 2012).

Compression ignition direct injection engines have a greater BSFC than traditional port-fuel-injected (PFI) spark ignition engines. Compression ratios are higher in compression ignition direct-injection engines (Zhao et al., 1999). Despite these benefits, the diesel engine produces more noise and has a lower speed range. Direct injection, four-stroke, spark ignition engine is nearest to accomplishing the objective of fuel economy and emissions reduction (Kim et al., 2015). An engine that does not control the load is unlikely to achieve these objectives. Research shows improvement in the level of brake specific fuel consumption (BSFC) from current SI engines.

Direct-injection, stratified-charge (DISC) engines operate with higher specific power and compression ratios. In DISC engines, atomized fuel is injected directly into combustion chamber directly as ignition commences. The intake air is cooled by the vaporization of the directly injected fuel (Park et al., 2012).

Direct injection spark ignition engines are classified into three types; wall guided, air guided and spray guided. Mass produced directly injected engines are wall guided and considered the first generation of DI engines (Gunasekaran & Dhandapani, 2012).

In the wall guided direct injection engines, the charge is injected towards the piston cavity and directed to the spark plug by the reflection on the cavity wall. Following this, hydrocarbon (HC) and nitrogen oxide (NO_x) emissions become a problem due to fuel adhesion to the cylinder wall (Cole et al., 1998; Stovell et al., 1999).

The introduction of directly-injected fuel on the piston and cylinder wall led to problems with the first generation of DI engines (Pontoppidan & Gaviani, 2018). These problems led to the development of air and spray-guided DI engines, which are now being considered for use in the next generation of DI engines (James Gunasekaran & Dhandapani, 2012). Spray-guided DI engines are designed to avoid the setbacks of air-guided and wall-guided systems, as well as the close proximity of the spark plug to centrally-mounted injectors. With spray-guided DI engines, wall-wetting is removed and stratified mixtures are formed close to the spark plugs. Spray-guided diesel engines produce very fine droplets of the charge ranging from 20 to 25µm. Swirl injectors show about 5% wall film quantity and the air-fuel ratio inside the combustion chamber is high. The creation of hydrocarbons (HC and NO_x) and low exhaust temperatures, are serious issues (Gunasekaran & Dhandapani, 2012). In 2012, researchers at the Indian Institute of Mechanical Engineers (IME) developed a diesel type high pressure fuel injector for petrol engines. This led to the development of models and computations on GDI engines with different fuel injection methods (Gunasekaran & Dhandapani, 2012).

DI engines use early injection to promote homogeneous charge and late injection to generate ultra-lean stratified charge. Late injection is not feasible under high-load

operation because a lean mixture produces a reduced torque output. However, some Japanese production DI engines use early injection for high-load operation and late injection for low-load operation (Kume et al., 1996). They reported a 40% or more improvement in fuel economy during idle (Harada et al., 1997; Iwamoto et al., 1997). Nonetheless, HC emissions for late injection was almost double as compared to early injection (Karl et al., 1997).

For these reasons, both early and late injection timing is considered in this study to analyze the effect of dual injection on combustion characteristics of GDI engine. The dual injection engine adopts two direct injection system, which is called dual- direct injection technology.

1.2 Statement of The Problem

The creation of hydrocarbons, carbon dioxide and nitrogen oxides during unthrottled stratified lean combustion in the GDI combustion systems are the main challenge. These greenhouse gas emissions have the potential to affect human health in several ways. These include an increase in the frequency of heat waves, weather events such as hurricanes, cyclones, and droughts, as well as a shift in the distribution of allergies and vector-borne infectious diseases around the world. The cardiovascular and gastrointestinal systems are particularly vulnerable to global warming's negative consequences. Furthermore, climate change affects some infectious diseases and their animal vectors, increasing the chance of infection with typhus, cholera, malaria, dengue fever, and West Nile virus (Franchini & Mannucci, 2015). In attempt to solve these setbacks, exhaust gas recirculation (EGR), common rail system has been introduced. There are a lot of research done on dual injection with respect to CI

engines and alternative fuels. It appears very few research has been focused on dual injection with respect to SI engines and for that matter using petrol as fuel for both DI injectors simultaneously.

1.3 Purpose of The Study

The study aims at modelling a new fuel injection system to help curb the issues emissions of the gasoline direct injection engine.

To achieve this, the following specific objectives would be pursued;

1. Analyze pre-combustion mixture formation characteristics in single GDI and dual direct GDI engines at early and late injection mode.
2. Compare combustion characteristics of single GDI and dual direct GDI engines for product dissociation potentials at early and late injection modes.
3. Analyze mass fractions of octane, air, carbon dioxide, water and predict thermal and prompt NO_x production at early and late injection modes.

1.4 Significance of The Study

This research is geared towards exhaust gas emission reduction and adherence of automobile pollutant legislation. Reduced exhaust gas emission means control of global warming. In addition to that, this work could be adopted by engine manufacturers to design a future GDI engines to be cleaner, less expensive, higher power, more efficient and environmentally friendly dual direct injection GDI engines. This work also touches on fuel consumption improvement due to crude oil reserves that are rapidly depleting. Researchers and developers could also use the results of this study to evaluate their work. Finally, research and development could also be

carried out following this work to reduce exhaust emissions and their attendant environmental pollution.

1.5 Organization of The Study

In this thesis, Chapter One introduces the work by describing the development of the spark ignition engine and the challenges which birthed the direct injection engine. Generations of GDI and their setbacks are discussed and finally introduces the reason for this thesis. Chapter Two, examines literature review. It describes the theoretical scholarly work upon which the researcher's thesis is based. Chapter Three details the methodology of the actual work. Results of the study are discussed in Chapter Four. Chapter Five concludes the thesis with summary of findings, conclusions and recommendations. Suggestions for further research was also made.



CHAPTER TWO

LITERATURE REVIEW

2.1 Introduction

This chapter presents various emission standards for emission control, some fuel injection advancement of vehicles, some technologies of fuel injection. The advancement of the injection system from port fuel injection, direct injection technology and their advantages and disadvantages compared. Gasoline direct injection and dual injection is also presented. The advantages of dual injection which includes control flexibility, enhanced cooling effect, knock mitigation, engine downsizing, fast combustion speed and extended lean burn limit are discussed.

2.2 Emission Standards

Volatile organic compound emissions from vehicles are accepted to assume a huge part in the arrangement of photochemical smog. This smog is experienced in areas with high vehicle population throughout the world (Perry & Gee, 1995). Photochemical smog is a mixture of secondary pollutants for instance as ozone, nitrogen dioxide, nitric acid, aldehydes and other organic compounds, formed from photolytic reactions between oxides of nitrogen and hydrocarbons. This goes on to tell that vehicle emission is dependent on the fuel standard. Three -way catalytic converter is one of the first technologies for gasoline engine emission control for metering stoichiometric air-fuel ratio and the overall management of the engine using sensors and actuators. Technologies for diesel engine emissions are normally focuses on after-treatment and in-chamber metering (Ayetor et al., 2020).

As shown in Table 2.1, a country that implements Euro 1 gasoline requirements will only accept the import of automobiles with the following minimal features: electronic

ignition instead of the mechanical distributor ignition system seen in older models, and three-way catalytic converter (TWC). Euro 2 has an EGR system that reduces NO_x emissions. Turbochargers are not required for Euro 1 diesel engines, however, an exhaust gas recirculation (EGR) system is necessary for NO_x reduction. To minimize PM to 0.08 g/km, Euro 2 requires either fuel injection or treatment afterwards. Euro 3 aims to reduce emissions during cold start for both engines. In comparison to Euro 3, diesel PM and NO_x emissions must be lowered by 50% in Euro 4. Turbochargers and a high-pressure common rail system are two technologies that can help cut PM even more. Gasoline NO_x and HC emissions will be cut in half in Euro 4 compared to Euro 3. NO_x is controlled in the EGR by combustion, while HC is constrained by reformulating the TWC. Euro 5 and 6 are centered around CO decrease. This is performed with gasoline direct injection in gasoline engines (GDI). In comparison to Euro 4, Euro 5 seeks to reduce PM by 80% in diesel engines. To minimize PM, the after-treatment includes diesel oxidation catalyst (DOC) and diesel particulate filter (DPF). In comparison to Euro 5, Euro 6 for diesel engines reduces NO_x by 66%.

Table 2.1: Limit of Sulphur and engine features about European standards.

Emission standard	Fuel Sulphur limit (ppm)	Gasoline engine features	Diesel engine features
Euro 1	2000	TWC integrated with oxygen sensors, electronic ignition, electronic injection	Mechanically controlled EGR, naturally aspirated engines, mechanical fuel injection.
Euro 2	500	TWC, multi-point fuel injection system (MPFI), electronic control unit (ECU), exhaust gas recirculation system (EGR) for NOx emission reduction	Rotary pump, electronic control, cooled EGR
Euro 3	350	Improved Engine management, EGR, heated oxygen sensor, on-board diagnostics, additional close-coupled catalyst	Electronically controlled injection, electronically controlled EGR, after treatment with oxidation catalysts
Euro 4	50	TWC formulation	Turbochargers with intercoolers, common rail injection system
Euro 5	10	Engine calibration, engine management, EGR, TWC formulation, improved oxygen sensors	DOC, DPF for variable fuel injection timing
Euro 6	Below 10	Gasoline Direct Injection, Engine calibration, engine management, EGR, TWC formulation, improved oxygen sensors Mechanically	Cooled EGR, SCR, LNT

Since Euro 5, a non-methane hydrocarbons (NMHC) limit of 68 mg/km has been added to the THC limit (European Commission, 2008). Only vehicles with DI engines are subject to the particulate matter (PM) limit, which is set at 4.5 mg/km when an

updated measurement technique is used (i.e., PMP). Cars with DI engines were subject to the particle number (PN) limit, which was set at 6×10^{12} #/km for the first three years of Euro 6 (European Commission, 2012).

Regulations to curb both air pollution and greenhouse gas emissions are becoming firm. The progression of emission limits for gasoline passenger cars from Euro 1 to Euro 6 is depicted in Table 2.1. Over the last three decades, limit values have been significantly decreased, and more pollutant species have been monitored. For example, the NO_x threshold in Euro 5 and 6 (European Commission, 2012) has diminished by 60%, from 0.15 g/km in Euro 3 (European Commission, 1998) to 0.06 g/km. The emission testing methods have become more comprehensive in Euro 6, despite the fact that the threshold values have remained unchanged since Euro 5. To begin, a Worldwide Harmonized Light Vehicles Test Procedure (WLTP) is implemented for type approval of new vehicles using chassis dynamometers, which is more indicative of real-world driving than the obsolete New European Driving Cycle (NEDC) (Tsokolis et al., 2016). A Real Driving Emissions (RDE) test has been implemented to calculate vehicle emissions in the real world using a Portable Emission Measurement System (PEMS) (European Commission, 2017), in addition to the laboratory-based WLTP. The RDE test intends to close the gap among research center, emission and fuel consumption (Huang et al., 2019). In 2017, a conformity factor of 2.1 was used with the aim of getting it down to 1.0 as soon as possible, preferably by 2023 (European Commission, 2017). In terms of greenhouse gas emissions regulations, the European Union has increased its fleet-wide average emission commitment from 130 g CO₂/km in 2015 to 95 g CO₂/km in 2021, equating to a petrol car fuel consumption of 4.1 L/100 km (European Commission, 2021). Until

the electrical discharge from the spark plug is started, it is important for the fuel to blend with the intake air and form a suitable mixture for SI engines.

Carburetors, port fuel injection (PFI), and the recent direct injection (DI) are the three most popular fuel injection technologies (Zhao et al., 1999). In the 1980s, PFI replaced carburetors due to its advantages in fuel savings through more precise fuel injection regulation and pollution reductions through exhaust after-treatment using a three-way catalyst (TWC). When compared to PFI, DI was built in the 1990s and provides additional fuel savings. Despite this, DI in modern SI engines has not fully replaced PFI.

PFI and DI have similar market shares (14 vs 16 engine models), as shown in Table 2.2, though DI is considered more advanced. This is due to the fact that each of these two fuel injection technologies has its own set of benefits and drawbacks. This leads to the innovative concept of combining DI and PFI in one engine (dual injection), which has the ability to combine their benefits while avoiding their disadvantages. Dual injection provides more control over mixture formation and combustion processes, making it a promising technology for meeting extremely strict emissions and fuel efficiency regulations. In recent years, dual injection has been in growth, and a few market vehicles, such as the Toyota RAV4, Toyota Camry, and Volkswagen Golf, have already embraced this design. These vehicles have outperformed their competitors in terms of engine downsizing (high compression ratios and turbocharging) and fuel economy.

Table 2.2 shows the fuel injection advancements of the top 20 most famous vehicle models in 2019 in Australia.

Table 2.2: Engine specifications of the top 20 most famous gasoline vehicle models in Australia in 2019

No.	Car model	Sales	Engine specifications					
			Engine model code	Displacement (L)	Air intake system	Injection system	Compression ratio	Fuel consumption (L/100km)
1	Toyota Hilux	47649	2TR-FE	2.7	aspirated	PFI	10.2:1	10.4-11.1
2	Toyota Corolla	30468	2ZR-FE	1.8	Aspirated	PFI	10.0:1	6.4-6.8
			2ZR-	1.8	Aspirated	PFI	13.0:1	3.5-4.2 (hybrid)
			FXE	2.0	Aspirated	DI	13.0:1	6.0-6.5
			M20A-FKS					
3	Ford Range	40690	No petrol model is available					
4	Hyundai i30	28378	Gamma	1.6	Turbocharged	DI	9.5:1	7.1-7.5
			Nu	2.0	Aspirated	DI	11.5:1	7.3-7.4
			G4KH	2.0	turbocharged	DI	9.5:1	8.0
5	Mitsubishi Triton	25819	4G64	2.4	Aspirated	PFI	9.0:1	11.4
			PE-VPS	2.0	Aspirated	DI	13.0:1	6.9
6	Mazda CX-5	25539	PY-VPR	2.5	Aspirated	DI	13.0:1	7.4
			PY-VPR	2.5	Turbocharged	DI	10.5:1	8.2
7	Toyota RAV4	24260	M20A-	2.0	Aspirated	DI+PF	13.0:1	6.5-6.8
			FKS	2.5	Aspirated	I	13.0:1	7.3
			A25A-FKS	2.5	Aspirated	DI+PF	14.0:1	4.7-4.8 (hybrid)
			A25A-FKS			I		
8	Mazda 3	24939	PE-VPS	2.0	Aspirated	DI	13.0:1	5.7-6.4
			PY-VPS	2.5	Aspirated	DI	13.0:1	6.0-6.6
9	Kia Cerato	21757	G4NA	2.0	Aspirated	PFI	10.3:1	7.4-7.6
			G4FJ	1.6	Turbocharged	DI	10.0:1	6.8
10	Mitsubishi ASX	20806	4B11	2.0	Aspirated	PFI	10.0:1	7.6-7.7
			4B12	2.4	Aspirated	PFI	10.5:1	7.9
11	Nissan X-Trail	19726	MR20D	2.0	Aspirated	DI	11.2:1	8.2
			D	2.5	Aspirated	PFI	10.0:1	7.9-8.3
			QR25D					
12	Toyota Landcruiser	18335	1UR-FE	4.6	Aspirated	PFI	10.2:1	13.4
13	Hyundai Tucson	18251	T-GDI	1.6	Turbocharged	DI	10.1:1	7.7
			2.0 GDI	2.0	Aspirated	DI	11.5:1	7.8-7.9
14	Mitsubishi Outlander	17514	4J11	2.0	Aspirated	PFI	10.5:1	7.0
			MIVEC					
			4B11	2.0	Aspirated	PFI		1.7 (plug-in hybrid)
			MIVEC					
			4J12	2.4	Aspirated	PFI	10.5:1	
15	Holden Colorado	17472	MIVEC	2.4	Aspirated	PFI		7.2
			MIVEC				12.0:1	1.9 (plug-in hybrid)

16	Isuzu D-Max	16892	No petrol model is available					
17	Toyota Camry	16768	2AR-FE	2.5	Aspirated	PFI	10.4:1	7.8-8.3
			A25A-FXS	2.5	Aspirated	DI+PF	10.4:1	4.2-4.5 (hybrid)
			2GR-FKS	3.5	Aspirated	I		
						DI+PF	11.8:1	8.7-8.9
18	Subaru Forester	15096	e-Boxer	2.0	Aspirated	DI	12.5:1	6.7 (hybrid)
			FB25	2.5	Aspirated	DI	12.0:1	7.4
19	Mazda CX-3	14813	SKYAC TIV-G	2.0	Aspirated	DI	13.0:1	6.3-6.7
20	Volkswagen Golf	14355	CZDA	1.4	Turbocharged	DI	10.0:1	5.4-5.7
			CJSB	1.8	Turbocharged	DI+PF		
			DJHB	2.0	Turbocharged	I	9.6:1	6.8
			CHHA	2.0	Turbocharged	DI+PF		
						I	9.3:1	7.2-7.3
					DI+PF			
					I	9.6:1	6.5	

* The 2019 new car sales were from the Federal Chamber of Automotive Industries at <https://www.caradvice.com.au/817278/vfacts-2019-new-car-sales-results>

† The engine specifications of 2019 car models were from <https://www.redbook.com.au/>

2.3 Technologies of Fuel Injection

2.3.1 Port Fuel Injection (PFI)

SI engine fuel injection technologies as indicated in Table 2.1, DI and PFI dominate modern SI engine fuel injection systems. Fuel is controlled by a nozzle and sprayed to the intake manifold, where it is delivered into cylinders by intake air in a PFI system. Single-point injection and multi-point injection are the two types of PFI multi-point injection injects fuel-air mixture at the back of each cylinder's intake valve(s), whereas single-point injection injects the mixture at the main intake manifold, which serves all cylinders. Because multi-point injection distributes fuel more evenly and accurately across cylinders than single-point injection, it is the most common type in current PFI engines.

2.2.2 Direct Injection (DI)

A high-pressure injector sprays gasoline directly into the engine combustion chamber in a DI system Fig 2.1. The two combustion modes used in DI engines are homogeneous stoichiometric combustion and stratified lean combustion (Lee et al., 2020). The homogeneous mode injects fuel during the early intake stroke, resulting in a homogeneous stoichiometric mixture at spark discharge. The stratified mode injects fuel later, bringing about an ignitable combination around the spark attachment. It is true that the stratified mode has a higher fuel efficiency but the TWC has a low conversion efficiency.

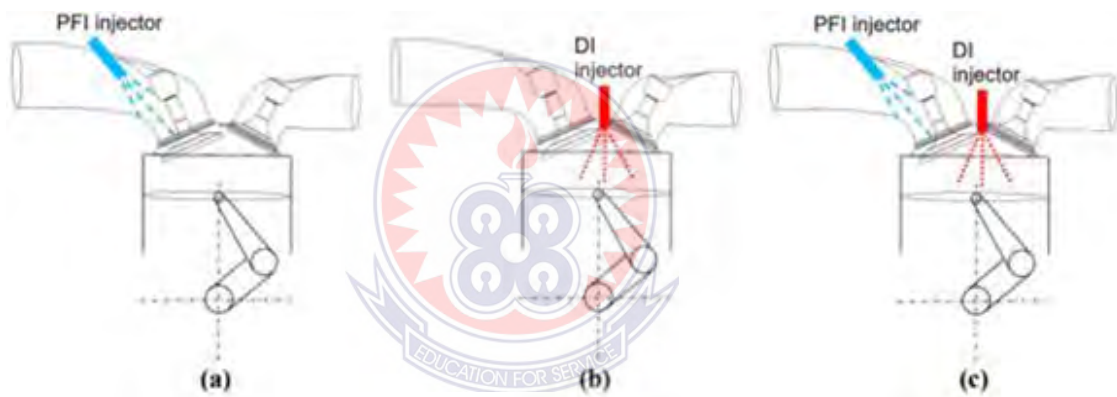


Figure 2.1. Schematics of (a)Port Fuel Injection (PFI), (b) Direct Injection (DI), (c) the current Dual injection(Dual DI) in use

Before the intake valves open and fuel films develop on the surfaces of the ports and valves, PFI regularly begins injection. The liquid fuel retains heat from the warmed surfaces and somewhat dissipates prior to being entrained by the intake air into the combustion chamber. Accordingly, PFI engine possess sufficient energy for fuel mixing and evaporation, and just utilize low injection. PFI engines have a high TWC conversion efficiency due to their homogeneous stoichiometric combustion. Furthermore, the efficient mixing processes and evaporation limit particle emissions. Port wall wetness, on the other hand, causes a delay between injection and fuel

delivery to the cylinders, resulting in metering errors and delayed transient responses. When the intake port is cold, over-fueling is required for a cold start, which results in poorer fuel economy and increased HC emissions.

DI engines inject fuel straight forwardly into every chamber, eliminating time lag and improving transient response. Fuel evaporation cools the air inside the combustion chamber, increasing volumetric efficiency and lowering knock tendency. To improve thermal efficiency, a larger compression ratio can be achieved. DI technology also has a higher tolerance limit for exhaust gas recirculation (EGR) and more possibility for system optimization (Zhao et al., 1999). All of these advantages, however, come at the expense. Because the amount of time available for fuel evaporation and mixing is restricted, fine spray droplets require high pressure injection of about 20 MPa. Over a wide operating range, fuel injection under high pressure and mixture formation have more control complexity, and fuel impingement on the cylinder and piston walls is possible. Spark timing will cause unevaporated fuel droplets to participate in diffusion burning, resulting in high particulate emissions similar to diesel engines. Saliba et al. (2017) examined the performance of DI and PFI light-duty petrol cars in terms of gaseous and particle emissions. The results showed very minimal difference in regulated gaseous emissions between PFI and DI vehicles. DI vehicles, then again, emitted much particulate matter than PFI cars by a factor of two. In studies with smaller sample sizes (Liang et al., 2013; Wen et al., 2020; Zhu et al., 2016), higher particle emissions of DI engines were also noted. PM and PN restrictions have been imposed by recent emission laws such as Euro 6. DI engines will need to use gasoline particulate filters to comply (Awad et al., 2020). Finally, DI engines face issues such as injector deposits and ignition fouling. Injector deposits accumulate as a result of

being exposed to a high-temperature combustion environment, which can limit injector fuel flow rates and modify the spray characteristics. Fuel-air mixture impingement on the electrodes of the spark plug causes ignition fouling due to the close distance between the injector and the spark plug (Zhao et al., 1999).

Table 2.3: Comparison between advantages and disadvantages PFI and DI technologies

	PFI	DI
Advantages	Long time for fuel evaporation and mixing Low cost of low-pressure injection system Low gaseous emissions with TWC Low PM and PN emissions	Improved transient response High compression ratio and fuel efficiency Low HC during cold start Extended EGR tolerance limit Enhanced potential for system optimization
Disadvantages	Fuel delivery delay due to port wall wetting Low compression ratio and fuel efficiency Fuel evaporation in intake port reduces volumetric efficiency Over fueling and high HC during cold start	Short time for fuel evaporation and mixing High cost of high-pressure injection system Reduced TWC efficiency under lean mode High PM and PN emissions In-cylinder fuel impingement Injector deposits and ignition fouling

2.2.3 Gasoline Direct Injection (GDI)

In modern spark ignition (SI) engines, gasoline direct injection (GDI) is a widely used method of injection due to its enhanced thermal efficiency and exhaust emission when compared to port fuel injection (Shuai et al., 2018).

In general, there are two types of GDI engines, each with its own injection strategy: early injection for homogenous charge and late injection for stratified charge. It is

suggested that the latter could realize the GDI engine's full potential in terms of fuel economy and emissions (Kalghatgi, 2019). From this, late injection GDI engine, as well as the mixture formation and fuel atomization processes that lead to fuel vaporization and combustion of the air-fuel combination, has become a study focus. Fuel is injected into the combustion chamber in a GDI engine directly, where an air-fuel mixture forms simultaneously, which appears to alleviate the mixture control problem that plagues PFI engines (Journal, 2019). In the later phase of the compression stroke, it uses charge stratification at part load to premix the fuels with air in the combustion chamber. In this situation, the air-to-fuel ratio is stoichiometric near the spark plug, but leaner near the cylinder walls, which reduces engine knock. As a result, the lean air-fuel mixture may result in better fuel economy. Furthermore, because of the stratified charge, progressive charge cooling is achieved, allowing for the use of greater compression ratios without the risk of engine knock. The thermal efficiency is greatly improved in such situations (Yang & Bandivadekar, 2017).

Furthermore, due to the lean combustion and the position of the injector, mixture management may not be dependent on throttling, and there is evidence that pumping loss due to cycle work may be minimized when compared to standard PFI engines (Huang et al., 2018). Despite the fact that the GDI engine produces more power at part load, current study shows that the lean mixture creation in the combustion chamber might cause misfires and unburned hydrocarbon emissions, potentially weakening the engine's advantage over the PFI engine. As a result, the quality of mixture creation in the GDI engine with late injection should be improved to offset the influence of potential downsides of lean mixture formation (Anenberg et al., 2019). The time for gasoline to combine with air in GDI engines with late injection is restricted. Strong

turbulence caused by tumble or swirl motion must be improved in order to attain an acceptable proportion of mixture. The injection geometry affects turbulence inside the cylinder, and this injection parameter appears to be sensitive to injector type (European Commission,2008). As a result, the use of suitable injectors is critical in improving mixture formation performance, which reduces emissions and improves fuel economy for GDI engines with late injection (European Commission,2012).

Swirl injectors and multi-hole injectors are frequently used, and a recent study showed that the latter has a substantial advantage over the former in terms of obtaining a higher quality of mixture formation (European Commission,1998). In GDI, the spark plug is positioned in the center of the combustion chamber, while the injector position can be adjusted. When it comes to the width of the gap between the spark plug and the injector, there are primarily two options: narrow spacing and wide spacing (European Commission, 2017). In GDI, the spark plug is positioned in the center of the combustion chamber, while the injector position can be adjusted. There are basically two ways for the positioning of injector in regard to the gap between spark plug and injector, namely, small spacing and wide spacing (European Commission, 2017). Because of its simplicity and lack of importance to air charge motion, it is suggested that the narrow spacing configuration is preferable. High thermal stress around the exhaust valve, on the other hand, could be a disadvantage. According to Fiengo (2013), three types of combustion systems for GDI engines with late injection are constructed based on a narrow spacing scheme, whereas charge stratification approaches are separated. Spray guided, wall-guided, and air-guided are three of these properties (Tsokolis et al., 2016). The injector in a spray-guided system is often placed near the center of the combustion chamber, and the stratification

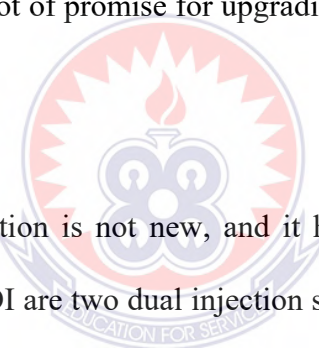
process is highly dependent on spray dynamics, whereas a cavity on the top of the piston interacts with spray in a wall-guided system (Y. Huang et al., 2019). Another aspect of this design is that the injection is placed close to the centrally positioned spark plug, avoiding the use of a hollow surface piston in the cylinder. Stratification is achieved in air guided systems primarily through the interaction between the fuel spray and the velocity of the air charge injected in the cylinder (Journal, 2019). The atomization process is also critical for spray generation, which is the process of breaking up liquid fuel into drops and is necessary for liquid fuel to burn properly in a combustion chamber (Fontaras et al., 2017).

It has been noticed that atomization of fuel is traditionally carried out by atomizers, which are most likely a component of the injector on the scope of the internal combustion engine, and one of the permissible categories of atomizer is based on the energy used for atomization (European Commission, 2017). It's also been proven that the swirl atomizer can create a powerful tumble or swirl for a GDI engine with late injection to accomplish the expected charge stratification for mixture formation. The jet atomizer aids in the investigation of the process of liquid disintegration into drops, which occurs at a distance from the atomizer. Many factors influence the degree of disintegration, including orifice size, discharge velocity, and ambient conditions. In most cases, increasing discharge velocity can hasten the break-up process (European Commission, 2021).

2.2.4 Dual Injection

When paired with renewable fuels, the potential for dual injection in terms of fuel savings and emissions reduction can be further expanded by utilizing their fuel qualities, such as high-octane number, greater cooling impact, and wide flammability

limit. In the fight against global warming and fossil fuel depletion, renewable fuels are becoming increasingly essential, with ethanol being the most extensively utilized alternative fuel for SI engines (Thakur et al., 2017; Thangavelu et al., 2016). Due to its limited supply and compatibility with existing engines, it is currently utilized to partially substitute fossil fuel by mixing with gasoline (e.g., E10). Blending renewable fuels with gasoline at fixed ratios, on the other hand, would not provide optimal performance throughout a wide range of engine operating circumstances. Thus, the dual injection concept's in-cylinder blending of gasoline and renewable fuels allows the option to use renewable fuels more effectively and efficiently than pre-blending. By adjusting the blending ratio and the method of injection according to the operating state, dual injection has a lot of promise for upgrading the combustion performance of SI engines.

The logo of the University of Education, Winneba, is a circular emblem. It features a central lamp with a flame, set against a background of a sunburst. The lamp is flanked by two stylized figures. The entire emblem is encircled by a border containing the text 'UNIVERSITY OF EDUCATION FOR SERVICE'.

The concept of dual injection is not new, and it has been widely researched in CI engines. DI+PFI and DI+DI are two dual injection systems that have been extensively studied in CI engines. Dual injection CI engines can operate in low temperature combustion (LTC) or conventional diesel combustion (CDC) mode, depending on the quantity of premixed fuel used. LTC acts more like a premixed flame, whereas CDC behaves more like a diffusion flame. Although DI+PFI is commonly investigated in LTC mode, such as reactivity regulated compression ignition (RCCI) (Liu et al., 2018; Reitz & Duraisamy, 2015) and dual fuel sequential combustion (DFSC) (Cui et al., 2021; Qian et al., 2016), it also works in CDC mode, such as natural gas/hydrogen/alcohols PFI + diesel DI (Chintala & Subramanian, 2017; Wei & Geng, 2016). Meanwhile, DI+PFI is being investigated in both LTC and CDC modes (e.g., intelligent charge combustion ignition (ICCI) (Zhao et al., 2020) and direct dual fuel

stratification (DDFS) (Shirvani et al., 2020). Dual injection, on the other hand, is a relatively new concept in SI engines that has gotten a lot of attention in recent years. There has been a paucity of critical review in this field thus far. The goal of this research is to examine recent developments in dual injection of gasoline in SI engines. Although there are a few studies on dual PFI (Y. Lee et al., 2018; Venugopal & Ramesh, 2014) and the combination of DI and PFI, the dual injection idea here explicitly refers to dual direct injection (Dual DI) that has gained the greatest study attention.

2.3 Advantages of Dual Injection

As previously discussed, both DI and PFI have their own set of benefits. Dual injection of DI+PFI is a novel concept that combines their benefits. The dual injection method allows for more control over mixture formation and combustion processes. It's also a more effective and efficient way of utilizing renewable fuels' limited supply than blending them with gasoline at fixed ratios. Furthermore, the use of renewable fuels can boost the benefits of dual injection by utilizing their fuel features such as higher enthalpy of vaporization, higher octane number, and a larger flammability limit. In particular, when compared to DI or PFI, dual injection offers the following benefits.

2.3.1 Control flexibility

Furthermore, by exploiting their fuel properties such as higher enthalpy of vaporisation, better octane number, and a higher flammability limit, renewable fuels can enhance the benefits of dual injection. When compared to DI or PFI, dual injection has the following advantages. Due to the fact that these phases of a test cycle generate the majority of particle emissions, dual injection has been advised to mitigate

the problem of excessive particulate emissions in cold-start and transient scenarios (Chen et al., 2019).

As the engine load grows, the percentage of DI fuel can be increased to lower the combustion temperature and thus reduce engine knock. Furthermore, employing fuels with a high RON and/or a large enthalpy of vaporization can greatly improve anti-knock effectiveness (such as ethanol and premium unleaded petrol). This method is known as octane-on-demand (Qian et al., 2019), and various patents have been issued based on it. In addition, depending on the operating conditions, dual injection can vary the renewable fuel and gasoline blending ratio in real time. Experiments revealed that varying biofuel-to-gasoline blending ratios are required for optimal engine performance under various operating situations (Phuangwongtrakul et al., 2016). Renewables have a finite supply and can only partially replace gasoline. Dual injection allows for on-demand modification of the in-cylinder blending ratio, making renewable fuels more effective and efficient than pre-blending them with gasoline at a fixed ratio. Daniel et al. (Daniel et al., 2013) examined the combustion performance of dual injection gasoline-biofuel blends to DI gasoline-biofuel blends. Dual injection outperformed DI in terms of combustion duration, cylinder pressure, and thermal efficiency, as well as decreased CO and mean particle matter diameter.

2.3.2 Enhanced Cooling Effect

Because of the evaporation of gasoline inside the combustion domain, DI has a greater cooling impact than PFI. SI engines benefit from this cooling effect in a variety of ways, including improved volumetric efficiency, fewer NO_x emissions, decreased knock propensity, bigger compression ratios, greater turbocharging, and

higher thermal efficiency. Furthermore, the cooling impact of DI might be amplified by employing fuels with higher vaporization enthalpies.

DI's cooling impact may be measured in a variety of ways. The most straightforward method is to take direct readings of the air temperature inside the cylinders. Due to the extremely transient nature of in-cylinder flows, cold-wire resistance thermometers were used to monitor in-cylinder air temperatures in PFI and DI engines (Price et al., 2007), which needed fast-response and thin sensors. As a result, to preserve the sensitive sensors, such tests were only done in non-firing situations. The in-cylinder gas temperature of a DI engine was measured using a tracer-based PLIF method established by Attar et al. (2014) during both driving and firing circumstances. The bulk of experimental investigations have measured characteristics related to charge cooling, such as in-cylinder pressures (Ahn et al., 2010), volumetric efficiencies and anti-knock effects (Kasseris & Heywood, 2012), to indirectly quantify the cooling impact. The volumetric air flow rate of a gasoline PFI with gasoline/DMF/ethanol DI engine was determined by Wu et al. (2011). They discovered that the DI ratio enhanced air flow rate, and that the rise was considerably greater for ethanol than DMF or gasoline. Zhuang and Hong (2013) discovered that the volumetric efficiency of a gasoline PFI Combined with ethanol DI engine improved with the DI ratio only when the injection occurred when the intake valve was open. Volumetric efficiency or intake flow rate, on the other hand, may only indicate a fraction of the charge cooling impact that occurs before the intake valves are closed. Fuel evaporation would continue in a DI SI engine during the compression stroke or even during combustion. As a result, knock onset was thought to be a superior metric for determining the cooling impact. The anti-knock property of DI can be attributed to two factors:

thermal (cooling effect) and chemical benefit (Kasseris & Heywood, 2012). It was discovered that the cooling impact of ethanol was equivalent to its greater RON. To compare the thermal and chemical advantages of ethanol, a one-point increase in the RON is comparable to an increase of 2-8 kJ/kg in mixture cooling power (Milpied et al., 2009), or adding 10% ethanol to gasoline raises the RON by five points (Ozsezen & Canakci, 2011).

Meanwhile, numerical simulation has been used to assess the cooling impact of DI and dual injection systems since it is a cost-effective and strong tool for overcoming the limitations of experimental techniques. Wyszynski et al. (2002) estimated the potential improvements in volumetric efficiency of DI over PFI using a 0-D model. Kasseris and Heywood (2012) evaluated the anti-knock advantages of a DI engine running on ethanol-gasoline mixtures using a 1-D model. The output information from 0-D and 1-D models, on the other hand, was typically quite limited because they were designed for certain purposes. Huang et al. (2015) investigated the cooling impact of a petrol PFI with ethanol DI dual injection engine using a three-dimensional computational fluid dynamics (CFD) model. Due to ethanol's low evaporation rate and in-cylinder wall wetting, they discovered that the overall cooling impact improved with DI ratios between 0% and 58 percent, but not with higher DI ratios. Under low-temperature conditions (such as naturally-aspirated engines), ethanol evaporates more slowly than gasoline (Huang et al., 2013), limiting the amount of ethanol-induced cooling. The air temperature can be raised to help with this. Kasseris and Heywood (2012) used 3-D CFD modeling to investigate the influence of intake air temperature on cooling effect. They discovered that with a high intake air temperature of 120 °C, they could achieve all of the expected cooling effects.

2.3.3 Knock Mitigation

In SI engines, RON describes a fuel's anti-knock ability. Renewable fuels all have a higher RON than gasoline. Dual injection of gasoline and alcohol fuels can further improve anti-knock performance by combining the cooling impact of DI with the greater enthalpies of vaporization of alcohols. As previously stated, the thermal and chemical advantages are equally important in knock mitigation (Stein et al., 2012). Engine experiments have thoroughly examined the benefits of dual injection in knock mitigation. Liu et al. (2014) studied the knock characteristics of a methanol PFI plus gasoline DI engine and found that dual injection successfully suppressed engine knock, extended the high-load limit, and improved fuel efficiency. When ethanol was fed during intake valve open, experiments on an ethanol PFI plus gasoline DI engine revealed simultaneous decreases in knock propensity and emissions (Kim et al., 2015). Meanwhile, Zhuang et al. (2017) investigated the potential of a gasoline PFI with ethanol DI engine to reduce knock. When compared to gasoline PFI or DI, they discovered that dual injection successfully reduced knock by raising the ethanol DI ratio and allowed for more advanced spark timing and greater intake air pressure. Experiments on a gasoline PFI with n-butanol DI engine, however, revealed that dual injection of 20% and 50% n-butanol had a higher knock propensity and intensity than gasoline PFI, despite dual injection having a higher indicated mean effective pressure (IMEP) (Feng et al., 2018).

2.3.4 Engine Downsizing

Engine downsizing is seen as a critical technology for meeting future carbon reduction goals (Fraser et al., 2009). Engine downsizing is the notion of using a smaller engine in a car to give equivalent power output as a larger engine by using a turbocharger and keeping the compression ratio as high as possible to obtain the optimum thermal efficiency. Lower mechanical and thermal losses, reduced engine

weight, and greater operation time inside an engine's optimal performance zone are the major benefits of engine downsizing (Gheorghiu, 2015).

Turner et al. (2014) proved that by reducing engine displacement by 60% and fuel consumption by 35%, it was feasible to obtain torque performance similar to that of a current big (e.g., 5.0 L) naturally-aspirated engine. However, higher knock propensity at high load and lower fuel economy at part load are two major drawbacks of SI engine downsizing (Fraser et al., 2009). Dual injection's increased control flexibility and anti-knock capabilities may be able to assist address these issues. The Toyota M20A-FKS/A25A-FKS/A25A-FXS naturally aspirated engines have reached high compression ratios of 14:1 in a hybrid arrangement and 13:1 in a conventional configuration in mass production automobiles by using dual injection, as indicated in Table 2.2 (i.e., Camry and RAV4 models). Dual injection systems are also used in the Volkswagen turbocharged engines CJSB/DJHB/CHHA. It's worth noting that both PFI and DI in these dual injection engines utilize the same fuel (gasoline). Due to their higher RON and enthalpies of vaporisation, it is predicted that combining renewable fuels with the dual injection idea will allow for more aggressive engine downsizing (e.g., higher turbocharging, bigger compression ratio, and more spark advance).

2.3.5 Fast Combustion Speed

The flame rates of renewable fuels are often faster than those of gasoline. As a result, incorporating renewable fuels into gasoline engines may improve the rate of combustion. Majority of research have found that dual injection systems have higher combustion rates, either indirectly through in-cylinder pressure related factors or directly by visualization of in-cylinder flows using experimental and computational

approaches. Experiments on engines using gasoline. The combustion process in a gasoline PFI + ethanol/DMF DI optical engine was shown by Jiang et al. (Jiang et al., 2012), who discovered that both gasoline ethanol and gasoline-DMF dual injection systems exhibited quicker combustion rates than gasoline PFI. When the ethanol ratio was less than 76 percent, CFD modeling findings of a gasoline PFI with ethanol DI engine revealed that dual injection had a faster flame propagation speed than gasoline PFI (Huang et al., 2015).

2.3.6 Extended Lean Burn Limit

Because of decreased pumping losses and combustion temperatures, lean burn technology is a successful method for reducing fuel consumption and NO_x emissions in SI engines (Alvarez et al., 2018). However, increased cyclic variation, lower combustion speed, and higher ignition energy limit the applicability of lean burn technology. The use of renewable fuels in tandem with fossil fuels has the potential to extend the lean burn limit. Hydrogen, in example, has a much higher flame velocity, a broader flammability limit, lower ignition energy, and a quicker diffusion rate than gasoline (White et al., 2006), and has therefore been widely explored for increasing the SI engine's lean burn limit. The addition of hydrogen to a gasoline PFI with hydrogen DI engine enhanced thermal efficiency and decreased cyclic variation under lean circumstances (Du et al., 2016). With 10.5 percent hydrogen (Niu et al., 2016), the lean burn limit rose with hydrogen DI ratio and could reach an excess air ratio of 2.65. Under lean-burn circumstances, hydrogen addition might also prolong the EGR limit (Yu et al., 2019). Gong et al. (2020) found that a dual injection engine with hydrogen PFI and methanol DI could successfully increase the lean-burn limit from 1.6 without hydrogen to 2.2 with 3–6% hydrogen DI, while also reducing cyclic fluctuation. Dual injection engines' lean-burn performance might be improved by

using liquid renewable fuels. When compared to gasoline PFI, the lean-burn limit of a gasoline PFI with ethanol DI engine was improved by on average 20%, according to Zhuang et al. (2018). In addition, when the ethanol ratio grew and DI time advanced, the lean burn limit increased. Under lean-burn circumstances, experiments on a dimethyl ether (DME) PFI + gasoline DI engine revealed enhanced thermal efficiency and reduced cyclic variation when using dual injection mode (Shi et al., 2019).

The dual injection concept's ultimate objective is to improve engine thermal efficiency and so conserve fossil fuels. The benefits stated above, in particular improved control flexibility, engine downsizing, quicker combustion speed, and longer low burn limit, have all contributed to this. In terms of pollutant emissions, the majority of dual injection investigations have shown that particle and particular gaseous emissions are reduced.



CHAPTER THREE

METHODS AND MATERIALS

3.1 Introduction

This section discusses the techniques utilized in completing the research: the numerical methods, species transport model, procedures and the geometry and mesh of the combustion chamber utilized for the study.

3.2 Numerical Methods

The investigation is about the computational fluids dynamics (CFD) modelling of two-stage steady injection measure in nonexclusive GDI engines to contemplate the highlights of fuel atomization, injection speed and its effect on turbulence utilizing ANSYS 2021. The geometry is designed using ANSYS software. The researcher has designed a typical dual injection spark ignition engine and made significant modifications to it, which is capable of meeting current design specifications and applications. The main concern areas under consideration, is to change the port fuel injector and make it two direct injectors significantly distant from one another, analyze the flow velocities and the turbulences during the combustion process.

Computational domain for simulations is the combustion chamber of the GDI engine in which the piston is near the top dead centre (TDC) on the compression stroke on one hand and at the bottom dead centre on the other hand representing the early and late injection strategies. The dimensions and 3D of the geometry are shown in Figures 3.1, - 3.5 with the inlet orifice simplified to be at the surface. The polyhedral mesh Figs 3.6-3.9 was used with the main specifications shown in Table 3.1 while mesh size for inlet region specified through the 'Relative to base' method. The percentage is determined automatically in terms of the proportion for the diameter of the inlet to that of the outlet. For the boundary conditions, magnitude normal to the

boundary is specified for the velocity. For turbulence specification method, the turbulent intensity is 5% and the turbulent viscosity ratio is 10. To study the mixture formation, contours plot of different injection velocities is selected such as 100m/s, 150m/s, 200m/s, 250m/s and 300m/s.

Chemical species of gasoline-air combustion are examined at both early and late injection modes using eddy-dissipation model in ANSYS fluent. physical models; heat transfer is enabled by the energy equation, standard k-epsilon turbulence model is selected in the viscous model and chemical species transport and reaction enabled by selecting the species transport model. select material properties, and define boundary conditions for a turbulent flow with chemical species mixing and reaction.

A generalized eddy-dissipation model to analyze the gasoline-air combustion system. The combustion will be modeled using a one-step reaction mechanism, assuming complete conversion of the fuel to CO₂ and H₂O. The reaction equation is $C_8H_{18} + 12.5 (O_2 + 3.76 N_2) \rightarrow 8 CO_2 + 9H_2O + 47 N_2$. This reaction will be defined in terms of stoichiometric coefficients, formation enthalpies, and parameters that control the reaction rate. The reaction rate will be determined assuming that turbulent mixing is the rate-limiting process, with the turbulence-chemistry interaction modeled using the eddy-dissipation model.

Default setting for the mixture is modified by enabling the gas law. By default, the mixture material uses constant properties. These constant property assumptions are retained, allowing only the mixture density to vary with temperature and composition. The influence of variable property inputs on the combustion prediction are examined

3.2 Geometry of the Combustion Chamber

The engine is designed using ANSYS 2021 Software. This software allows two-

dimensional (2D) and three-dimensional (3D) data design integration. It is possible to create a virtual pictorial representation of the final product that users can validate the form, fit, and function of products before it is manufactured. There are four combustion chamber models in consideration; two models with the piston at bottom dead centre (BDC) for single injection and dual injection and two models with the piston at top dead centre (TDC) for both single and dual injection engines.

The geometry consists of a chamber of which the piston position is at bottom dead centre (BDC), a direct fuel injector for the GDI and two direct fuel injectors for the dual injection engine.

Table 3.1: Main technical parameters of the engine

Engine	Spark ignition, four cylinders, dual-injection
Compression	9.6:1
Displacement	1.984L
Cylinder Bore and stroke	82.5 mm x 92.8mm
Maximum Power	137KW (5000rpm)
Maximum Torque	320Nm(1600-4000rpm)

A cylinder with a centrally mounted swirl injector is designed. The atomizing nozzle diameter is 0.1mm to enable fuel injection at high pressure into the combustion chamber.

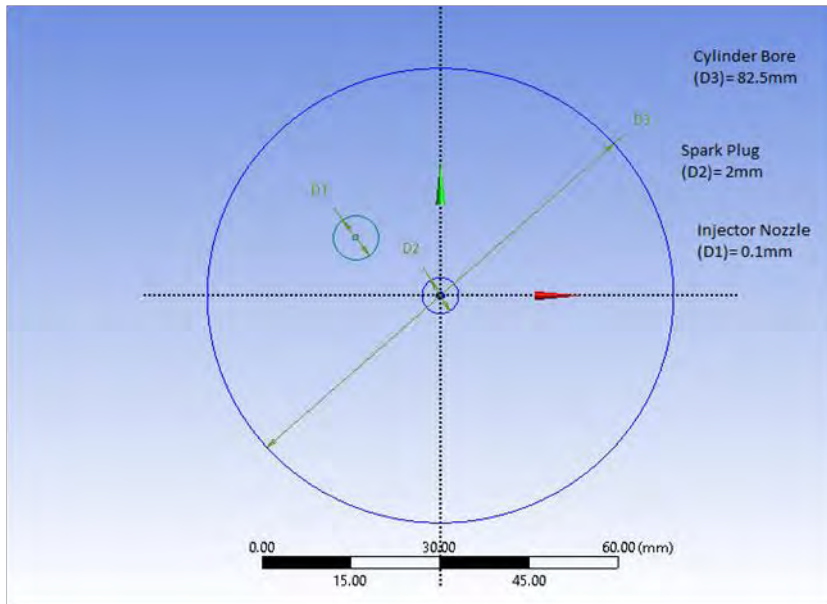


Figure 3.1: Dimension of cylinder

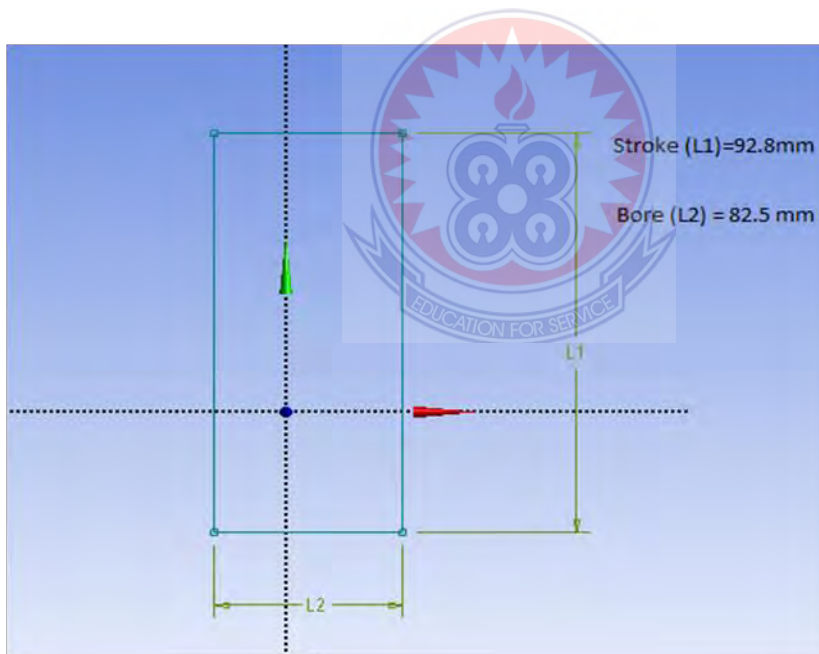


Figure 3.2: Dimension of cylinder bore and stroke

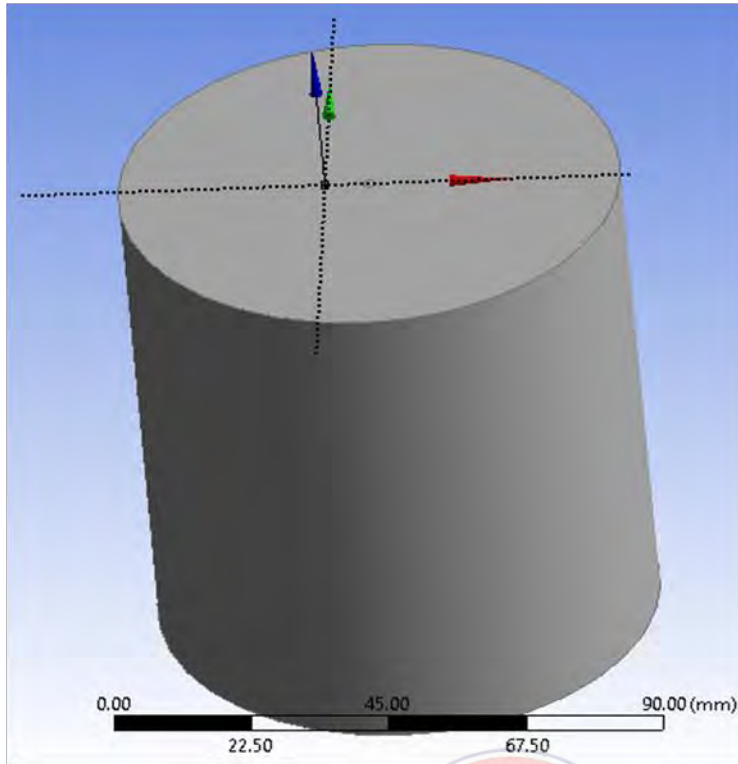


Figure 3.3: 3D geometry of a computational domain with piston at BDC.

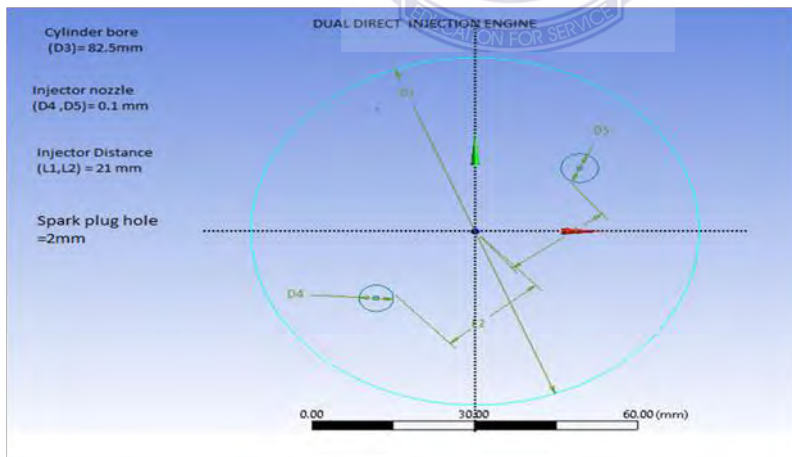


Figure 3.4: Dimensions of the dual direct injection model

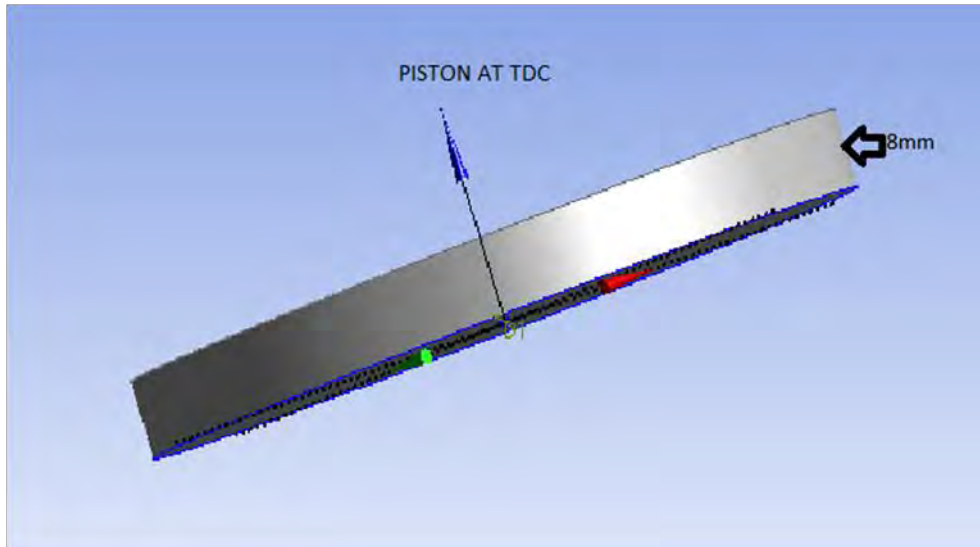
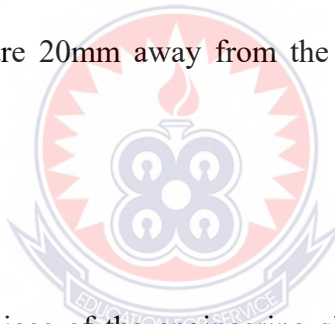


Figure 3.5: 3D geometry of the computational domain with piston at TDC

The injector nozzle which is the inlet to the computational domain is 0.1mm in diameter. The injectors are 20mm away from the walls and 21mm from the spark plug.



3.3 Meshing

Meshing is a necessary piece of the engineering simulation process where complex geometry is partitioned into straightforward components that can be utilized as discrete approximations of the bigger area. The mesh impacts the precision, convergence and speed of the simulation. In the case of meshing being precise, then, at that point the results are additionally expected to be practical.

The present geometry is a mesh in ANSYS Software for the GDI and Dual injection engines

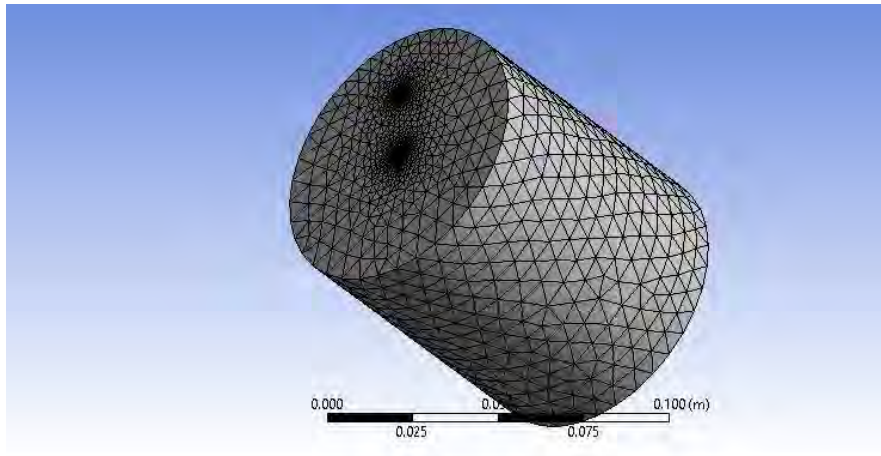


Figure 3.6: Mesh of cylinder with single direct injector at BDC

This is an automatic mesh of a single injector computational domain at the bottom dead centre. The mesh has 6694 nodes and 34806 elements.

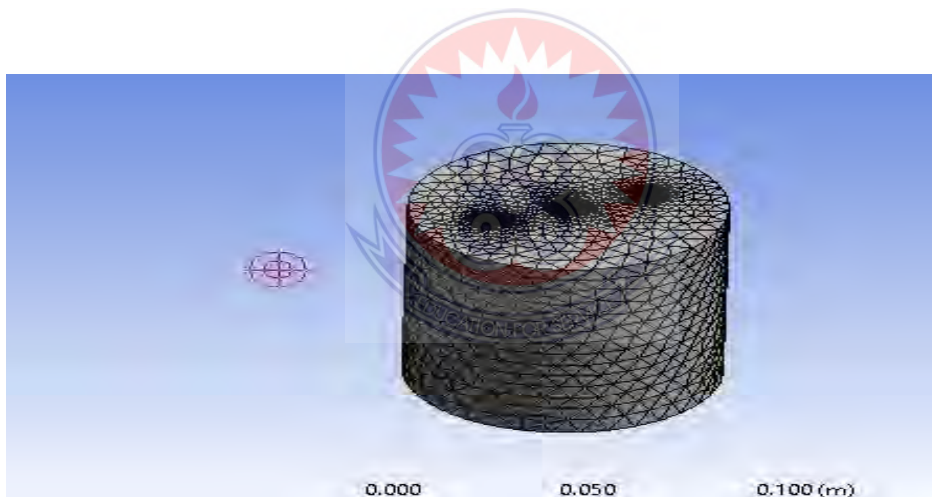


Figure 3.7: Mesh of cylinder with dual direct injector at BDC

This is an automatic mesh of a dual direct injector computational domain at bottom dead centre. The mesh has 9272 nodes and 48752 elements.

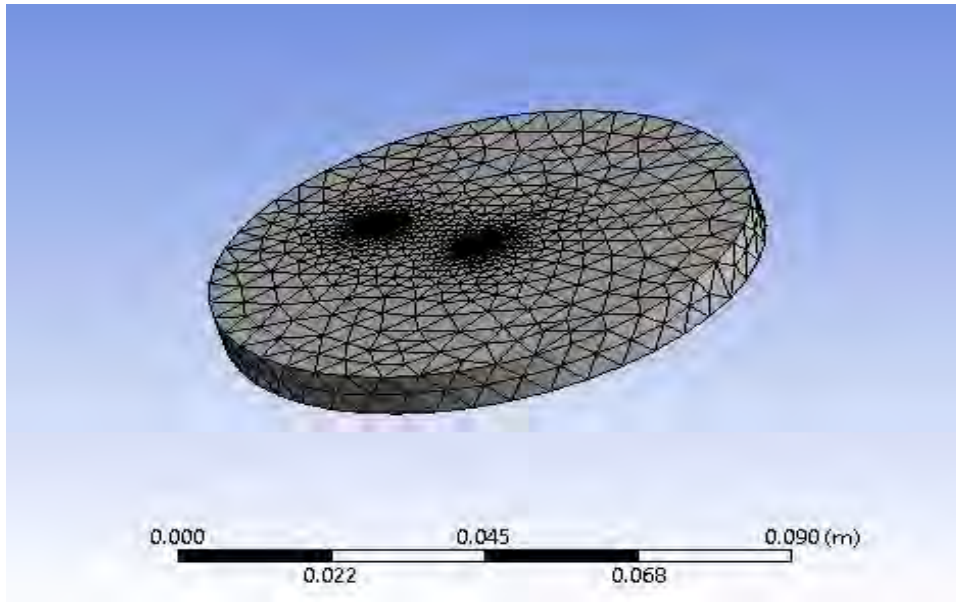


Figure 3.8: Mesh of cylinder with single direct injector at TDC

This is an automatic mesh of a single direct injector computational domain with the piston at top dead centre. The mesh has 4885 nodes and 24589 elements.

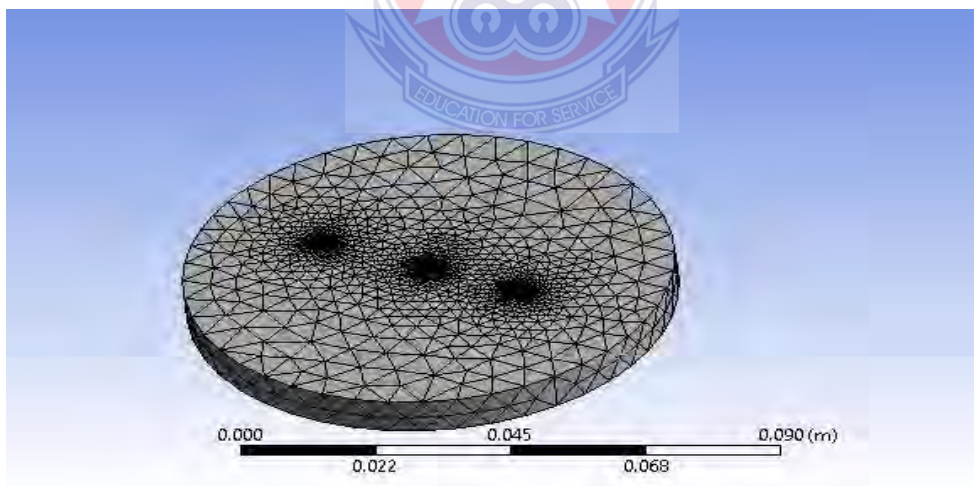


Figure 3.9: Mesh of cylinder with dual direct injector at TDC

This is an automatic mesh of a dual direct injector computational domain at top dead centre. The mesh has element of 38073 and 7412 nodes having the element size to be $5.8473e-003$ m.

3.4 Procedural Approach

A fuel injector is a component that administers fuel into an engine utilizing electronic control valves equipped for opening and shutting frequently. It has a nozzle that distributes fuel equally for ideal combustion and efficiency. In this research a two-stage flow injector with combustion chamber has been simulated by Ansys fluent software. For mixture formation, standard K-Epsilon model is used for the flow analysis from the viscous model. Viscous model allows the analysis of turbulence flow in a medium. Air and gasoline are the fluids under consideration in the computational domain. The boundary conditions for the computational domain are set to compute from the inlet with velocity at the inlet (velocity-inlet). The velocity magnitude of the inlet ranges from 100m/s to 300m/s while maintaining a constant injection pressure of 20Mpa. Acceleration due to gravity 9.81m/s^2 acts in the Z direction and a specific operating density of 1.22kg/m^3 . A standard initialization is commenced to compute from the inlet. In running the calculations, the time step method was automatic with the time scale factor of 1 for a conservative length scale method. It was set to calculate hundred iterations.

Fluent launcher was also used to start the 3D version of ANSYS FLUENT with double precision enabled for combustion and post combustion analysis. The imported mesh is checked to ensure that the reported minimum volume is positive. Heat transfer is activated by enabling the energy equation in the model. standard k-epsilon turbulence model is also selected from the viscous model and finally, chemical species transport and reaction model is enabled in the species model. Eddy-dissipation in the turbulence chemistry interaction is enabled to compute the rate of reaction under the assumption that chemical kinetics are fast as compared to the rate at which

reactants are mixed by eddies. Gasoline-air is selected in the species model and 1000J/Kg-K is entered for a constant specific heat value in the Cp drop down.

Intensity and hydraulic diameter are selected for specification method for the air inlet zone. velocity magnitude of air is set to 0.5m/s, default setting for turbulence intensity is retained at 10% and the hydraulic diameter set to 0.44m, the air temperature at 300K and 0.23 for O₂ species mass fraction. Intensity and hydraulic diameter are also selected for specification method for fuel inlet zone. Fuel velocity magnitude of air is set to 80m/s, default setting for turbulence intensity is retained at 10% and the hydraulic diameter set to 0.01m, the air temperature at 300K and 1 for C₁₆H₂₉ species mass fraction. The gauge pressure value for the pressure outlet is 0Pa. intensity and hydraulic diameter is selected for its specification method. Backflow turbulent intensity is set to 10% in the backflow diameter of 0.45m at a backflow total temperature of 300K and 0.23 species mass fraction for O₂. Temperature of 300K is selected for the thermal condition of the outer wall. The solution is first done with constant heat capacity with the default solution parameters retained in the solution methods. Under -relaxation factors for the species were set to 0.95 since the default parameters in ANSYS FLUENT are set to high value.

Plotting of residual during calculation is enabled in the monitor. Field variables are initialized by computing from selecting all-zone from the drop-down list and the variables are initialized. Calculation is started by requesting 500 iterations.

For solution with varying heat capacity, composition dependence of the specific heat is enabled by selecting mixing law from Cp drop down in the properties group box mixture selection. This is to ensure that specific heat of the mixture is based on a local mass-fraction weighted average of all the species. Temperature dependence of

specific heat is enabled for CO₂, O₂, C₁₆H₂₉, and H₂O by ensuring piecewise polynomial in the Cp drop down is selected. 500 more iterations are requested and calculations ran.

3.5 Species Transport Model

The governing transport equations, including mass, momentum, energy, and species conservations, were solved numerically under steady-state and turbulent flow conditions with a set of finite-rate reaction kinetics and eddy-dissipation rates.

In this study the Navier-Stokes equations are considered as

$$\nabla \cdot (\rho \vec{v}) = -\nabla p + \nabla \cdot (\bar{\tau}) + S_i \quad (3.1)$$

Where the stress tensor $\bar{\tau}$ is given by

$$\bar{\tau} = \mu \left[(\Delta \vec{v} + \nabla \vec{v}^T) - \frac{2}{3} \nabla \cdot \vec{v} I \right] \quad (3.2)$$

and the porous media source term, S_i , is expressed as

$$S_i = -\left(\frac{\mu}{\alpha} V_i + C_2 \frac{1}{2} \rho |V_i| |V_i| \right) \quad (3.3)$$

The permeability, α , and inertial loss coefficient, C_2 , can identified as

$$\alpha = \frac{D_p^2}{150} \frac{\varphi^3}{(1-\varphi)^2} \text{ and } C_2 = \frac{3.5(1-\varphi)}{D_p \varphi^3} \quad (3.4)$$

The continuity equation is expressed as follows:

$$\nabla \cdot (\rho \vec{v}) = 0 \quad (3.5)$$

The energy transport equation is solved with the modification of the conduction flux, using the effective conductivity, including turbulent contribution, as

$$\nabla \cdot (\vec{v}(ph + p)) = \nabla \cdot (k_{eff} \nabla T - \sum_j h_j \vec{J}_j) + S_h \quad (3.6)$$

Where the sensible enthalpy, h , and the effective thermal conductivity, k_{eff} , are defined as

$$h = \sum_j Y_j h_j \text{ and } k_{eff} = \alpha c_p \mu_{eff} \quad (3.7)$$

Similarly, the transportation of species is expressed as

$$\nabla \cdot (p \vec{v} Y_i) = -\nabla \cdot \left(- \left(p D_{i,m} + \frac{\mu_t}{Sc_t} \right) \nabla Y_i \right) + R_i \quad (3.8)$$

Where i denotes the CO, CO₂, O₂, CH₄, H₂, H₂O, C, and N₂ species, R_i is the net rate of production of the species i by chemical reactions, and Sc_t is the turbulent Schmidt number, which is a ratio of the turbulent viscosity to the eddy diffusivity.

Because the flow was turbulent, a Reynolds-averaging technique was employed to derive the Reynolds-averaged Navier-Stokes (RANS) equations (Eqs. (3.1) – (3.7)). Subsequently, the additional Reynolds stresses, representing the effects of turbulence, introduced in Eq. (1), were modeled using the Boussinesq hypothesis approach. It relates the Reynolds stresses to turbulent viscosity, μ_t , which is a function of the turbulence kinetic energy, k , and turbulence dissipation rate, ε . Subsequently, the two additional transport equations for k and ε were solved simultaneously using the RANS equations. The RNG-based k - ε turbulence model, using a mathematical technique called a renormalization group method, was more accurate and reliable, and can be expressed as

$$\frac{\partial}{\partial x_i} (p k u_i) = \frac{\partial}{\partial x_j} \left(\alpha_k \mu_{eff} \frac{\partial k}{\partial x_j} \right) \frac{\partial u_j}{\partial x_i} + G_k - \rho \varepsilon \quad (3.9)$$

$$\frac{\partial}{\partial x_i} (p\varepsilon u_i) = \frac{\partial}{\partial x_j} \left(\alpha_\varepsilon \mu_{eff} \frac{\partial \varepsilon}{\partial x_j} \right) + C_{1\varepsilon} \frac{\varepsilon}{k} (Gk) - C_{2\varepsilon} \rho \frac{\varepsilon^2}{k} - R_\varepsilon \quad (3.10)$$

The right-hand terms represent the diffusion, generation, and destruction, respectively. In these equations, μ_{eff} is the turbulent or eddy viscosity. The model constants $C_{1\varepsilon}$ and $C_{2\varepsilon}$ in Eq. (10) had values derived analytically using RNG theory. These values are $C_{1\varepsilon} = 1.42$, $C_{2\varepsilon} = 1.68$.



CHAPTER FOUR

RESULTS AND DISCUSSION

4.1 Introduction

This chapter discusses the results from mixture formation and combustion of gasoline-air. For mixture formation, turbulent kinetic energy (TKE), velocity magnitude, turbulence dissipation rate, turbulent intensity and turbulent viscosities are compared in single GDI and dual GDI at both early and late injection conditions. In the species transport analysis flame temperature at constant heat capacity and varying heat capacity, mixture specific heat, turbulent burning velocities, mass fractions of $C_{16}H_{29}$, O_2 , N_2 , CO_2 , H_2O and NO_x prediction comparison are made for single GDI and dual GDI engine at early and late injection modes.

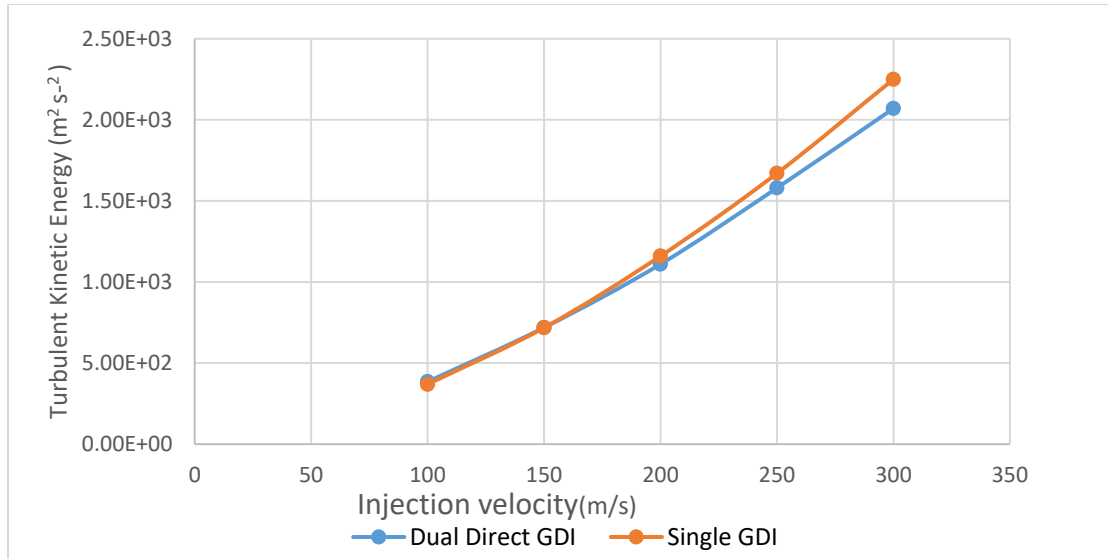
4.2 Comparison of dual GDI and Single GDI engines at late and early injection modes

A comparative simulation is ran between models of single DI and dual DI at both TDC and BDC. The injecting pressure of the injector is 20Mpa with a wide range of velocities, thus, 100m/s, 150m/s, 200m/s, 250m/s and 300m/s to determine the turbulent kinetic energy (TKE), turbulent dissipation rate, turbulent viscosity, turbulent intensity and velocity magnitude.

The analysis is based on results of simulations that was calculated using the flow velocities that the injector sprays at 20Mpa pressure in the computational domain.

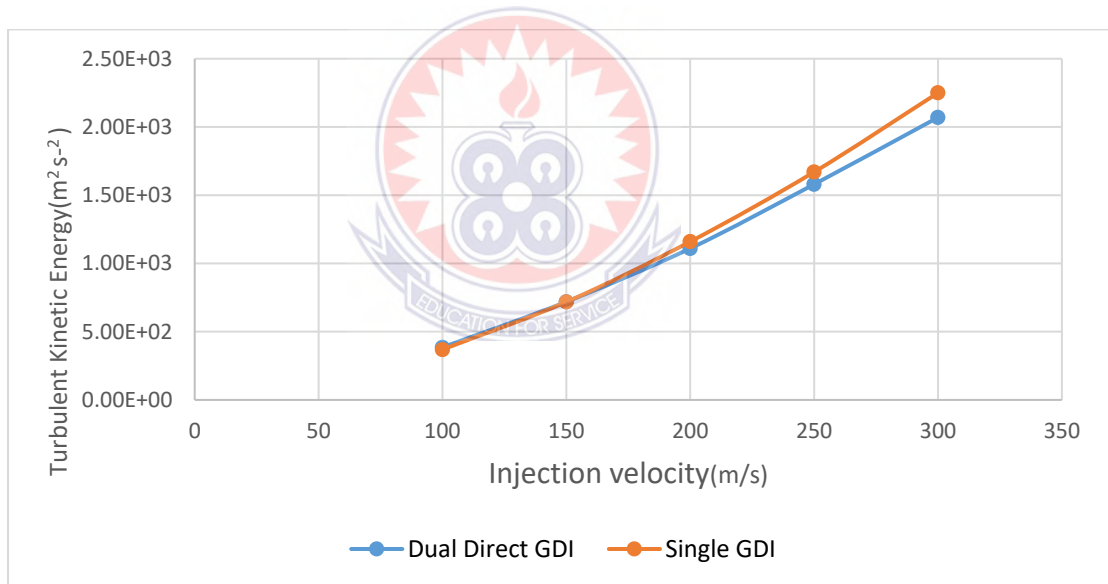
4.2.1 Turbulent Kinetic Energy

The results in Fig.4.1a showed that at late injection mode, the TKE of the eddies were directly proportional to the injection velocity.



(a)

During the early injection mode as shown in Fig.4.1b, the TKE of the eddies increased proportionally as the injection velocity



(b)

Figure 4.1: Turbulent Kinetic Energy against Injection velocity at (a)TDC, (b)BDC

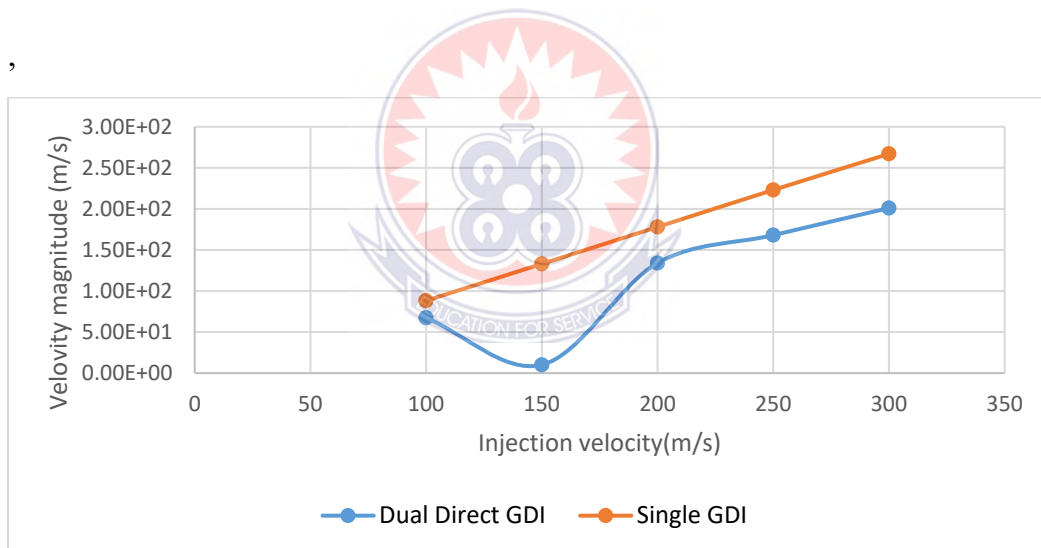
At the lowest velocity of 100m/s in in Fig.4.1a, the TKE of the single GDI engine was higher and that of the dual direct injection was about the same. At 300m/s the KTE of the single DI engine is about 15% higher than that of the dual GDI. During the early injection mode as shown in Fig.4.1b, the TKE of the eddies increased

proportionally as the injection velocity. At the lowest velocity of 100m/s, the TKE of the single GDI engine was slightly higher than that of the dual direct injection. At 150m/s both jet flows had about the same Turbulent kinetic energy. At higher injection velocities 200m/s, 250m/s and 300m/s, the KTE of the single GDI engine was higher than that of the dual GDI.

The results is consistent with that results of Carroll and Blanquart (2014) that the injection velocity produce turbulent kinetic energy.

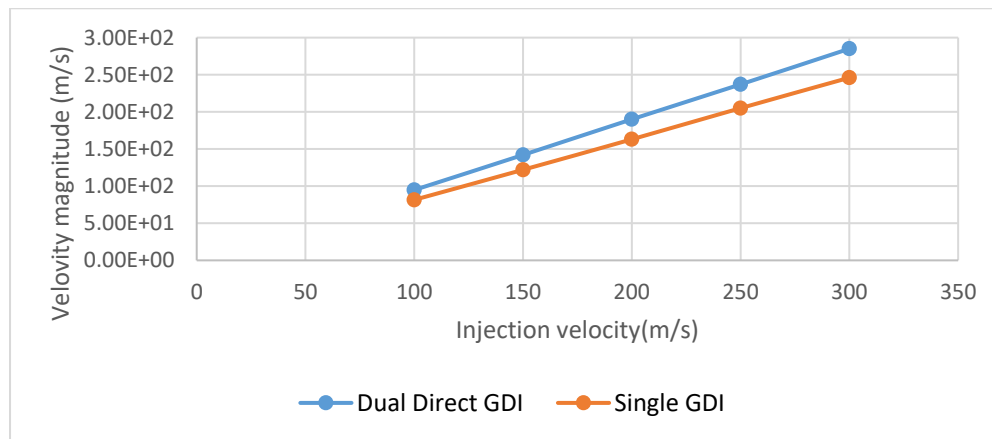
4.2.2 Velocity Magnitude

The results in Fig,4.2a shows the velocity magnitude of the eddies in the direction of the flow when fuel was injected late.



(a)

The results in Fig.4.2b shows the velocity magnitude of the eddies in the direction of the flow in early injection mode.



(b)

Figure 4.2: Velocity Magnitude against Injection Velocity at (a) BDC, (b)TDC

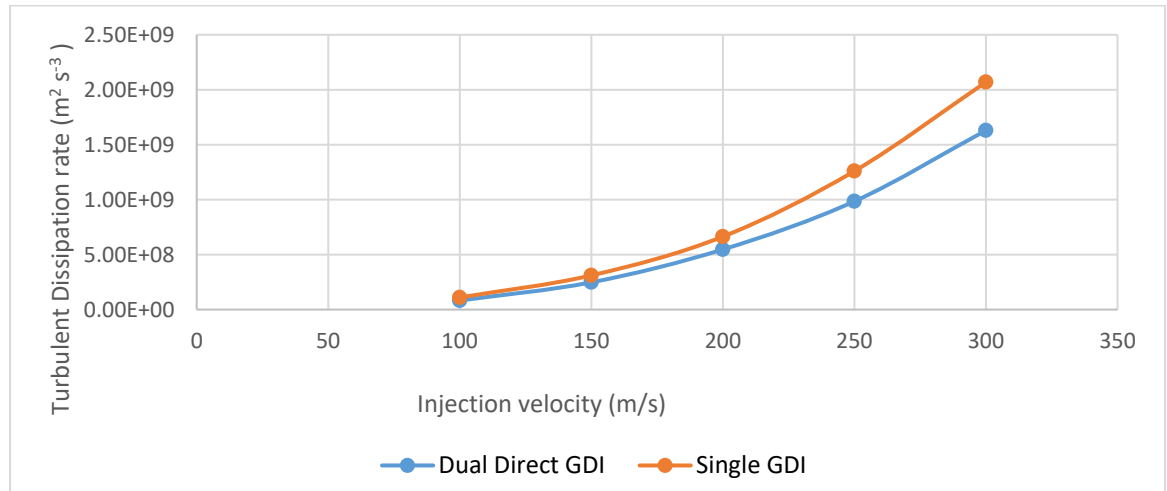
When the fuel was injected late as seen in Fig.4.2a, the velocity magnitude of the eddies in the direction of the flow were steady in the single GDI from 8.82×10^2 m/s at 100 m/s to 2.67×10^2 at 300 m/s while that of the dual GDI declined from 6.73×10^1 m/s at 100 m/s to 1.01×10^1 m/s at 150 m/s. The velocities of the flow then rose sharply to 1.34×10^2 m/s at 200 m/s and steadily to 2.01×10^2 m/s.

On the other hand, in Fig.4.2b, the velocity magnitude of the eddies in the direction of the flow were steady for both single GDI and dual GDI. The velocity magnitude of the mass of eddies of the dual direct injection was higher as compared to the single direct injection. The jet velocity rose steadily from 9.48×10^1 m/s at 100 m/s to 2.85×10^2 m/s at 300 m/s in dual GDI engine against 8.15×10^1 at 100 m/s to 2.46×10^2 m/s in the single GDI engine.

The results agrees with the results of López et al. (2012) that higher injection velocities justifies the increase in effective velocity magnitude.

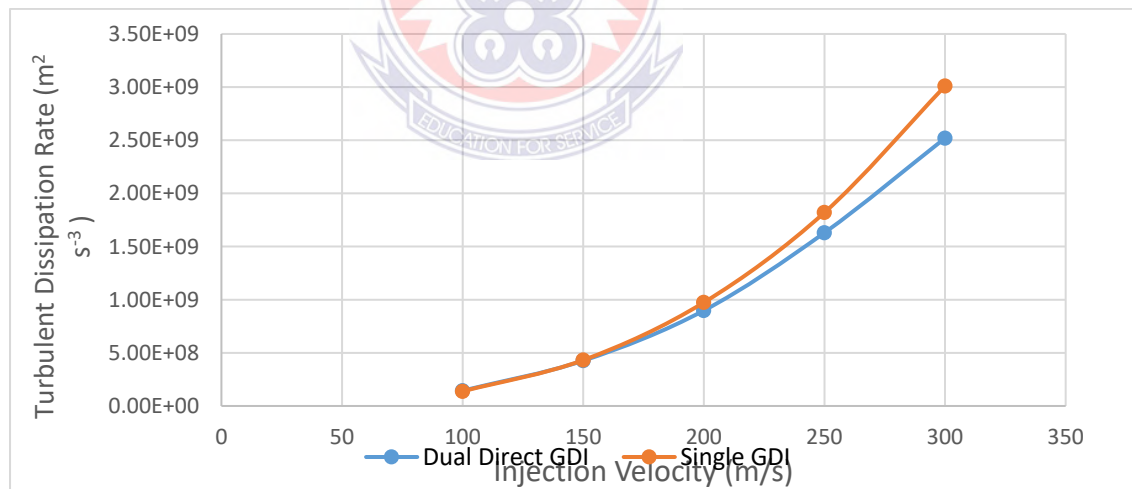
4.2.3 Turbulent Dissipation Rate

Figure 4.3a shows the results of the rate of dissipation of TKE against injection velocity when fuel is injected late into the cylinder.



(a)

Figure 4.3b shows the results of the turbulent dissipation rate against injection velocity in early injection mode.



(b)

Figure 4.3: Turbulent Dissipation Rate against Injection velocity at (a) BDC, (b)TDC

From Fig 4.3a when fuel is injected late into the cylinder, the rate of diffusion of TKE in single GDI engine is quite lower than that of the dual GDI. At the 100m/s, the lowest rate at which turbulent eddies dissipates energy in single GDI was 1.10e+08

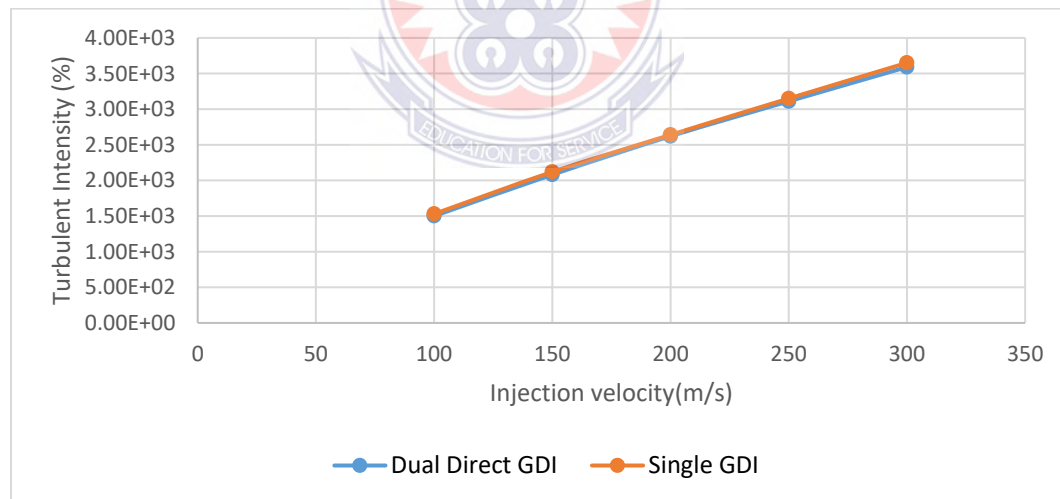
$\text{m}^2 \text{s}^{-3}$ as against $8.23\text{e}+07 \text{ m}^2 \text{s}^{-3}$ in the dual GDI. This is true for all injection velocities, at 300m/s the minimum dissipation rate at which the TKE was still diffused in the single DI was $2.07\text{e}+09 \text{ m}^2 \text{s}^{-3}$ against $1.63\text{e}+09 \text{ m}^2 \text{s}^{-3}$ in the dual GDI.

In the early injection mode as seen in Fig.4.3b, the rate of diffusion of TKE in single GDI engine was almost same as that of the dual direct injection at lower injection velocities 100m/s and 150m/s. At higher injection velocity 300m/s the single GDI dissipates the TKE at higher peak value of $3.01\text{e}+09 \text{ m}^2 \text{s}^{-3}$ against $2.52\text{e}+09 \text{ m}^2 \text{s}^{-3}$ in the dual GDI.

The results is consistent with the results of Liu et al. (2019) that the injection velocity does not have any critical influence on the rate of dissipation.

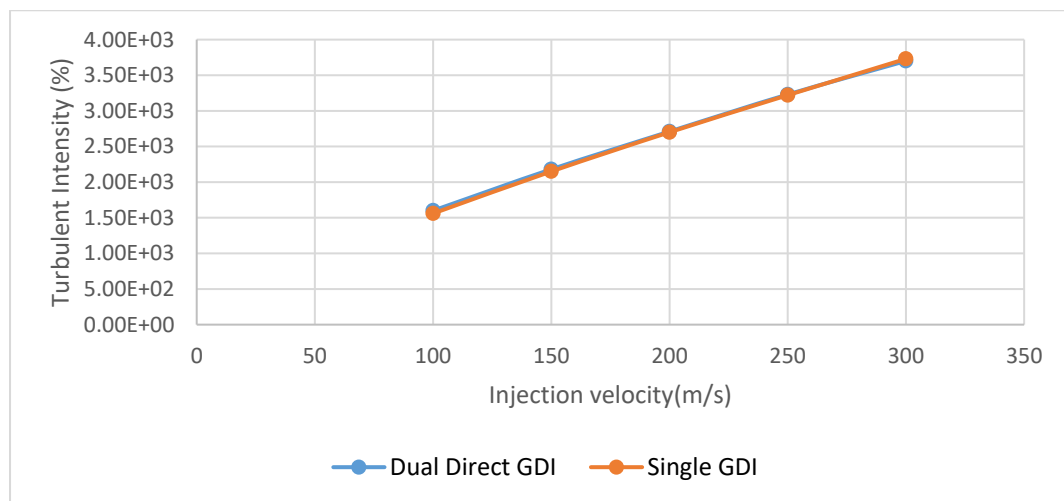
4.2.4 Turbulent Intensity

Figure 4.4a shows the results of the turbulent intensity against injection velocity during late injection mode.



(a)

Figure 4.4b shows the results of the turbulent intensity against injection velocity during early injection mode.



(b)

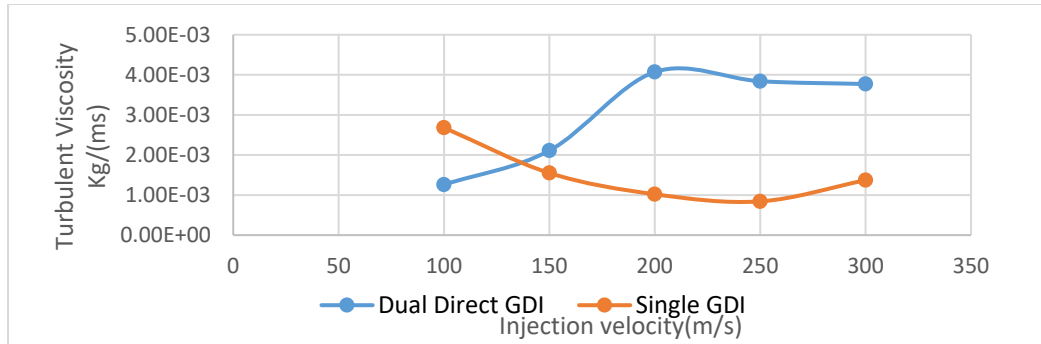
Figure 4.4: Turbulent Intensity against Injection velocity at (a) BDC, (b)TDC

At 100m/s from Fig 4.4a, the turbulent intensity in Single GDI engine was slightly higher during late injection mode than that of the dual GDI. The turbulence intensity was almost same for both single GDI and dual GDI engine at injection velocity of 200m/s and then rose further high on higher injection velocities.

At 100m/s as shown in Fig 4.4b, the turbulent intensity in dual GDI engine operating at early injection mode was slightly higher than that of the single DI. The turbulence intensity was almost same for both single GDI and dual GDI engine at an injection velocity of 200m/s and 250m/s. The turbulent intensity in the single DI rose a little high on higher injection velocities. The results is consistent with the results of Gummesson and Becquin (n.d.) that turbulent intensity is dependent on the fuel injection velocity

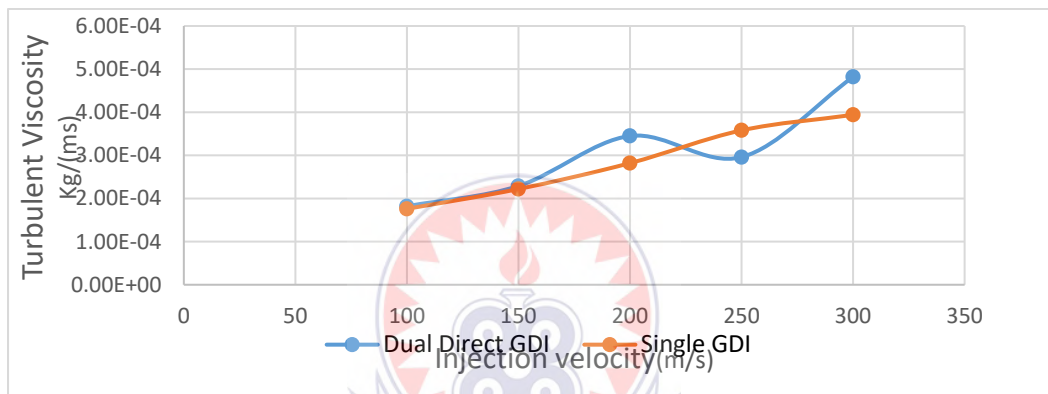
4.2.5 Turbulent Viscosity

Figure 4.5a shows the turbulent viscosity to the flow in the combustion chamber at different injection velocities during late injection mode.



(a)

Figure 4.5b shows the turbulent viscosity to the flow in the combustion chamber at different injection velocities during early injection mode.



(b)

Figure 4.5: Turbulent Viscosity against Injection velocity at (a)TDC, (b)BDC

At an injection velocity of 100m/s as in Fig.4.5a, the internal resistance to the flow in the combustion chamber was 2.68e-03 Kg/(ms) single GDI engine during late injection as compared to a higher 1.26e-03 Kg/(ms) for dual GDI engine. The turbulence viscosity increases with increasing injection velocities in the single GDI engine to about 8.42e-03 Kg/(ms) limiting the rate at which the TKE can cover the combustion domain before decay. The turbulent viscosity in the dual GDI engine decreases right from the high resistance of 1.26e-03 Kg/(ms) at the nozzle to 4.07e-03 Kg/(ms).

At an early injection velocity of 100m/s as seen in Fig.4.5b the internal resistance to the flow of eddies in the combustion chamber was 1.76×10^{-4} Kg/(ms) for single GDI engine as compared to a higher 1.82×10^{-4} Kg/(ms) for dual GDI. The turbulence viscosity decreases with increasing injection velocities in the single GDI engine to about 3.94×10^{-4} Kg/(ms). The turbulent viscosity in the dual GDI engine also decreases right from 1.82×10^{-4} at the nozzle to 4.82×10^{-4} Kg/(ms).

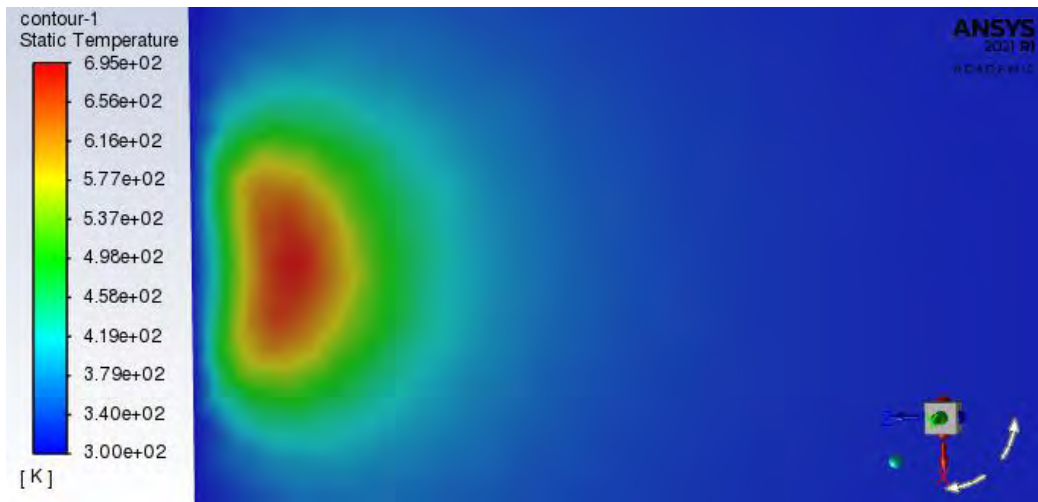
The results is consistent with the findings of López et al. (2012) that higher injection velocities results in lower turbulent viscosities.

4.3 Species transport

The eddy-dissipation model computes the rate of reaction under the assumption that chemical kinetics are fast compared to the rate at which reactants are mixed by turbulent fluctuations (eddies). The combustion is modeled using a one-step reaction mechanism, assuming complete conversion of the fuel to CO₂ and H₂O. The reaction equation is $C_8H_{18} + 12.5 (O_2 + 3.76 N_2) \rightarrow 8 CO_2 + 9H_2O + 47 N_2$. This reaction will be defined in terms of stoichiometric coefficients, formation enthalpies, and parameters that control the reaction rate. The reaction rate is determined assuming that turbulent mixing is the rate-limiting process, with the turbulence-chemistry interaction modeled using the eddy-dissipation model.

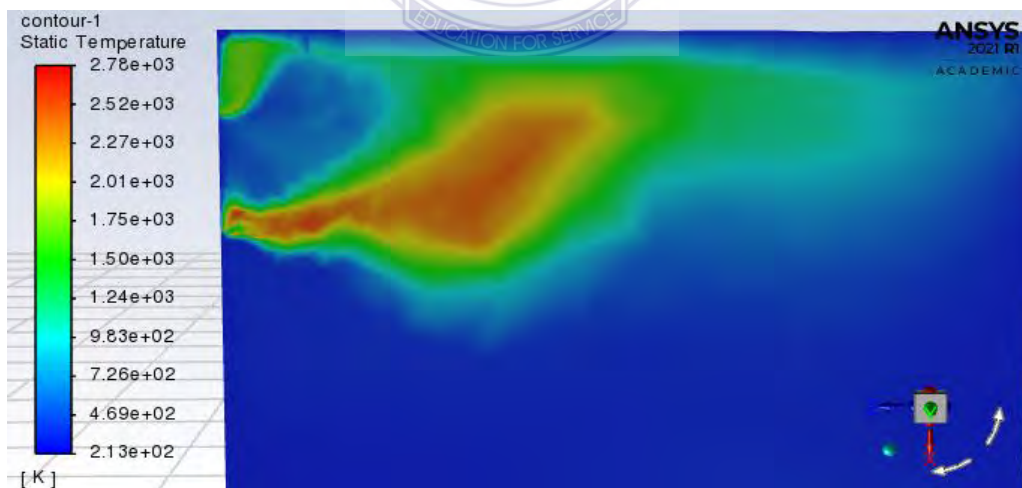
4.3.1 Flame Temperature at Late injection mode

Figure 4.6a shows the Contour plot of temperature distribution at constant heat capacity of $1000 \text{ J/kg} - \text{K}$ in a single GDI engine in late injection mode.



(a)

Figure 4.6b shows the Contour plot of temperature distribution at constant heat capacity of $1000 \text{ J/kg} - \text{K}$ in a dual DI engine in late injection.



(b)

Figure 4.6: Contour plot of temperature distribution at constant heat capacity of $1000 \text{ J/kg} - \text{K}$ of (a) single GDI and (b) dual GDI

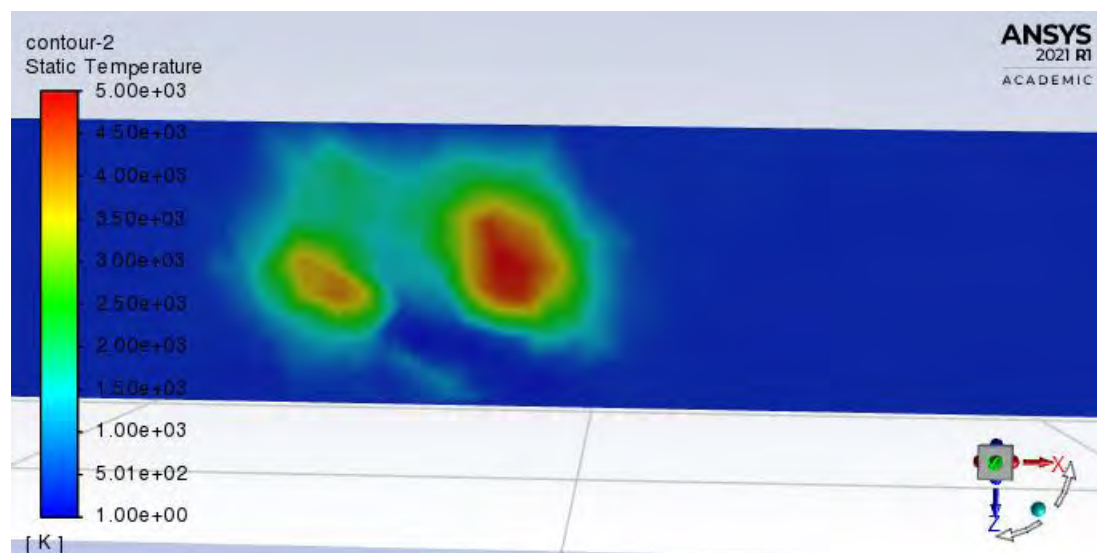
In Fig. 4.6a, the flame temperature is at its peak around the region of the fuel inlet of the single DI engine. The peak flame temperature, predicted using a constant heat capacity of $1000 \text{ J/kg} - \text{K}$, is 695K . The flame temperature reduces to an average temperature of $4.98\text{e}+02\text{K}$ as the eddies fluctuate in the domain. The minimum flame temperature of combustion at the constant heat capacity is $3.00\text{e}+02\text{K}$. The peak flame temperature is below 1816K which makes dissociation insignificant.

In Fig. 4.6b, the peak flame temperature, predicted using a constant heat capacity of $1000 \text{ J/kg} - \text{K}$, is 2780K in the dual DI engine. The average temperature of the combustion flame is $1.50\text{e}+03\text{K}$ and least predicted temperature is $2.13\text{e}+02\text{K}$.

The hotter the flame, the greater the amount of dissociation forming increasing number of unburned products. Dissociation breaks down some of the combustion products down to carbon mono oxide, hydrogen, oxygen and oxides of nitrogen. The peak flame temperature is 2780K in the late injection mode which threatens dissociation of combustion products in harmful exhaust emissions.

4.3.2 Flame temperature at Early injection mode

Figure 4.7a shows the Contour plot of temperature distribution at constant heat capacity of $1000 \text{ J/kg} - \text{K}$ in a single GDI engine in early injection.



(a)

Figure 4.7b shows the Contour plot of temperature distribution at constant heat capacity of $1000 \text{ J/kg} - \text{K}$ in a dual DI engine in early injection.



(b)

Figure 4.7: Contour plot of temperature distribution at constant heat capacity of $1000 \text{ J/kg} - \text{K}$ of (a) single GDI and (b) dual GDI

In Fig.4.7a, the peak flame temperature, predicted using a constant heat capacity of $1000 \text{ J/kg} - \text{K}$, is 5000K in the single DI engine. The average temperature of the combustion flame is $2.50\text{e}+03\text{K}$ and least predicted temperature is $1.00\text{e}+00\text{K}$.

5000K flame temperature possess a greater risk in the amount of dissociation forming increasing number of unburned products and NO_x . The peak flame temperature 5000K in the early injection mode of the single direct injection engine may threaten dissociation of combustion products into harmful exhaust emissions.

In Fig. 4.7b, the flame temperature is at its peak around the region of the fuel inlet of the dual DI engine. The peak flame temperature, predicted using a constant heat capacity of $1000 \text{ J/kg} - \text{K}$, is 700K . The flame temperature reduces to an average temperature of $5.00\text{e}+02\text{K}$ as the eddies fluctuate in the domain. The minimum flame

temperature of combustion at the constant heat capacity is $3.00 \times 10^3 \text{K}$. The peak flame temperature is below 1816K which makes dissociation insignificant.

4.3.3 Comparison of flame temperatures of single direct injection engine at different injection modes

Figure 4.8 shows the results of comparison of Peak flame temperature of single GDI engine at both late and early injection modes.

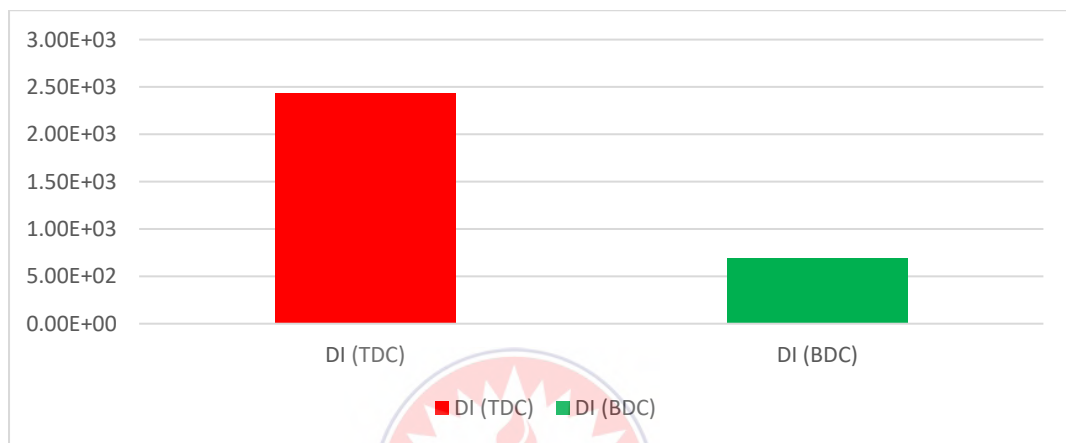


Figure 4.8: Peak flame temperature of single DI engine at TDC and BDC

It could be observed from Fig. 4.8 that the peak flame temperature of the mixture under temperature and composition dependent heat capacity is high when the engine is running on early injection mode. At 2430K flame temperature, dissociation of combustion products; CO, HC, NO_x, O, C may commence to produce harmful exhaust pollutant. The opposite is also true for the late injection mode under the same conditions. It could be observed that under the peak flame temperature for the single direct injection engine operating at late injection mode is 692K . At a flame temperature of 692K , dissociation of combustion product is practically insignificant.

The results follow the work of Chen et al. (2019) who also stated in their research that lower the combustion temperature leads to reduced engine knock. The single DI engine operating at both early and late injection mode has a tendency to mitigate engine knock.

4.3.4 Comparison of flame temperatures of dual direct injection (DI) engine at different injection modes

Figure 4.9 shows the results of comparison of Peak flame temperature of dual DI engine at both late and early injection modes.

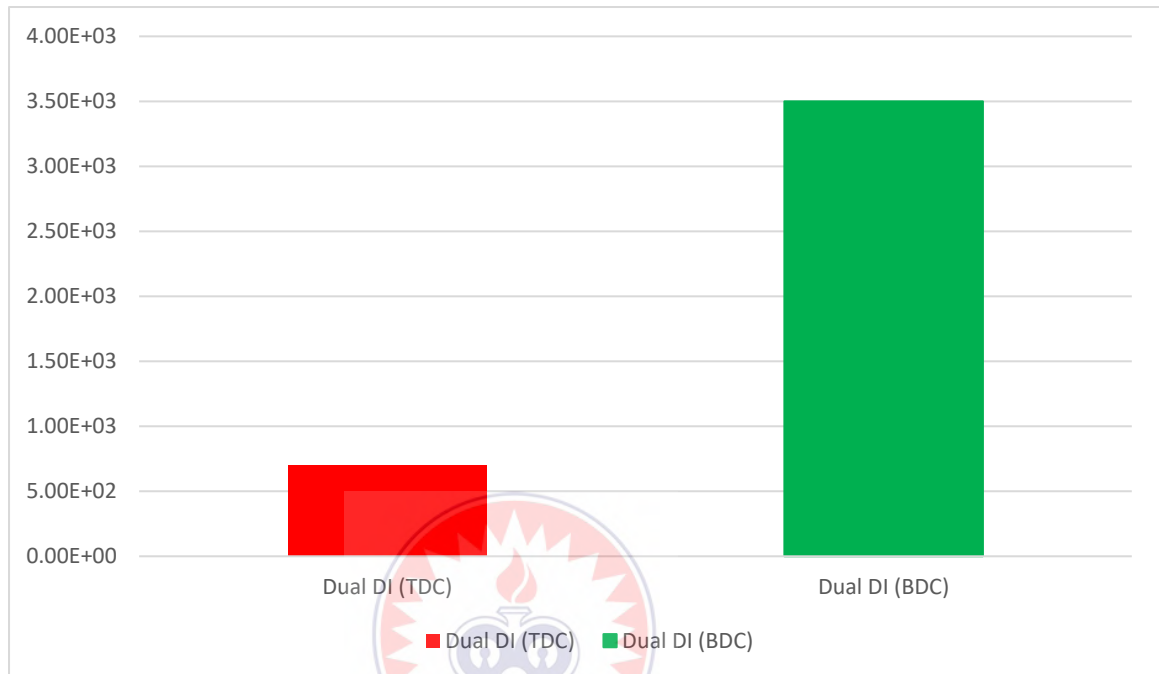


Figure 4.9: Peak flame temperature of Dual DI engine at TDC and BDC

From Fig 4.9, the peak flame temperature of the dual DI at early injection mode operates at 698K. it burns the mixture at a low temperature that makes it almost impossible for dissociation of combustion products to occur. The late injection mode under the same conditions threatens the release of high pollutant number when the flame temperature is as high as 3500K. from the foregoing, dual DI at late injection mode has a tendency of producing higher pollution that single direct injection engine operating at early injection mode which could product some amount of pollutant at 2430K.

Also, the flame temperature 3500K of dual DI engine operating at early injection mode has a tendency to exhibit engine knock in its operation as Chen et al. (2019) also stated in their work.

4.3.5 Temperature and Composition Dependent Heat Capacity at Late injection mode

Figure 4.10 shows the result of the peak flame temperature as a result of temperature and composition-dependent specific heat in single GDI at late injection mode.

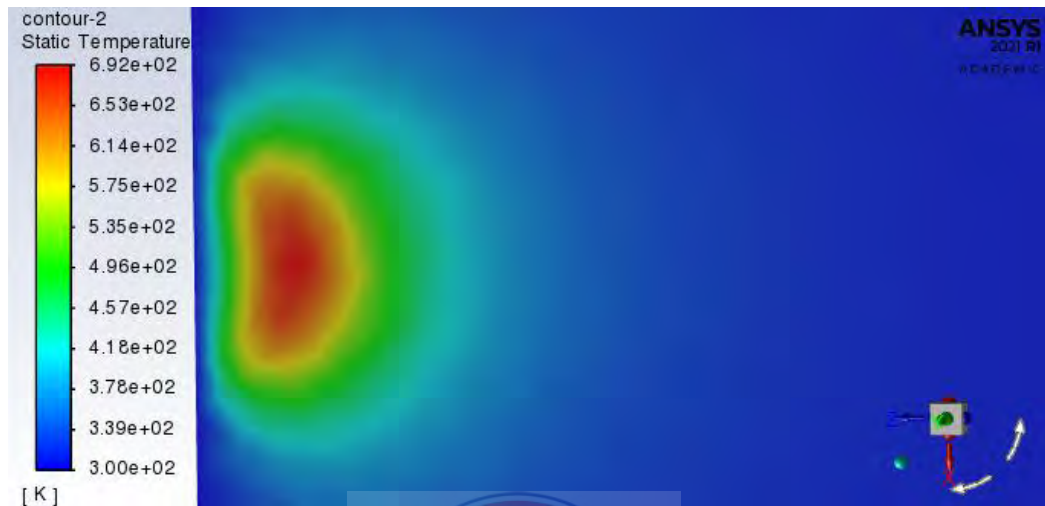


Figure 4.10: Contours diagram of Temperature distribution for Variable Cp of single GDI

Figure 4.10 in comparison to fig 4.6a, the peak flame temperature of 695K has dropped to approximately 692 K as a result of the temperature and composition-dependent specific heat. The temperature is not high enough to cause dissociation of combustion product for harmful exhaust emissions.

Figure 4.11 shows the result of the peak flame temperature as a result of temperature and composition-dependent specific heat in dual DI at late injection mode.

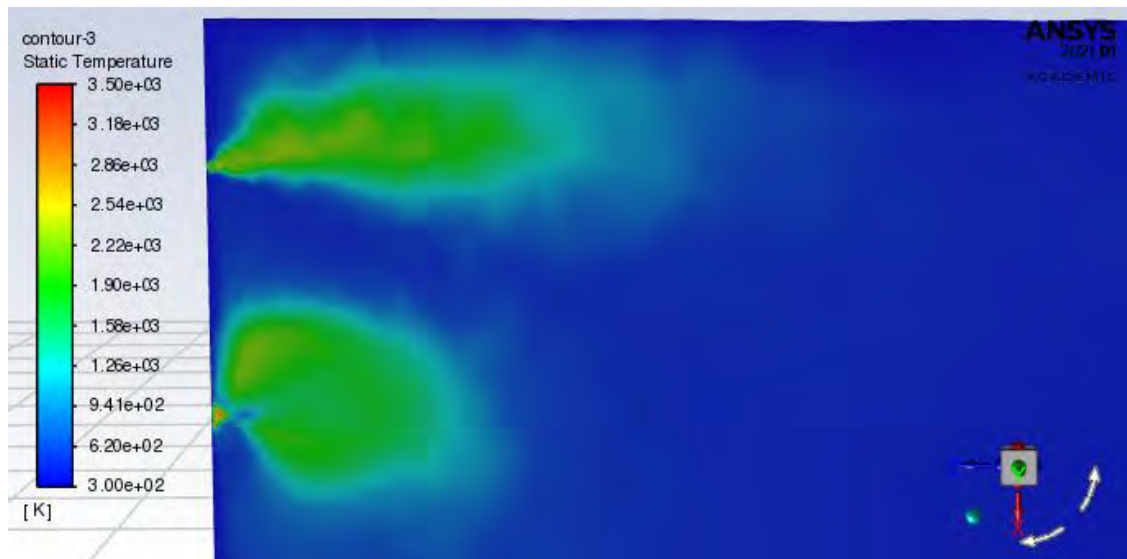


Figure 4.11: Diagram of Temperature distribution for Variable Cp of dual GDI

The peak temperature has risen from 2780K in Fig.6b to approximately 3500 K as a result of the temperature and composition-dependent specific heat in Fig 4.11. The peak flame temperature threatens further dissociation of combustion products into harmful exhaust emissions for environmental pollution.

4.3.6 Temperature and Composition Dependent Heat Capacity at Early injection mode

The result in Fig. 4.12 shows the peak flame temperature as a result of temperature and composition-dependent specific heat in single GDI at early injection mode.

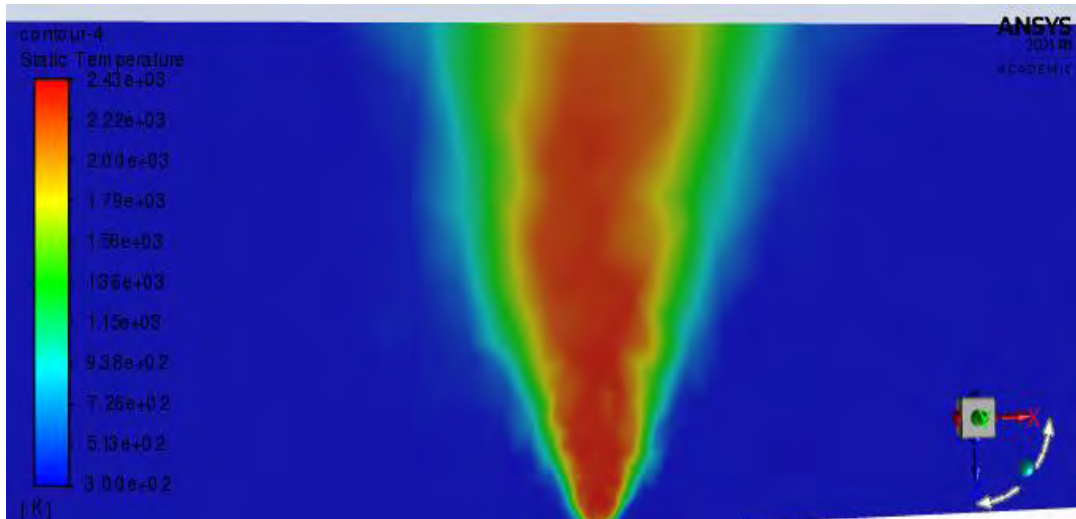


Figure 4.12: Contours plot of Temperature distribution for Variable Cp of single GDI

The peak temperature of the flame has dropped from 5000K in Fig. 4.7a with a constant heat capacity to approximately 2430 K as a result of the temperature and composition-dependent specific heat in Fig.4.12. The tendency of NO_x and other pollutant production in the combustion is considerably reduced.

Figure 4.13 shows the result of the peak flame temperature as a result of temperature and composition-dependent specific heat in dual DI at early injection mode.



Figure 4.13: Contours plot of Temperature distribution for Variable Cp of dual GDI

The peak temperature of the flame has dropped from 700K in fig.4.7b to approximately 698 K in fig. 4.13 as a result of the temperature and composition-

dependent specific heat. The temperature of the burning mixture is not high enough to cause dissociation of combustion product for harmful exhaust emissions.

4.3.7 Mixture specific heat (Cp) at Late injection mode (Piston at BDC)

Figure 4.14 presents the results of specific heat capacity of the mixture during late injection mode in single GDI engine.



Figure 4.14: Contours plot of Temperature distribution for Specific Heat of single GDI

The mixture highest specific heat is recorded as $1.17e+03$ J/(KgK) to raise the temperature of the mixture to its highest. The mixture specific heat is largest where the $C_{16}H_{29}$ is concentrated, near the fuel inlet, and where the temperature and combustion product concentrations are large. The average specific heat of the mixture is $9.43e+02$ J/(KgK) which is around the tip of the nozzle and the minimum specific heat of the mixture being $7.20e+02$ J/(KgK) at the nozzle.

Figure 4.15 presents the results of specific heat capacity of the mixture during late injection mode in dual DI engine.



Figure 4.15: Contours plot of Temperature distribution for Specific Heat of dual GDI

The mixture highest specific heat is $1.43e+03$ J/ (Kg K) to raise the temperature of the mixture to its highest. The mixture specific heat is largest where the $C_{16}H_{29}$ is concentrated which the jet from the injector and where the temperature and combustion product concentrations are large. The average specific heat of the mixture is $7.24e+02$ J/ (Kg K) which is around the tip of the nozzle and the minimum specific heat of the mixture being $1.38e+01$ J/ (Kg K) at the nozzle.

4.3.8 Mixture specific heat (Cp) at Early injection mode (Piston at TDC)

Figure 4.16 presents the results of specific heat capacity of the mixture during early injection mode in single GDI engine.

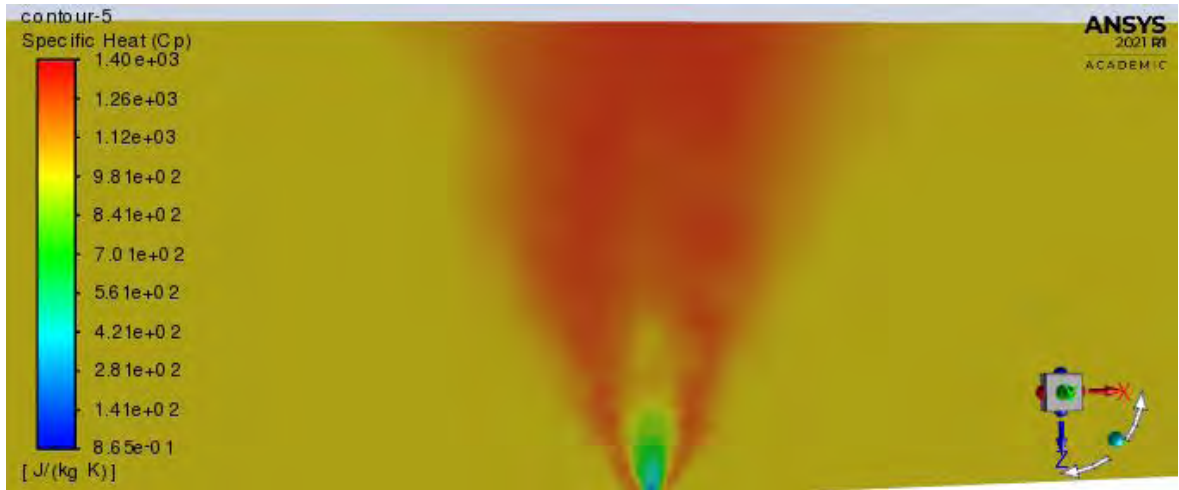


Figure 4.16: Contours of Temperature distribution for Specific Heat of single GDI

The mixture highest specific heat is $1.40e+03 \text{ J/(Kg K)}$ to raise the temperature of the mixture to its highest. The average specific heat of the mixture is $7.01e+02 \text{ J/(Kg K)}$ which is around the tip of the nozzle and the minimum specific heat of the mixture being $8.65e-01 \text{ J/(Kg K)}$ at the nozzle

Figure 4.17 presents the results of specific heat capacity of the mixture during early injection mode in dual DI engine.



Figure 4.17: Contours plot of Temperature distribution for Specific Heat of dual GDI

The highest specific heat of the mixture is 1.17×10^3 J/ (Kg K) to raise the temperature of the mixture to its peak. The average specific heat of the mixture is 8.98×10^2 J/ (Kg K) which is around the tip of the nozzle and the minimum specific heat of the mixture being 6.29×10^2 J/ (Kg K) at the nozzle.

4.3.9 Comparison between mixture specific heat of single DI engines at early and late injection modes

Figure 4.18 shows the results of the comparison between mixture specific heat (C_p) of single GDI Engine operating modes.

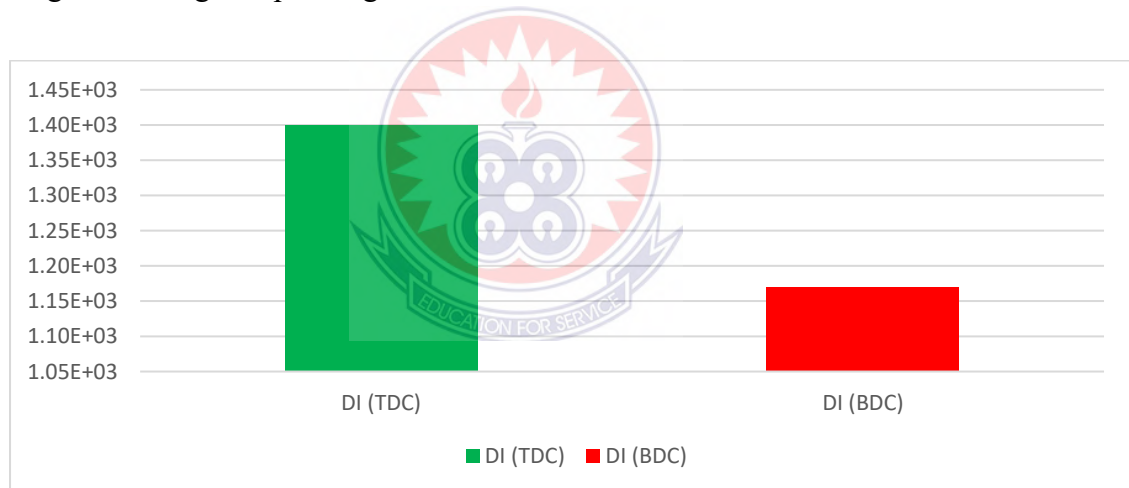


Figure 4.18: Mixture specific heat (C_p) of single GDI Engine operating modes

The peak specific heat capacity of the mixture in the single GDI injected early has a higher specific heat capacity of 1.40×10^3 as compared to the specific heat capacity of 1.17×10^3 of same engine when operated at late injection mode. Increased heat capacity substantially increases the peak flame temperature, and consequently threatens cylinder misfire and the dissociation of combustion products to form harmful exhaust pollutants like CO, HC and NO_x. The heat capacity of the late

injected fuel is rather low in comparison to that of the early injection, lower flame temperature and results in lower NO_x formation which is in disagreement with the results of Pedrozo et al.,(2016) which says high heat capacities rather lowers NO_x formation.

4.3.10 Comparison between mixture specific heat of dual DI engines at early and late injection modes

Figure 4.19 shows the results of the comparison between mixture specific heat (C_p) of dual DI Engine operating modes.

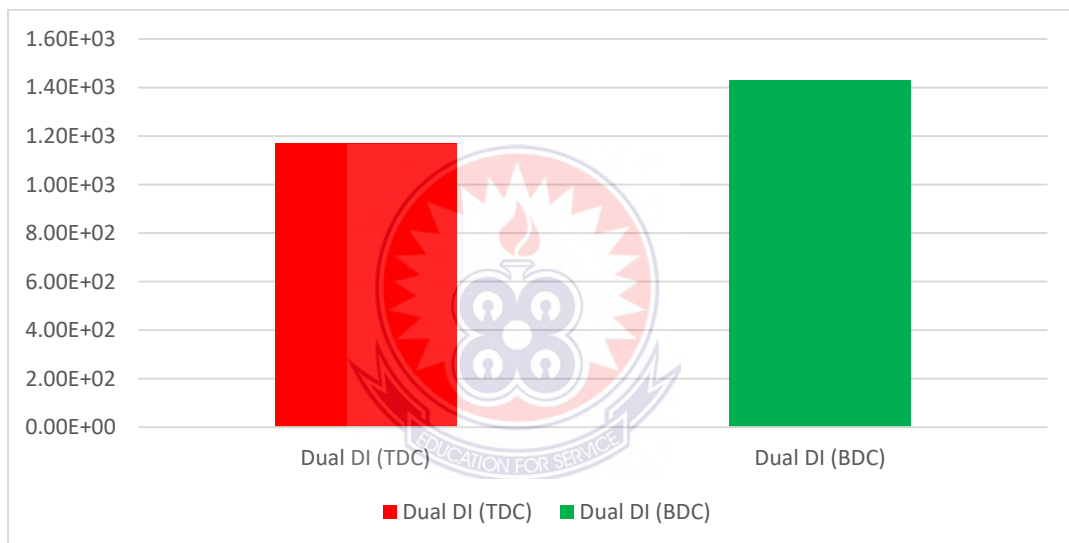


Figure 4.19: Mixture specific heat (C_p) of dual GDI Engine operating modes

The peak specific heat capacity of the mixture in the dual GDI injected late has a higher specific heat capacity of 1.43e+03 as compared to the specific heat capacity of 1.17e+03 of same engine when operated at early injection mode. Increased heat capacity substantially increases the peak flame temperature, and consequently threatens cylinder misfire and the dissociation of combustion products to form harmful exhaust pollutants like CO, HC and NO_x. The heat capacity of the early injected fuel is lower in comparison to that of the late injection, lower flame temperature and results in lower NO_x formation. The results is in variance with the

work of Pedrozo et al.,(2016) that higher heat capacity of the in-cylinder charge curbed nitrogen oxides (NO_x) formation.

4.3.11 Turbulent burning velocity at late injection mode (Piston at BDC)

Figure 4.20 presents the Velocity Vectors contour plot for the turbulent burning velocity of the mixture at late injection mode in a single GDI engine.

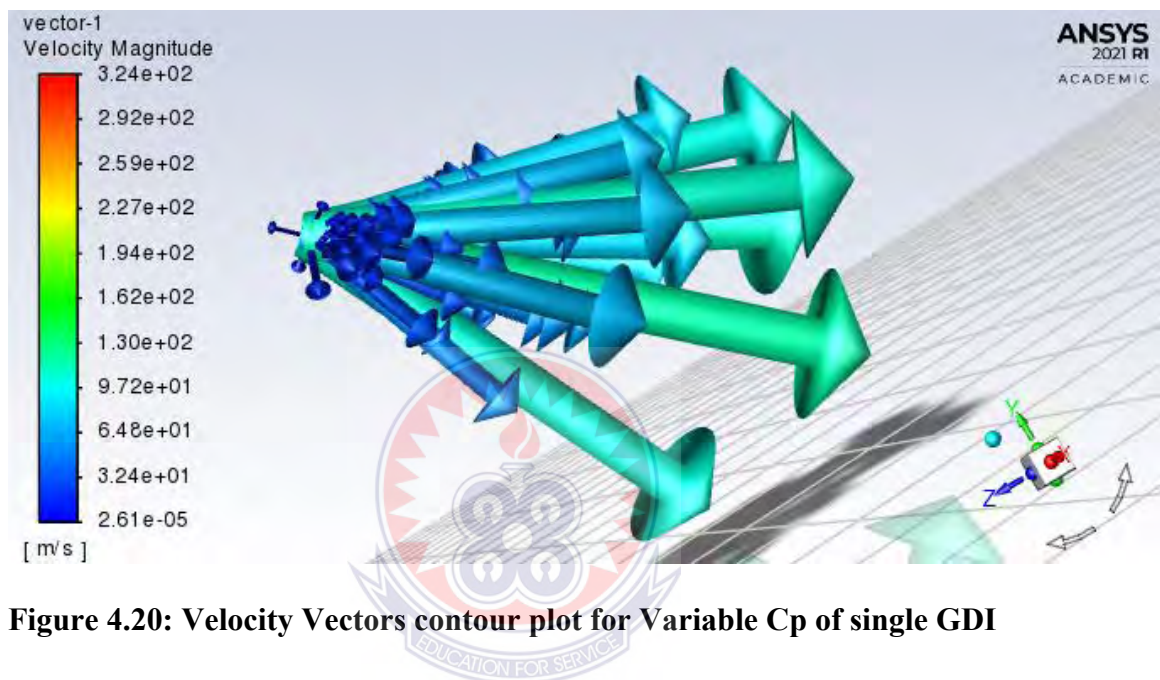


Figure 4.20: Velocity Vectors contour plot for Variable Cp of single GDI

From Fig. 4.20, the maximum burning velocity is recorded as 324 m/s. This means that the flame is propagating to burn the unburnt fuel-air mixture at a maximum velocity of 324m/s. The minimum speed of the flame at which it will still propagate to burn the air-fuel mixture is 2.61e-05m/s.

Figure 4.21 presents the Velocity Vectors contour plot for the turbulent burning velocity of the mixture at late injection mode in a dual DI engine.

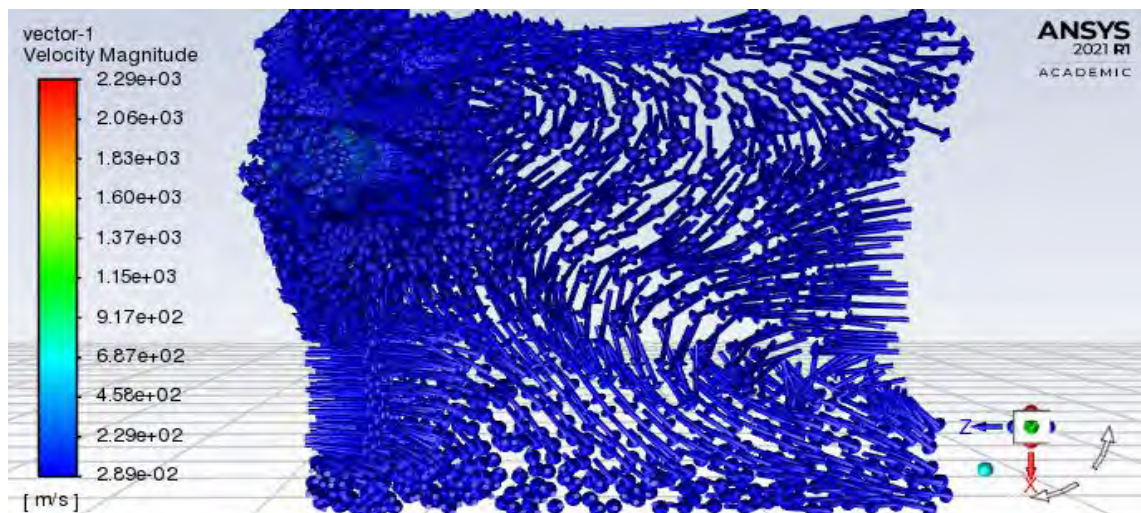


Figure 4.21: Velocity Vectors contour plot for Variable Cp of dual GDI

The maximum burning velocity of the dual injection engine at late injection mode is 2290 m/s. this literary means that the speed of the burning mixture to cover the unburnt mixture is 2290m/s which is seven times as fast as the velocity of the single injection. Combustion of the mixture will continue until the velocity decays to its minimum of 2.89e-02m/s. The result is in agreement with the findings of Huang et al. (2015) who also concluded that Dual injection has faster flame propagation.

From the foregoing, it appears that fuel injected late in Dual DI engine serves to increase local turbulence in the region of the spark which in turn leads to much faster combustion as confirmed by Cracknell et al. (2013) than that of the single direct DI engine. They also reiterated that faster flame speed formulations are known to give superior acceleration, thus, the Dual DI engine operated at late injection mode stands to give superior acceleration than its single DI engine.

4.3.12 Turbulent burning velocity at early injection mode (Piston at TDC)

Figure 4.22 shows the Velocity Vectors contour plot for the turbulent burning velocity of the mixture at early injection mode in a single GDI engine.

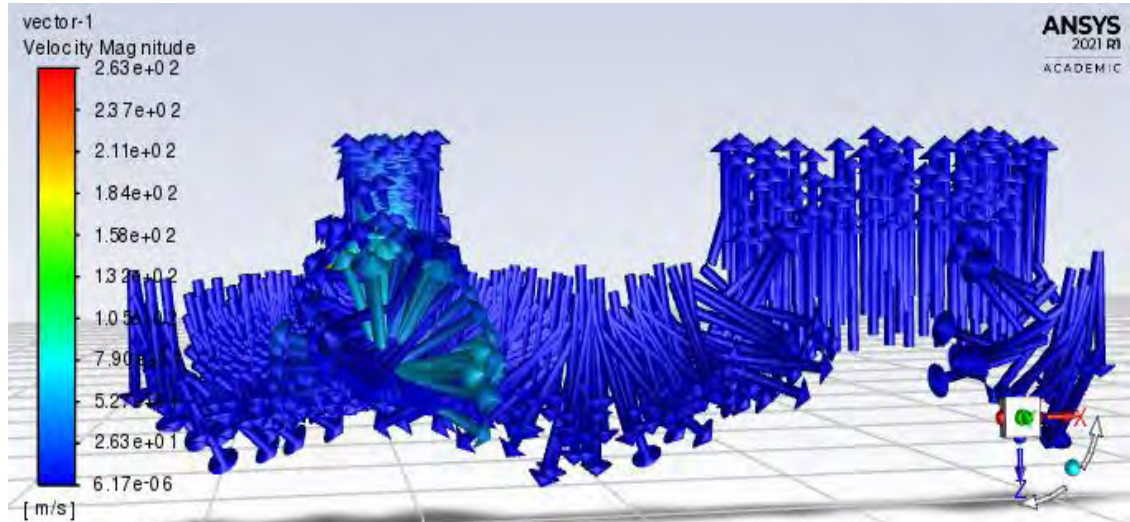


Figure 4.22: Velocity Vectors contour plot for Variable Cp of single GDI)

The maximum burning velocity of the dual injection engine at early injection mode is 263 m/s. Combustion of the mixture will continue until the velocity decays to its minimum of 6.17e-06 e-02m/s.

Figure 4.23 shows the Velocity Vector contour plot for the turbulent burning velocity of the mixture at early injection mode in a dual DI engine.

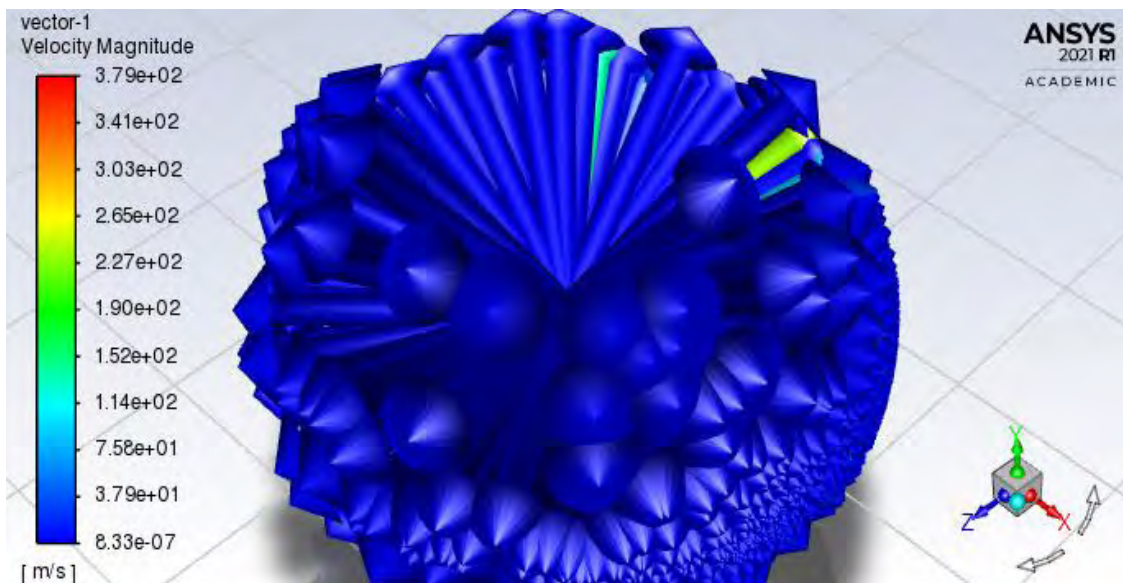


Figure 4.23: Velocity Vectors contour plot for Variable Cp of dual GDI

The maximum burning velocity of the dual injection engine at early injection mode is 3.79×10^2 m/s. This literary means that the speed of the burning mixture to cover the unburnt mixture about 30% faster than the velocity of the single injection under the same condition as Huang et al. (2015) also stated. Combustion of the mixture continues until the velocity decays to its minimum of 8.33×10^{-7} m/s. The results is in agreement with the findings of Cracknell et al. (2013) that fuel with a higher burning velocity results in faster combustion in an engine. This goes to tell that dual direct injection engine operating at early injection mode burns its mixture about 30% faster and has superior acceleration than single direct injection engine operating under the same condition.

4.3.13 Comparison of Turbulent burning velocities of single DI engine at early and late injection modes

Figure 4.24 shows the results of the comparison between turbulent burning velocities of single GDI Engine operating modes

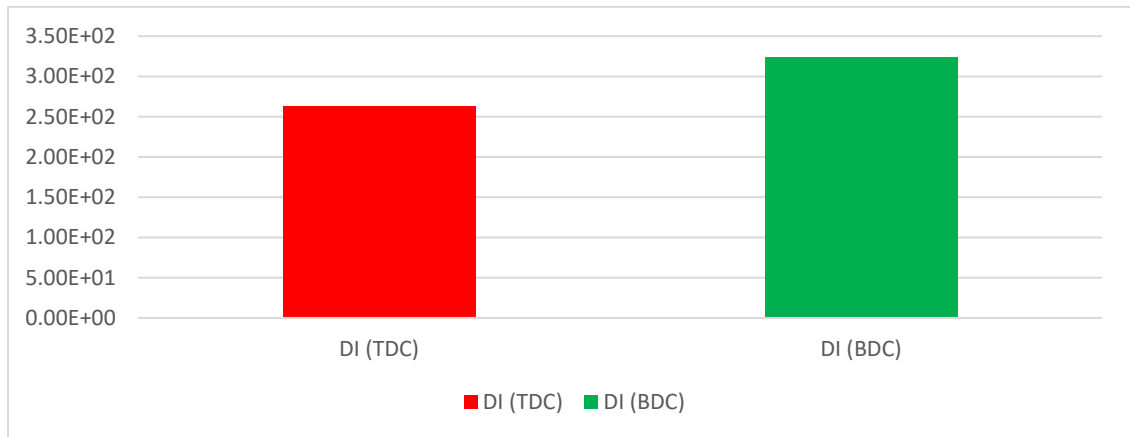


Figure 4.24: Turbulent burning velocities of single GDI Engine operating modes

The peak burning velocity of the engine operated at late injection mode is 324m/s while that of the same engine operated at early injection mode is 263m/s. The results follows the work of Cracknell et al. (2013) that engines fuel injected late in the engine increases local turbulence around the spark which in turn results in much faster combustion.

4.3.14 Comparison of Turbulent burning velocities of Dual DI engine at early and late injection modes

Figure 4.25 shows the results of the comparison between turbulent burning velocities of dual GDI Engine operating modes

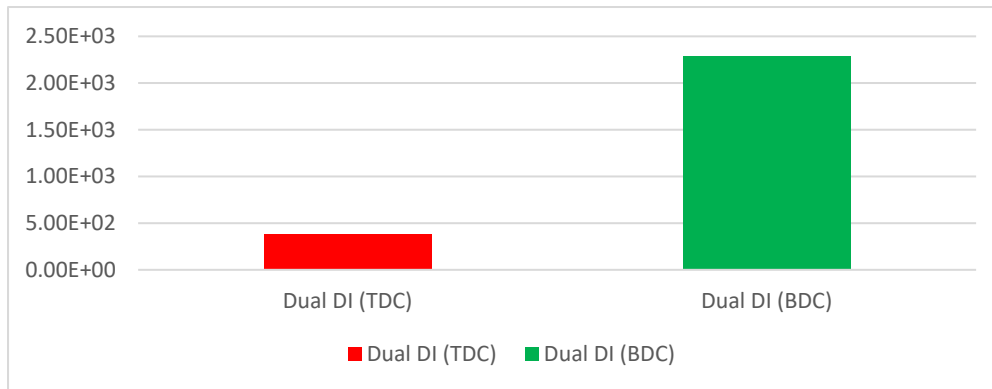


Figure 4.25: Turbulent burning velocities of dual GDI Engine operating modes

The peak burning velocity of the dual GDI engine operated at late injection mode is 2290 m/s while that of the same engine operated at early injection mode is 379 m/s. The late injected fuel burns at a higher velocity resulting in faster combustion and superior acceleration than the fuel injected early. The results follows the work of Cracknell et al. (2013) that engines fuel injected late in the engine increases local turbulence around the spark which in turn results in much faster combustion.

4.3.14 Mass fraction of Octane at Late injection mode (Piston at BDC)

Figure 4.25 presents the mass fraction of Octane at late injection mode in a single GDI engine.



Figure 4.25: Contours plot of Octane Mass Fraction of single GDI

At the beginning of combustion, the fraction of the mass of petrol otherwise called gasoline in the whole mixture is recorded as $5.40e-01$. Continuous burning reduces the mass fraction to an average of $2.70e-01$ until complete combustion occurs at $0.00e+00$ where there is no mass of petrol.

Figure 4.26 presents the mass fraction of Octane at late injection mode in a dual DI engine.



Figure 4.26: Contours plot of Octane Mass Fraction of dual GDI

At the beginning of combustion, the mass fraction of the petrol (octane) otherwise called gasoline of the mixture is recorded as $9.90\text{e-}01$. Continuous burning reduces the mass fraction to an average of $4.95\text{e-}01$ until complete combustion occurs at $0.00\text{e+}00$ where there is no mass of petrol.

In sum, the late injection dual DI engine injects more octane into the cylinder for combustion than the single DI engine that injects the fuel late.

4.3.15 Mass fraction of Octane at Early injection mode (Piston at TDC)

Figure 4.27 presents the mass fraction of Octane at early injection mode in a single GDI engine.



Figure 4.27: Contours plot of Octane Mass Fraction of single GDI

Octane mass fraction is high at the start of combustion at $9.96\text{e-}01$ when injected early. The mass of octane in the combustion reduces as combustion progresses to an average mass fraction of $4.98\text{e-}01$ until the quantity of octane in the mixture is exhausted to $0.00\text{e+}00$ at the end of the combustion. The results follow that of Solaka et al. (2012) that the octane is high at start of injection and decreases due to the activities of the O_2 fraction.

Figure 4.28 presents the mass fraction of Octane at early injection mode in a dual DI engine.

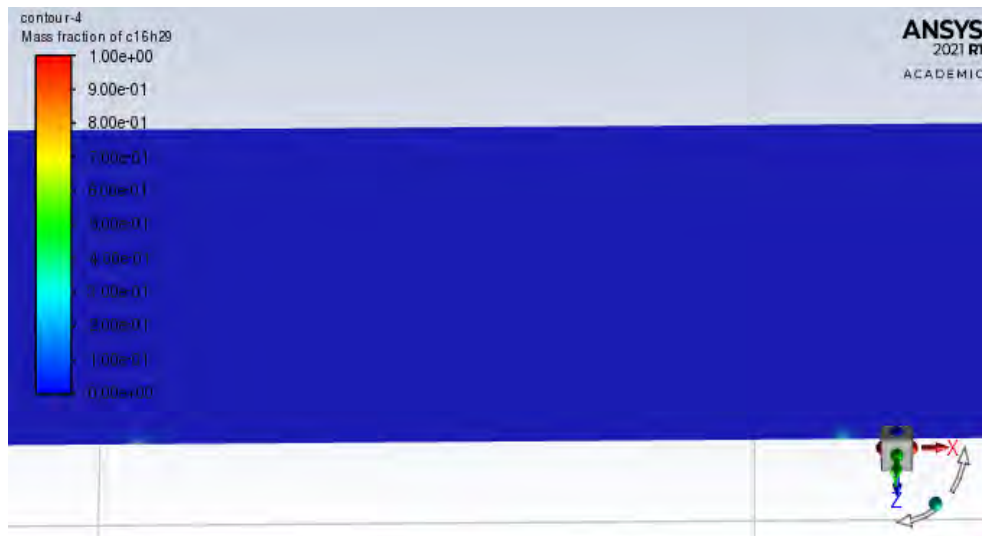


Figure 4.28: Contours plot of Octane Mass Fraction of dual GDI

Octane mass fraction is high at the start of combustion at $1.00e+00$ when injected early. The mass of octane in the combustion reduces as combustion progresses to an average mass fraction of $5.00e-01$ until the quantity of octane in the mixture is completely burnt to $0.00e+00$ at the end of the combustion. The results is in line with the results of Solaka et al. (2012).

4.3.16 Comparison of mass fractions of octane(C16H29) in single DI engine at early and late injection modes

Figure 4.29 shows the peak mass fraction of Octane in single GDI at both early and late injections.

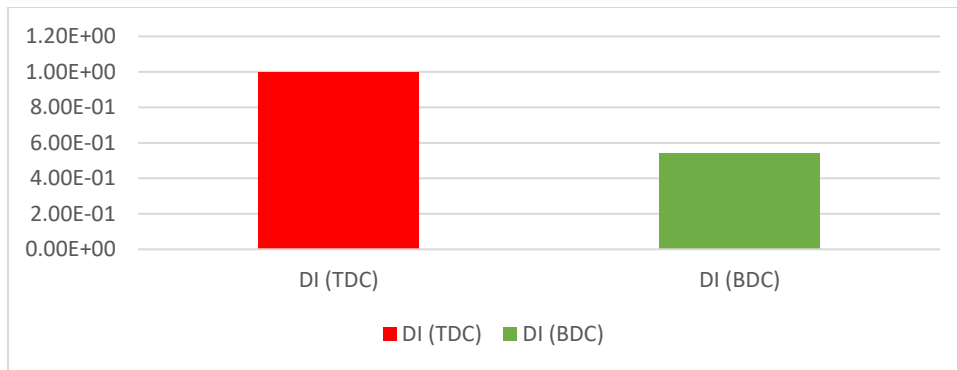


Figure 4.29: Mass fraction of Octane of single GDI Engine operating modes

At early injection mode, the peak mass fraction of octane that mixes with the air is 9.96×10^{-1} as against 5.40×10^{-1} as around the spark plug at the start of combustion. Lean mixture is created in the engine when fuel is injected late more than the early injection mode. The results follow that of Anenberg et al. (2019) that lean mixture creation in the combustion chamber causes misfires and unburnt hydrocarbon emissions.

4.3.17 Comparison of mass fractions of octane (C₁₆H₂₉) in Dual DI engine at early and late injection modes

Figure 4.30 shows the peak mass fraction of Octane in dual DI at both early and late injections.

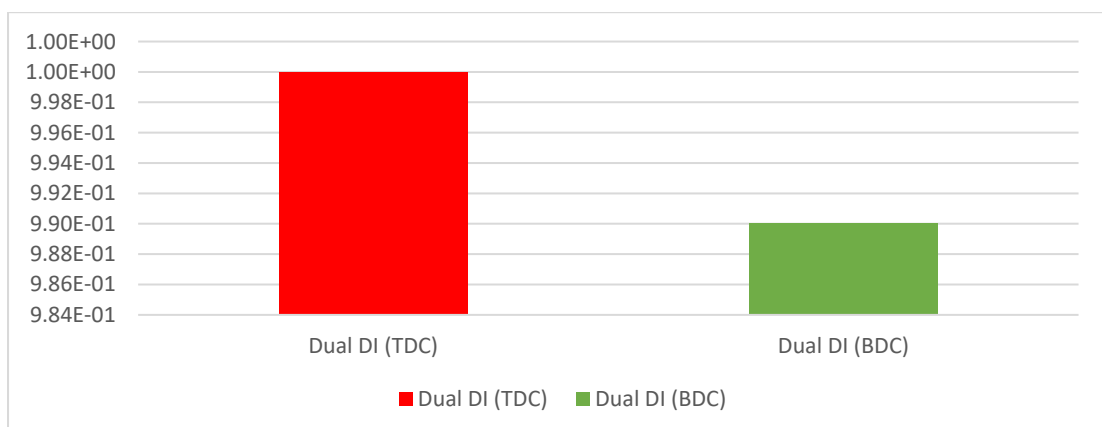


Figure 4.30: Mass fraction of Octane of dual GDI Engine operating modes

At early injection mode, the peak mass fraction of octane that mixes with the air is $1.00e+00$ as against $9.90e-01$ as around the spark plug at the start of combustion.

Lean mixture is created in the engine when fuel is injected late more than the early injection mode. The results agree with Cho and He, (2007) that lean mixture creation in the combustion chamber might cause unburnt hydrocarbon emissions.

4.3.18 Mass fraction of Oxygen (O_2) at Late injection mode (Piston at BDC)

The results in Fig. 4.31 shows the mass fraction of oxygen gas in the single GDI engine at late injection mode



Figure 4.31: Contours plot of Oxygen Mass Fraction of single GDI

The mass fraction of oxygen in the cylinder before the commencement of combustion was at its highest of $2.30e-01$. The quantity of oxygen is used up during combustion leaving burnt mixture to have a minimum mass of oxygen molecules. From fig. 4.31, the minimum mass fraction recorded after combustion is $2.83e-05$ and the average mass fraction of oxygen gas that could be present in the course of combustion is $1.15e-01$.

The results in Fig. 4.32 shows the mass fraction of oxygen gas in the dual Di engine at late injection mode

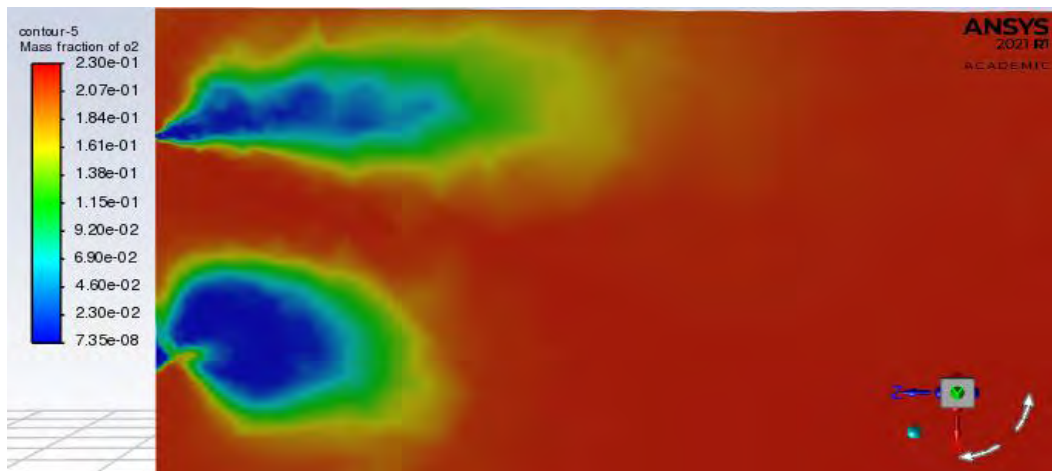


Figure 4.32: Contours plot of Oxygen Mass Fraction of dual GDI

The mass fraction of oxygen in the dual injection cylinder before the commencement of combustion was at its highest of 2.30×10^{-1} . The quantity of oxygen is used up during combustion leaving burnt mixture to have a minimum mass of oxygen molecules. From fig 4.32, the minimum mass fraction after combustion is 7.35×10^{-8} and the average mass fraction of oxygen gas that could be present combustion progresses is 1.15×10^{-1} .

4.3.19 Mass fraction of Oxygen (O₂) at Early injection mode (Piston at TDC)

The results in Fig. 4.33 shows the mass fraction of oxygen gas in the single GDI engine at early injection mode

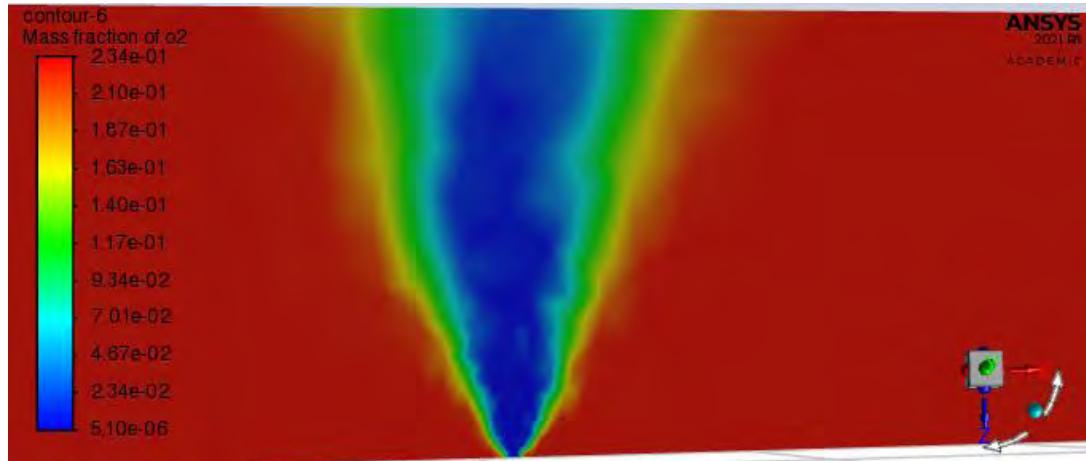


Figure 4.33: Contours plot of Oxygen Mass Fraction of single GDI

From Fig.4.33, the mass fraction of oxygen in the dual injection cylinder before the commencement of combustion was at its highest of 2.34e-01. The quantity of oxygen is used up during combustion leaving burnt mixture to have a minimum mass of oxygen molecules. The minimum mass fraction after combustion is 5.10e-06 and the average mass fraction of oxygen gas that could be present combustion progresses is 1.17e-01.

The results in Fig. 4.34 shows the mass fraction of oxygen gas in the dual Di engine at early injection mode

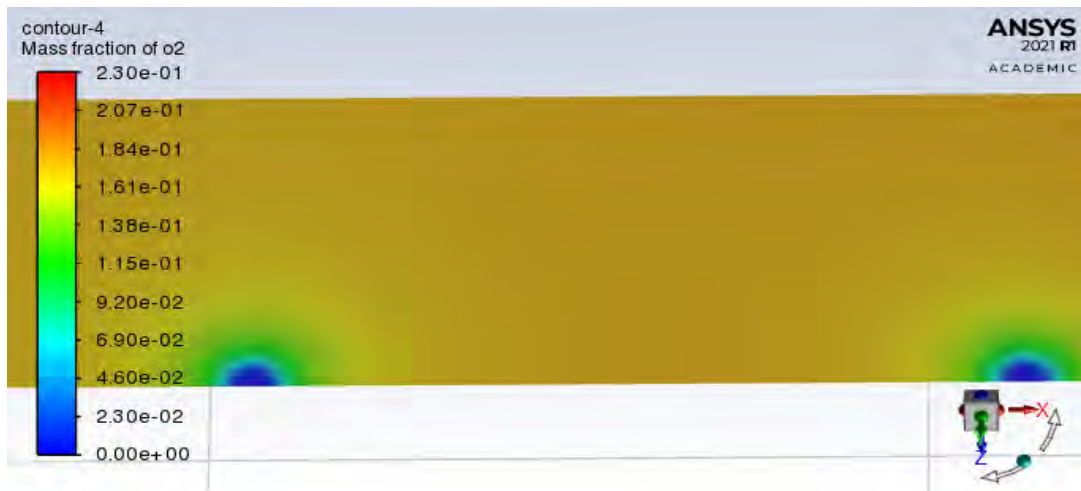


Figure 4.34: Contours plot of Oxygen Mass Fraction of dual GDI

Figure 4.34 shows the mass fraction of oxygen in the dual injection cylinder before the commencement of combustion was at its highest of 2.30e-01. The quantity of oxygen is used up during combustion leaving burnt mixture to have a minimum mass of oxygen molecules. The minimum mass fraction after combustion is 0.00e+00 and the average mass fraction of oxygen gas that could be present combustion progresses is 1.15e-01.

4.3.20 Comparison of mass fractions of oxygen (O₂) in single DI engine at early and late injection modes

Figure 4.35 shows the peak mass fractions of Oxygen gas in single GDI at both early and late injections.

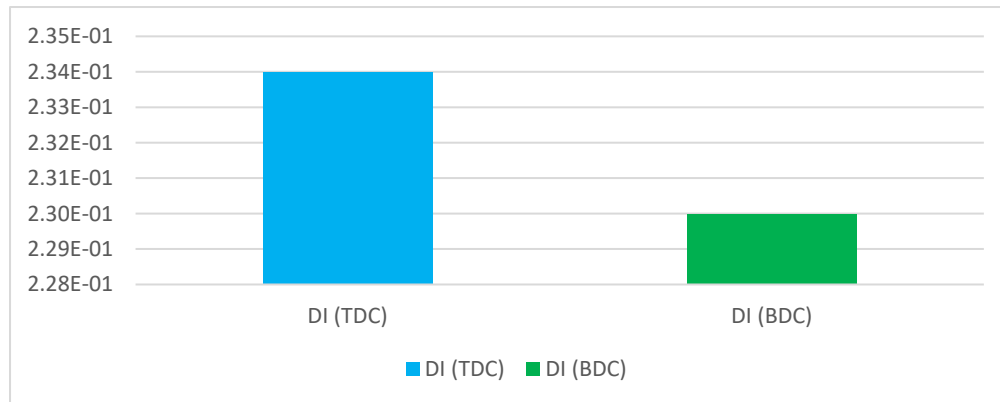


Figure 4.35: Mass fraction of Oxygen of single GDI Engine operating modes

At the commencement of the combustion in the early injection mode, the mass fraction of oxygen in the combustion chamber is 2.34e-01 as against 2.30e-01 when fuel is injected late. This indicates that a little more oxygen is used in combustion when the engine operates at early injection mode leaving a lower oxygen concentration in the cylinder than in the late injection modes of the single GDI engine.

The results is in agreement with the results of Pedrozo et al. (2016) whose results also showed lower oxygen concentration in the cylinder. The results also confirm the work of Bari (1996) that the amount of oxygen found by dissociation of CO₂ increased the oxygen concentration.

4.3.21 Comparison of mass fractions of oxygen (O₂) in Dual DI engine at early and late injection modes

Figure 4.36 shows the peak mass fraction of Oxygen gas in dual DI at both early and late injections.

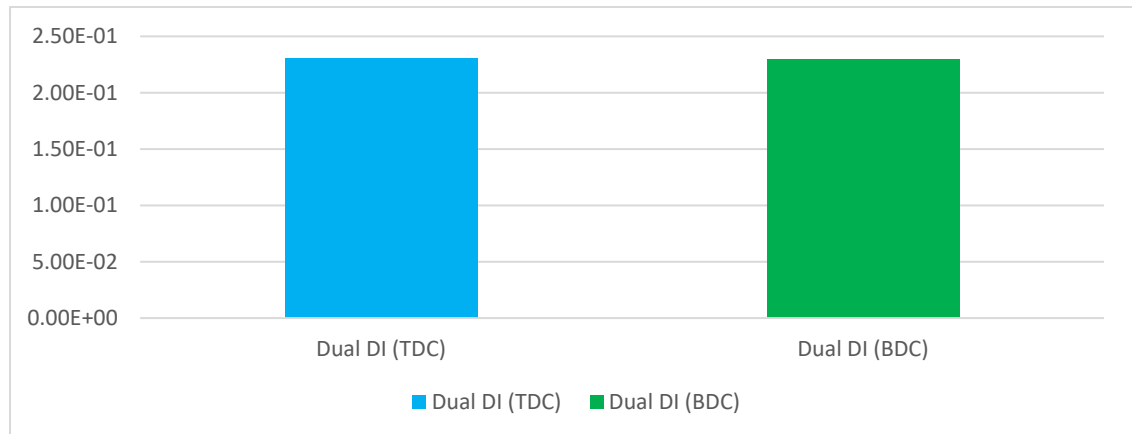


Figure 4.36: Mass fraction of Oxygen of dual GDI Engine operating modes

At the commencement of the combustion in both early and late injection mode, the mass fraction of oxygen in the combustion chambers are 2.30e-01. This indicates that in the dual direction injection engine, oxygen requirement of the engine is virtually same at both early and late injection modes. The results agrees with the results of Pedrozo et al. (2016) whose results also recorded lower oxygen concentration in the cylinder.

4.3.22 Mass fraction of Nitrogen (N₂) at Late injection mode (Piston at BDC)

The results in Fig. 4.37 shows the mass fraction of Nitrogen gas in the single GDI engine at late injection mode



Figure 4.37: Contours plot of Nitrogen Mass Fraction of Single GDI

The mass fraction of Nitrogen gas in the cylinder before the start of combustion was at its highest of 7.70e-01. The quantity of Nitrogen reacts during combustion leaving burnt mixture to have a minimum mass of Nitrogen molecules. From fig 4.65, the minimum mass fraction recorded during combustion is 3.21e-01 and the average mass fraction of oxygen gas that could be present in the course of combustion is 5.46e-01.

The results in Fig. 4.38 shows the mass fraction of Nitrogen gas in the dual Di engine at late injection mode



Figure 4.38: Contours plot of Nitrogen Mass Fraction of dual GDI

At the start of combustion, the mass fraction of Nitrogen is at its peak of 8.12e-01. The burning mixture has the minimum mass fraction of Nitrogen of 7.21e-03 since it reacts with oxygen and octane. As the flame propagates into the unburnt mixture, the Nitrogen molecules further reacts in the burning process to an average of 4.1e-01.

4.3.23 Mass fraction of Nitrogen (N₂) at Early injection mode (Piston at TDC)

Figure 4.39 shows the mass fraction of Nitrogen gas in the single GDI engine at early injection mode.

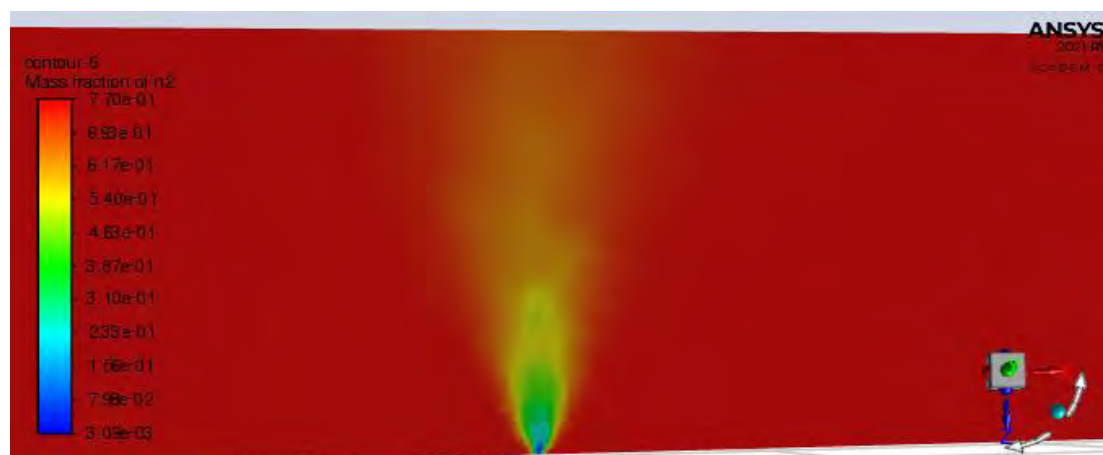


Figure 4.39: Contours plot of Nitrogen Mass Fraction of Single GDI

At the start of combustion, the mass fraction of Nitrogen is at its peak of $7.70e-01$. The burning mixture has the minimum mass fraction of Nitrogen of $3.09e-03$ since it reacts with oxygen and octane. As the flame propagates into the unburnt mixture, the Nitrogen molecules further reacts in the burning process to an average of $3.87e-01$.

Figure 4.40 shows the mass fraction of Nitrogen gas in the dual Di engine at early injection mode

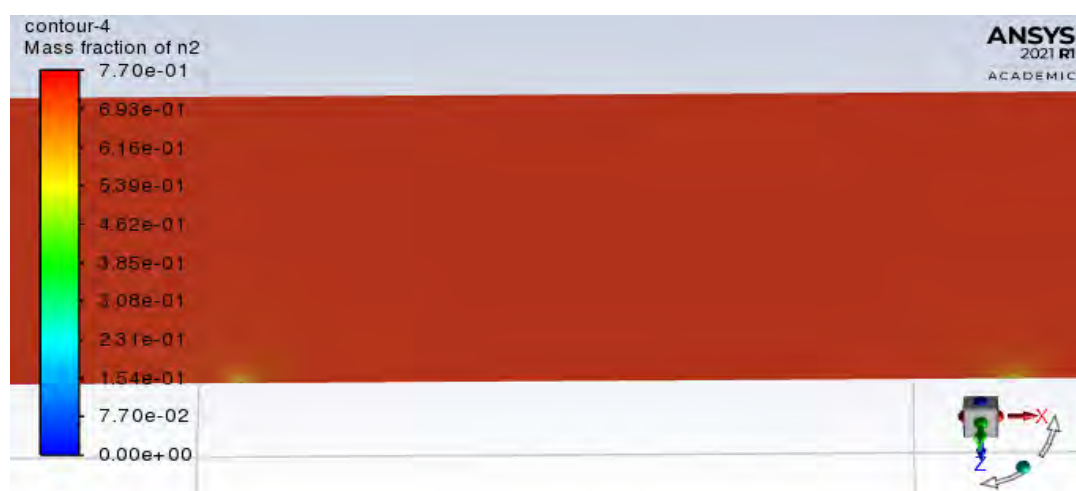


Figure 4.40: Contours plot of Nitrogen Mass Fraction of dual GDI

At the start of combustion, the mass fraction of Nitrogen is at its peak of 7.70×10^{-1} . As the flame propagates into the unburnt mixture, the Nitrogen molecules further reacts in the burning process to an average of 3.85×10^{-1} . The burning continues until there is no more nitrogen in the combustion chamber.

4.3.24 Comparison of mass fractions of Nitrogen N_2 in Single DI engine at early and late injection modes

Figure 4.41 shows the peak mass fraction of Nitrogen gas in single GDI at both early and late injections.

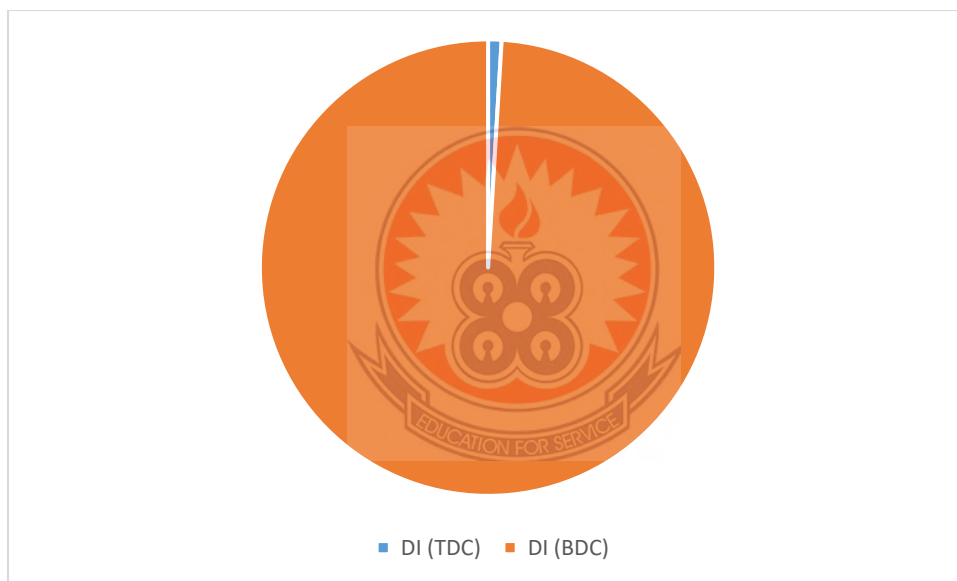


Figure 4.41: Mass fraction of Nitrogen of single GDI Engine operating modes

At the end of the combustion in the early injection mode, the mass fraction of nitrogen in the combustion chamber is 3.09×10^{-3} as against 3.21×10^{-1} in the case of late injection. This indicates that a little more nitrogen is used in combustion when the engine operates at early injection mode to the disadvantage of NO_x formation than in the late injection modes of the single GDI engine.

4.3.25 Comparison of mass fractions of Nitrogen (N₂) in Dual DI engine at early and late injection modes

Figure 4.42 shows the peak mass fraction of Nitrogen gas in dual DI at both early and late injection modes.

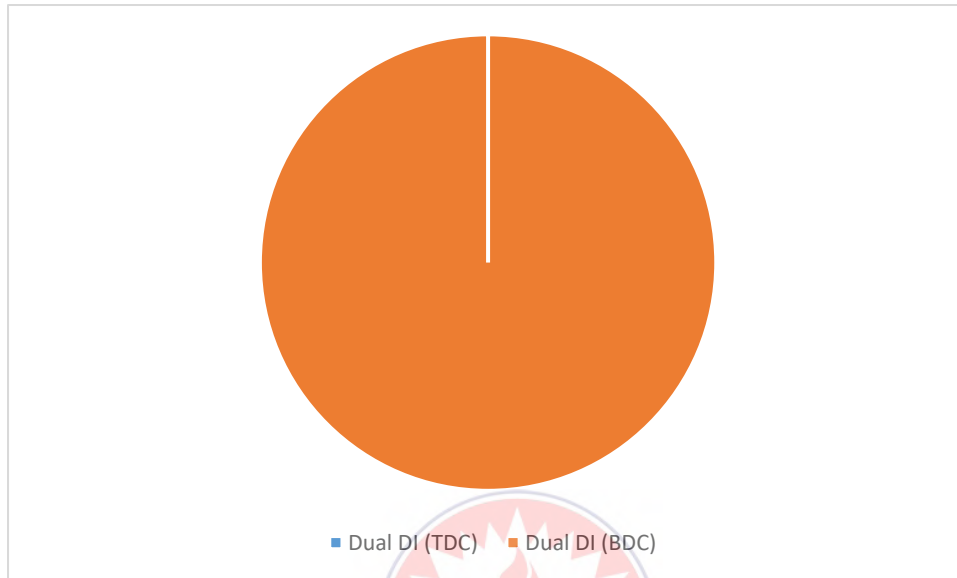


Figure 4.42: Mass fraction of Nitrogen of dual GDI Engine operating modes

At the end of the combustion in the early injection mode, the mass fraction of nitrogen in the combustion chamber is $0.00e+00$ as against $7.21e-03$ in the case of late injection. This indicates that all the nitrogen is used in combustion when the engine operates at early injection mode to the disadvantage of NO_x formation than in the late injection modes of the dual GDI engine.

4.3.26 Mass fraction of Carbon dioxide (CO₂) at Late injection mode (Piston at BDC)

The results in Fig. 4.43 shows the mass fraction of CO₂ in the single GDI engine at late injection mode.



Figure 4.43: Contours plot of Carbon dioxide Mass Fraction of single GDI

The highest concentration of carbon dioxide is 2.05e-01 during combustion. It is high around areas with high concentration of the exhaust gas. The average mass fraction of CO₂ is 1.02e-01 around the burning mixture and 0.00e+00 where the mixture is unburnt.

The results in Fig. 4.44 shows the mass fraction of CO₂ in the dual Di engine at late injection mode

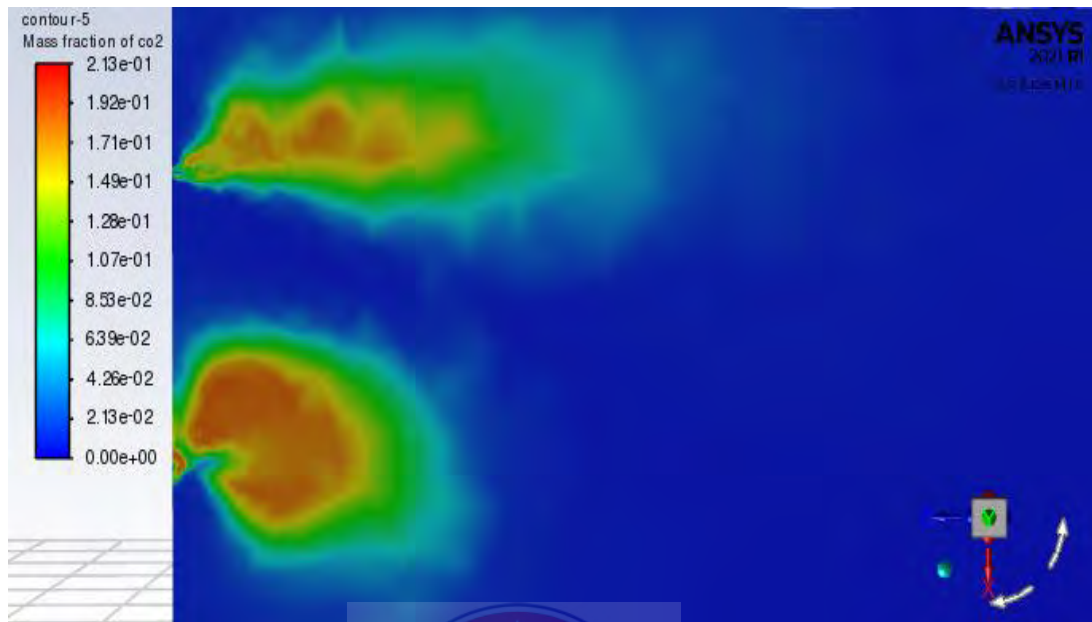


Figure 4.44: Contours plot of Carbon dioxide Mass Fraction of dual GDI

The highest concentration of carbon dioxide is 2.13×10^{-1} in the burnt mixture. It is high around areas with high concentration of the exhaust gas. The average mass fraction of CO₂ is 1.02×10^{-1} around the burning mixture and 0.00×10^0 where the mixture is unburnt.

4.3.27 Mass fraction of Carbon dioxide (CO₂) at Early injection mode (Piston at TDC)

The results in Fig. 4.45 shows the mass fraction of CO₂ in the single GDI engine at early injection mode

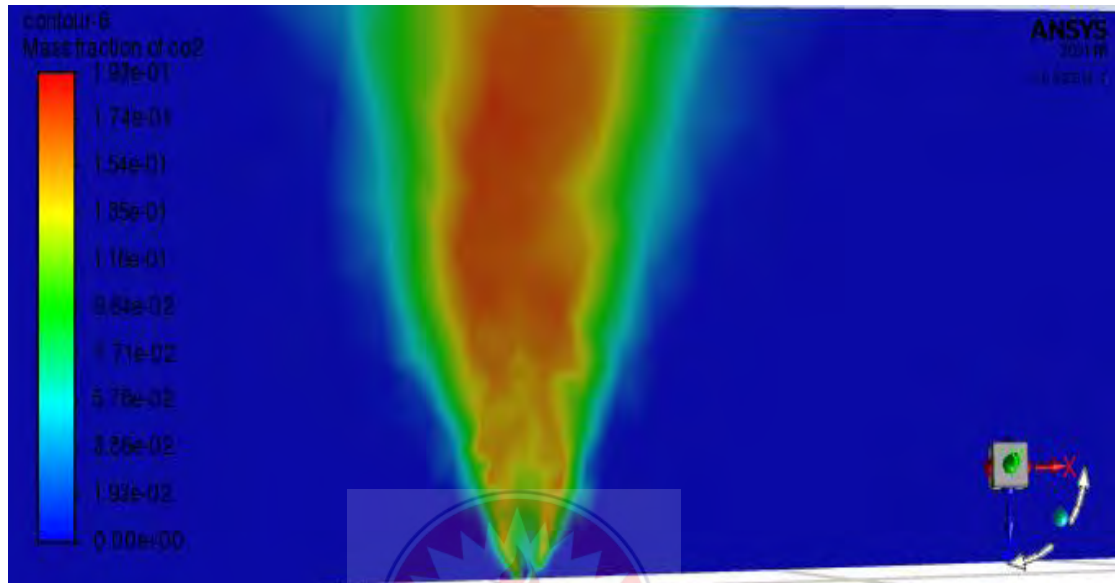


Figure 4.45: Contours plot of Carbon dioxide Mass Fraction of single GDI

From Fig. 4.45, The highest concentration of carbon dioxide is 1.93e-01 in the burnt mixture. The average mass fraction of CO₂ is 9.64e-02 around the burning mixture and 0.00e+00 where the mixture is unburnt.

The results in Fig. 4.46 shows the mass fraction of CO₂ in the dual Di engine at early injection mode

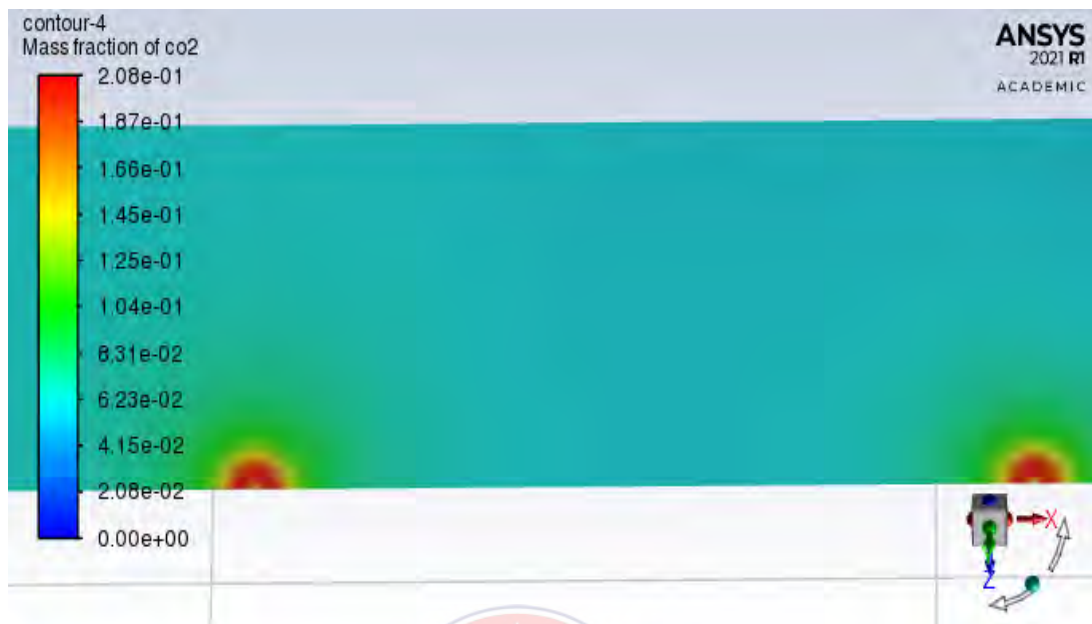


Figure 4.46: Contours plot of Carbon dioxide Mass Fraction of dual GDI

The highest concentration of carbon dioxide is 2.08e-01 in the burnt mixture. The average mass fraction of CO₂ is 1.04e-01 around the burning mixture and 0.00e+00 where the mixture is unburnt.

4.3.28 Comparison of mass fractions of Carbon dioxide (CO₂) in single DI engine at early and late injection modes

Figure 4.47 shows the peak mass fraction of Carbon dioxide in single GDI at both early and late injection modes.

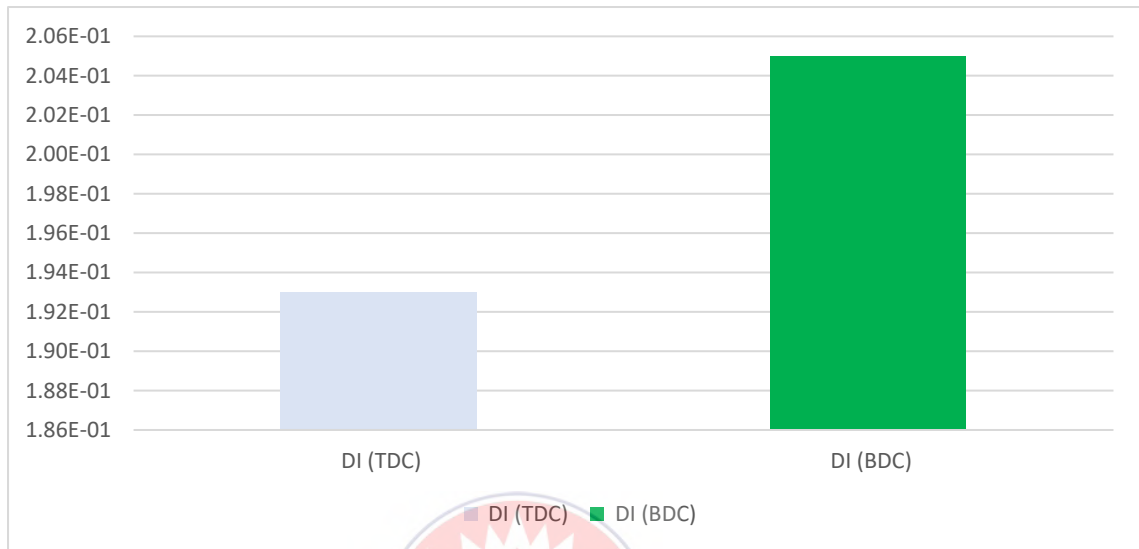


Figure 4.47: Mass fraction of Carbon dioxide of single GDI Engine operating modes

At the end of the combustion in the early injection mode, the mass fraction of CO₂ in the combustion chamber is 1.93e-01 as against 2.05e-01 in the case of late injection. This shows that the carbon dioxide produced from the combustion when the engine operates at early injection mode is lower than in the late injection modes of the single GDI engine.

4.3.29 Comparison of mass fractions of Carbon dioxide (CO₂) in Dual DI engine at early and late injection modes

Figure 4.48 shows the peak mass fraction of Carbon dioxide in dual DI at both early and late injection modes.

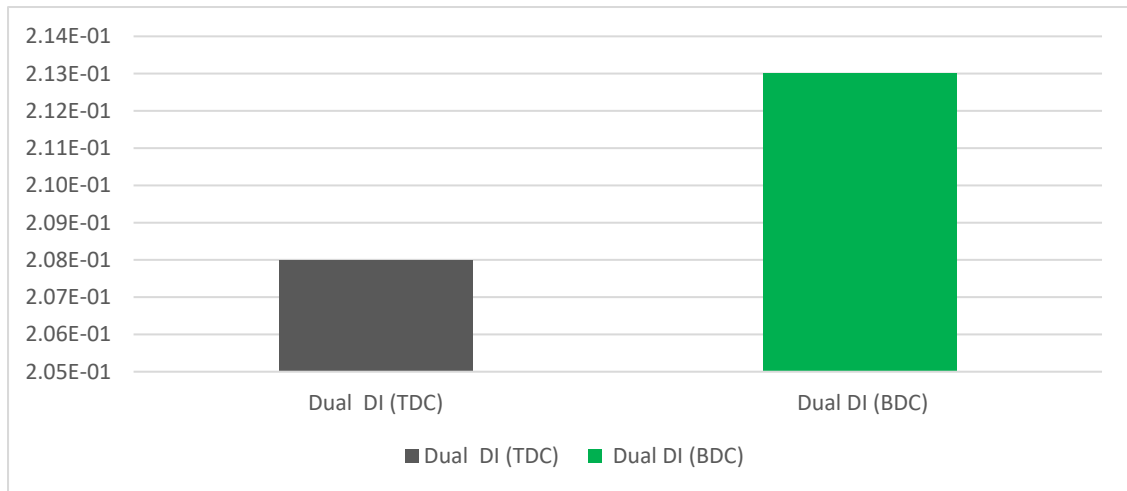


Figure 4.48: Mass fraction of Carbon dioxide of single GDI Engine operating modes

At the end of the combustion in the early injection mode, the mass fraction of CO₂ in the combustion chamber is 2.08e-01 as against 2.13e-01 in the case of late injection. This shows that the quantity of carbon dioxide produced from the combustion process when the engine operates at early injection mode is lower than in the late injection modes of the dual GDI engine.

4.3.30 Mass fraction of Water Vapour (H₂O) at Late injection mode (Piston at BDC)

The contour plot in Fig. 4.49 shows the mass fraction of H₂O in the single GDI engine at late injection mode.



Figure 4.49: Contours plot of Water Mass Fraction of single GDI

The mass fraction of water vapour in the combustion chamber is at its peak of 8.22e-02 around regions that has completed combustion is H₂O is a product of combustion. The burning mixture has less water vapour of 4.11e-02 averagely as combustion is ongoing. Mass fraction of H₂O vapour in the unburnt mixture is 0.00e+00.

The contour plot in Fig. 4.50 shows the mass fraction of H₂O in the dual Di engine at late injection mode

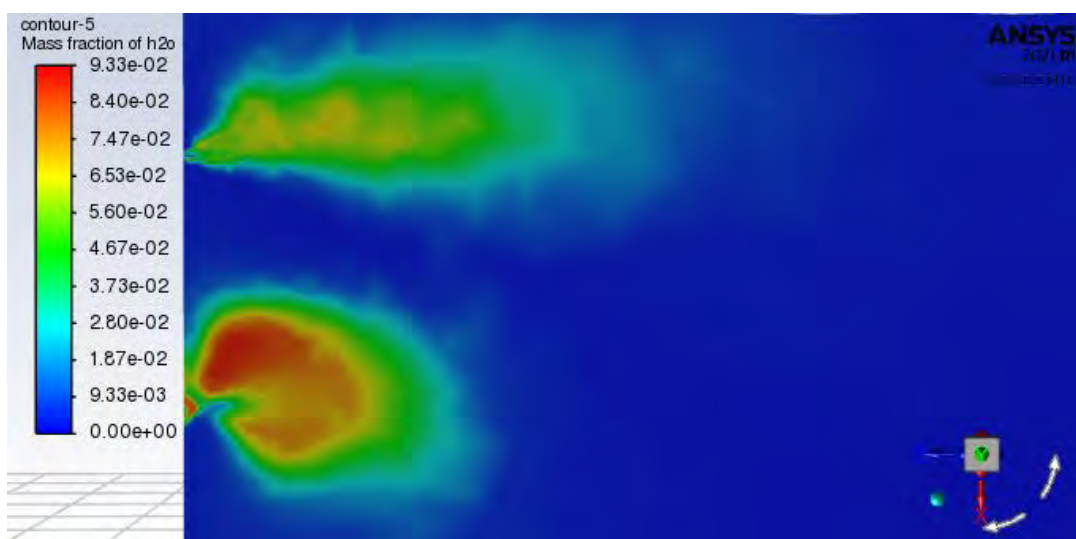


Figure 4.50: Contours plot of Water Mass Fraction of dual GDI

For late injection dual direct engine, the mass fraction of water vapour in the combustion chamber is at its peak of $9.33\text{e-}02$ around regions that has completed combustion is H_2O is a product of combustion. The burning mixture has less water vapour of $4.67\text{e-}02$ averagely as combustion is ongoing. Mass fraction of H_2O vapour in the unburnt mixture is $0.00\text{e+}00$

4.3.31 Mass fraction of Water Vapour (H_2O) at Early injection mode (Piston at TDC)

The contour plot in Fig. 4.51 shows the mass fraction of H_2O in the single GDI engine at early injection mode.

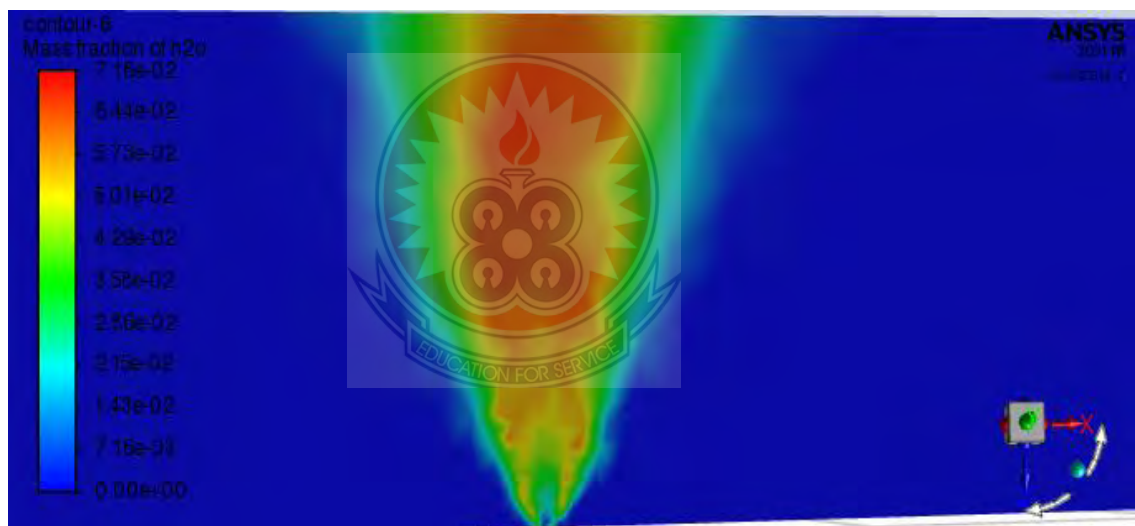


Figure 4.51: Contours plot of Water Mass Fraction of single GDI

The mass fraction of water vapour in the single DI combustion chamber is at its peak of $7.16\text{e-}02$ around regions that has completed combustion is H_2O is a product of combustion. The burning mixture has less water vapour of $3.58\text{e-}02$ averagely as combustion is ongoing. Mass fraction of H_2O vapour in the unburnt mixture is $0.00\text{e+}00$.

The contour plot in Fig. 4.52 shows the mass fraction of H₂O in the dual DI engine at early injection mode

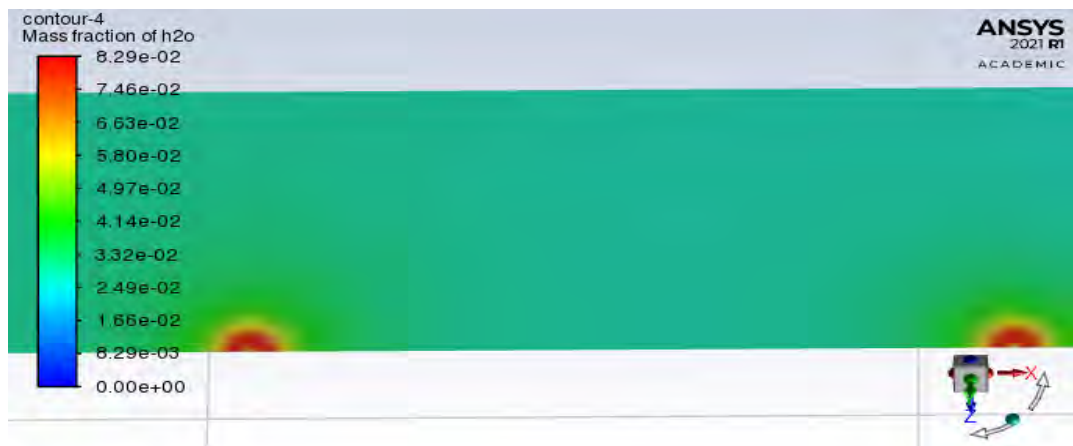


Figure 4.51: Contours plot of Water Mass Fraction of dual GDI

The mass fraction of water vapour in the dual injection combustion chamber that injected its fuel/air mixture early is at its peak of 8.29e-02 around regions that has completed combustion is H₂O is a product of combustion. The burning mixture has less water vapour of 4.14e-02 averagely as combustion is ongoing. Mass fraction of H₂O vapour in the unburnt mixture is 0.00e+00.

4.3.32 Comparison of mass fractions of Water vapour (H₂O) in single DI engine at early and late injection modes

Figure 4.52 shows the peak mass fraction of Water vapour in single GDI at both early and late injection modes.

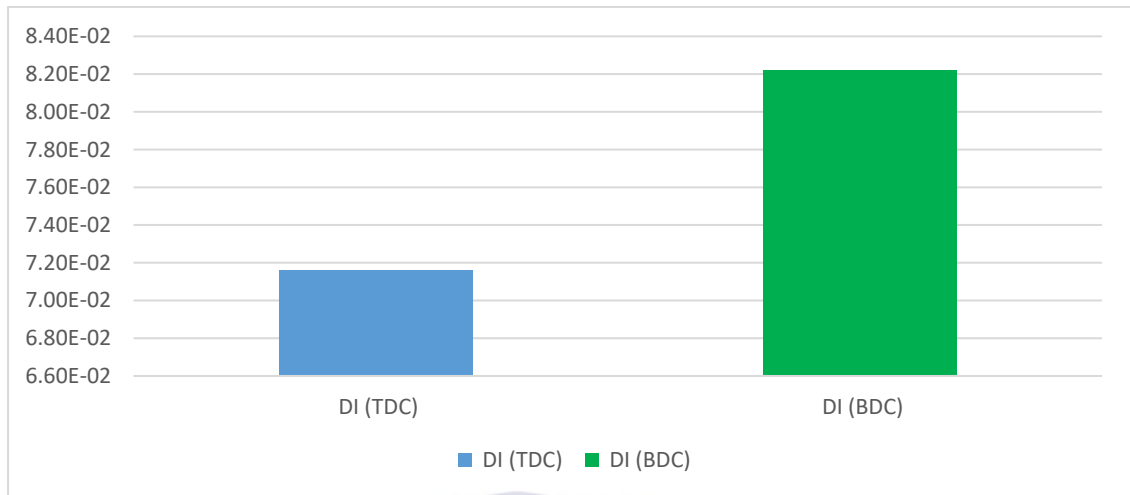


Figure 4.52: Mass fraction of water of single GDI Engine operating modes

At the end of the combustion in the early injection mode, the mass fraction of H₂O in the combustion chamber is 7.16e-02 as against 8.22e-02 in the case of late injection.

This shows that the quantity of water produced from the combustion process when the engine operates at late injection mode is more than in the early injection modes of the single GDI engine. The result is in line with the findings of Kumar and Rao (2013) who also identified traces of H₂O after combustion.

4.3.32 Comparison of mass fractions of Water vapour (H₂O) in Dual DI engine at early and late injection modes

Figure 4.53 shows the peak mass fraction of Water vapour in dual DI at both early and late injection modes.

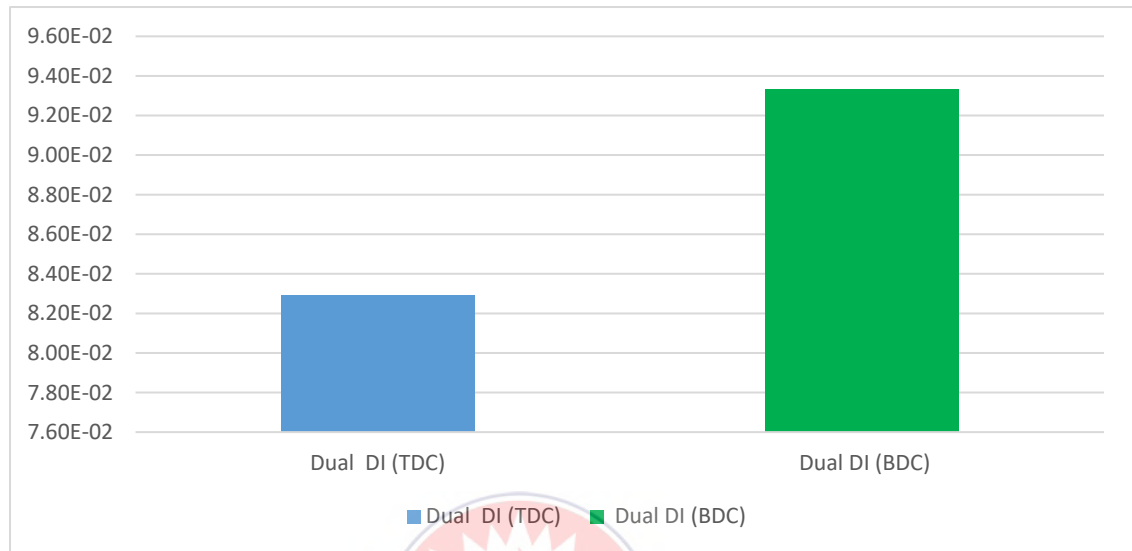


Figure 4.53: Mass fraction of water of dual GDI Engine injection modes

At the end of the combustion in the late injection mode, the mass fraction of H₂O in the combustion chamber is 9.33e-02 as against 8.29e-02 in the case of early injection.

This shows that the quantity of water produced from the combustion process when the engine operates at late injection mode is more than in the early injection modes of the single GDI engine. The results agrees with the finding of Kumar and Rao (2013) who also identified some amount of water vapour after combustion.

4.3.33 NO_x Production at Late injection mode (piston at BDC)

The contour plot in Fig. 4.54 shows the mass fraction of NO_x in the single GDI engine at late injection mode

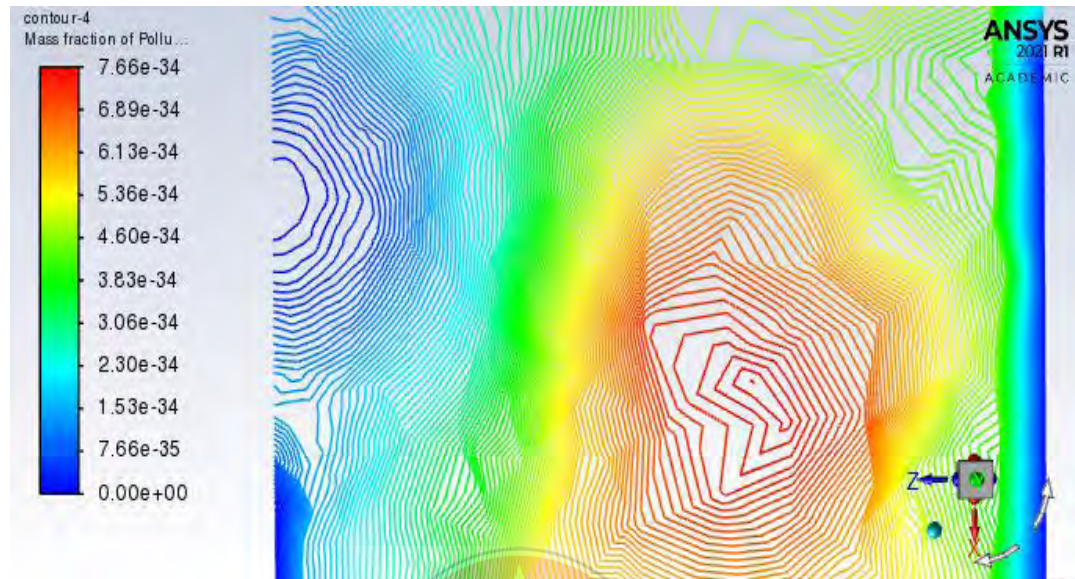


Figure 4.54: Contours plot of NO_x Mass Fraction—Prompt and Thermal NO_x Formation of single GDI

The peak concentration of NO_x is located in a region of high temperature where oxygen and nitrogen are available. The high concentration area has the highest mass fraction of NO_x of 7.66×10^{-34} . The moderate temperature, oxygen and nitrogen concentrated area has an average mass fraction of 3.83×10^{-34} . The region of low temperature with lower oxygen and nitrogen has no mass fraction of NO_x formed there and records 0.00×10^0 .

With the mass fraction of 7.66×10^{-34} , the Mass-Weighted Average shows that the exiting NO_x mass fraction through the exhaust is 0.0

The contour plot in Fig. 4.55 shows the mass fraction of NO_x in the dual Di engine at late injection mode

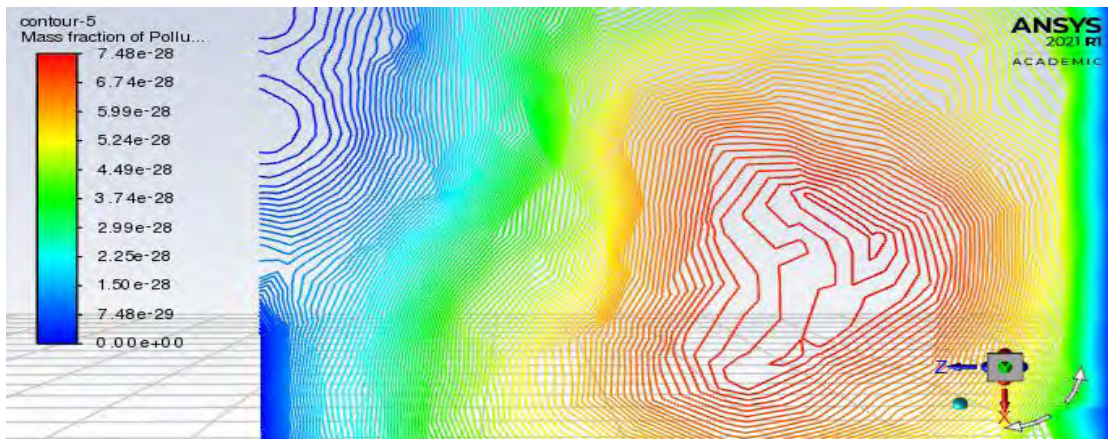


Figure 4.55: Contours plot of NO_x Mass Fraction—Prompt and Thermal NO_x Formation of dual GDI

The peak concentration of NO_x is located in a region of high temperature where oxygen and nitrogen are available. The high concentration area has the highest mass fraction of NO_x of 7.48e-28. The moderate temperature, oxygen and nitrogen concentrated area has an average mass fraction of 3.74e-28. The region of low temperature with lower oxygen and nitrogen has no mass fraction of NO_x formed there and records 0.00e+00. With the mass fraction of 7.48e-28, the Mass-Weighted Average shows that the exiting NO_x mass fraction through the exhaust is 0.0.

4.3.34 NO_x Production at Early injection mode (piston at TDC)

The contour plot in Fig. 4.56 shows the mass fraction of NO_x in the single GDI engine at early injection mode.

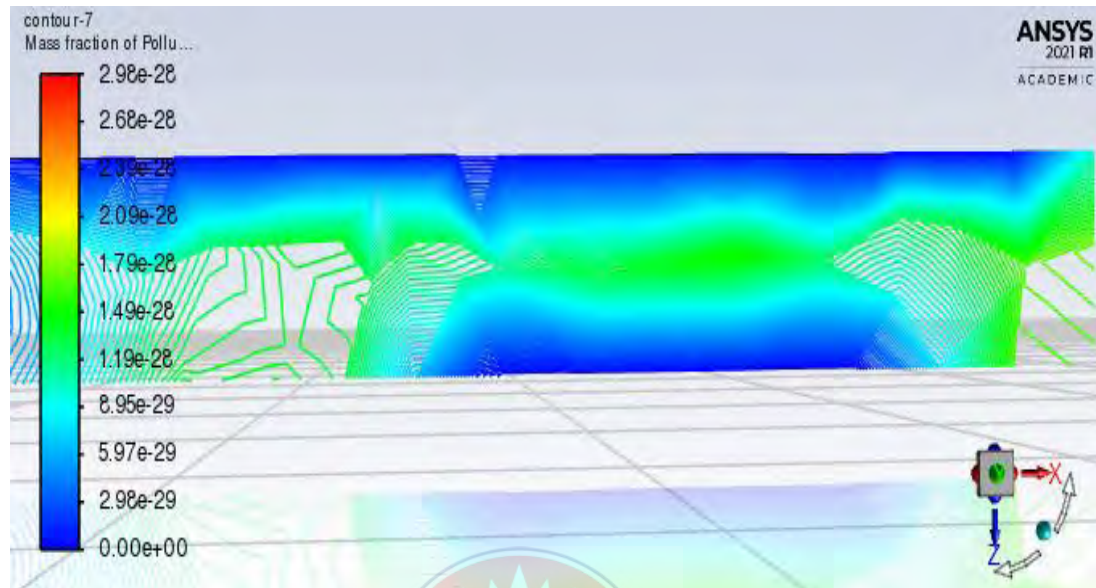


Figure 4.56: Contours plot of NO_x Mass Fraction—Prompt and Thermal NO_x Formation of single GDI

The peak concentration of NO_x is located in a region of high temperature where oxygen and nitrogen are available. The high concentration area has the highest mass fraction of NO_x of 2.98e-28. The moderate temperature, oxygen and nitrogen concentrated area has an average mass fraction of 1.49e-28. The region of low temperature with lower oxygen and nitrogen has no mass fraction of NO_x formed there and records 0.00e+00. With the mass fraction of 2.98e-28, the Mass-Weighted Average shows that the exiting NO_x mass fraction through the exhaust is 0.0

The contour plot in Fig. 4.57 shows the mass fraction of NO_x in the dual Di engine at early injection mode

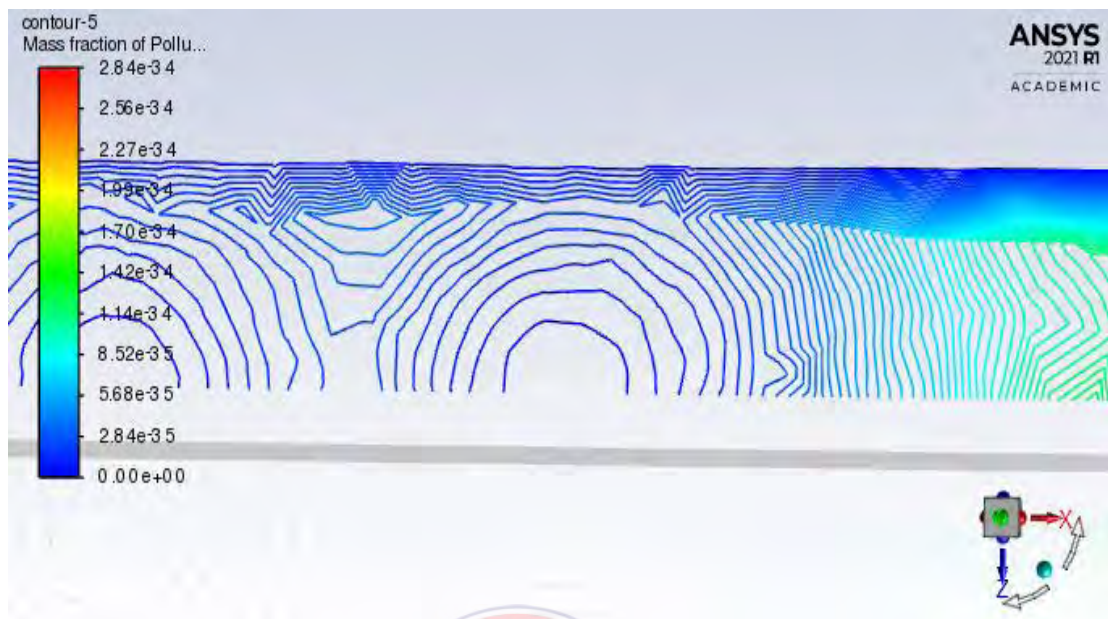


Figure 4.57: Contours plot of NO_x Mass Fraction—Prompt and Thermal NO_x Formation of dual GDI

The peak concentration of NO_x is located in a region of high temperature where oxygen and nitrogen are available. The high concentration area has the highest mass fraction of NO_x of 2.84×10^{-34} . The moderate temperature, oxygen and nitrogen concentrated area has an average mass fraction of 1.42×10^{-34} . The region of low temperature with lower oxygen and nitrogen has no mass fraction of NO_x formed there and records 0.00×10^0 . With the mass fraction of 2.84×10^{-34} , the Mass-Weighted Average shows that the exiting NO_x mass fraction through the exhaust is 0.0

4.3.35 Comparison of NO_x mass fractions of single DI engines at early and late injection modes

Figure 4.58 shows the peak mass fraction of NO_x in single GDI at both early and late injection modes.

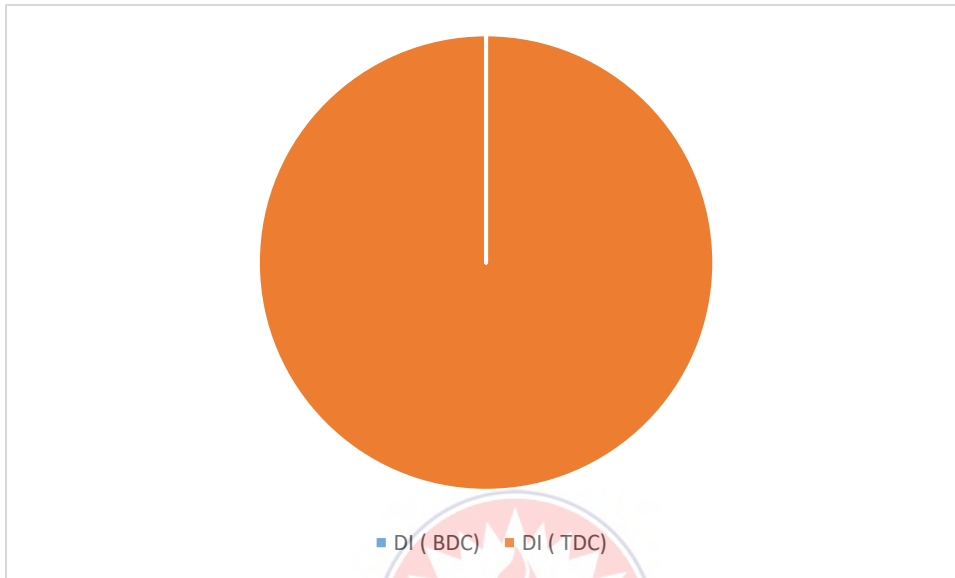


Figure 4.58: Mass fraction of NO_x of single GDI Engine injection modes

From Fig 4.58, the formation of NO_x in the single DI engine that injects fuel early is as high as 2.98e-28. On the other hand, the formation of NO_x when the fuel is injected late in the single DI engine is 7.66e-34 which is far lower. In sum, when fuel-air mixture is injected late into the single DI engine, NO_x formation is much improved as compared to early injection of fuel. The results for the single GDI engine varies from the results of Zheng et al. (2007) that homogenous charge reduces NO_x production in the single GDI.

4.3.36 Comparison of NO_x mass fractions of dual DI engines at early and late injection modes

Figure 4.59 shows the peak mass fraction of NO_x in dual DI at both early and late injection modes.

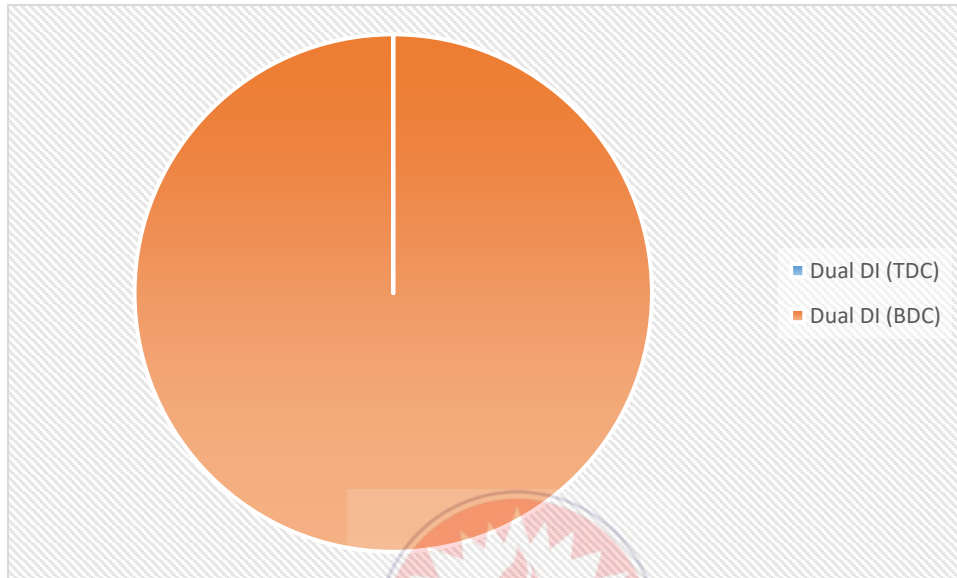


Figure 4.59: Mass fraction of NO_x of dual GDI Engine injection modes

From Fig. 4.59, the formation of NO_x in the dual DI engine that injects fuel late is as high as 7.48×10^{-28} . On the other hand, the formation of NO_x when the fuel is injected early in the dual DI engine is 2.84×10^{-34} which is far lower. In sum, when fuel-air mixture is injected early into the dual DI engine, NO_x formation is by far improved than in the late fuel injection mode. This results agrees with the findings of Zheng et al. (2007) that early injection mode promises the reduction of NO_x.

CHAPTER FIVE

SUMMARY OF FINDINGS, CONCLUSIONS AND RECOMMENDATIONS

5.1 Introduction

This chapter presents the summary of research findings, conclusion and recommendation for further research.

5.2 Summary of Findings

1. The results showed that at late injection mode, the TKE of the eddies were directly proportional to the injection velocity. At the lowest velocity of 100m/s, the TKE of the single GDI engine was higher and that of the dual direct injection was about the same. At 300m/s the KTE of the single DI engine is about 15% higher than that of the dual DI.

During the early injection mode, the TKE of the eddies increased as the injection velocity. At the lowest velocity of 100m/s, the TKE of the single GDI engine was slightly higher than that of the dual direct injection. At 150m/s both jet flows had about the same Turbulent kinetic energy. At higher injection velocities 200m/s, 250m/s and 300m/s, the KTE of the single GDI engine was higher than that of the dual GDI.

2. When the fuel was injected late, the velocity magnitude of the eddies in the direction of the flow were steady in the single GDI from $8.82e+02$ m/s at 100m/s to $2.67e+02$ m/s at 300m/s while that of the dual GDI declined from $6.73e+01$ at 100m/s to $1.01e+01$ at 150m/s. The velocities of the flow then rose sharply to $1.34e+02$ m/s at 200m/s and steadily to $2.01e+02$ m/s.

On the other hand, the velocity magnitude of the eddies in the direction of the flow were steady for both single GDI and dual GDI. The velocity magnitude of the mass of eddies of the dual direct injection was higher as compared to

the single direct injection. The jet velocity rose steadily from 9.48×10^1 m/s at 100m/s to 2.85×10^2 m/s at 300m/s in dual GDI engine against 8.15×10^1 m/s at 100m/s to 2.46×10^2 m/s in the single GDI engine.

3. When fuel is injected late into the cylinder, the rate of diffusion of TKE in single GDI engine is quite lower than that of the dual GDI. At the 100m/s, the lowest rate at which turbulent eddies dissipates energy in single GDI was $1.10 \times 10^8 \text{ m}^2 \text{ s}^{-3}$ as against $8.23 \times 10^7 \text{ m}^2 \text{ s}^{-3}$ in the dual GDI. This is true for all injection velocities, at 300m/s the minimum dissipation rate at which the TKE was still diffused in the single DI was $2.07 \times 10^9 \text{ m}^2 \text{ s}^{-3}$ against $1.63 \times 10^9 \text{ m}^2 \text{ s}^{-3}$ in the dual GDI.

In the early injection mode, the rate of diffusion of TKE in single GDI engine was almost same as that of the dual direct injection at lower injection velocities 100m/s and 150m/s. At higher injection velocity 300m/s the single GDI dissipates the TKE at higher peak value of $3.01 \times 10^9 \text{ m}^2 \text{ s}^{-3}$ against $2.52 \times 10^9 \text{ m}^2 \text{ s}^{-3}$ in the dual GDI.

4. At 100m/s, the turbulent intensity in Single GDI engine was slightly higher during late injection mode than that of the dual GDI. The turbulence intensity was almost same for both single GDI and dual GDI engine at injection velocity of 200m/s and then rose further high on higher injection velocities.

At 100m/s, the turbulent intensity in dual GDI engine operating at early injection mode was slightly higher than that of the single DI. The turbulence intensity was almost same for both single GDI and dual GDI engine at an injection velocity of 200m/s and 250m/s. The turbulent intensity in the single DI rose a little high on higher injection velocities.

5. At an injection velocity of 100m/s, the turbulent viscosity of the flow in the combustion chamber was $2.68e-03$ Kg/(ms) in the single GDI engine during late injection as compared to a higher $1.26e-03$ Kg/(ms) for dual GDI engine. The turbulence viscosity increases with increasing injection velocities in the single GDI engine to about $8.42e-03$ Kg/(ms) limiting the rate at which the TKE can cover the combustion domain before decay. The turbulent viscosity in the dual GDI engine decreases right from the high resistance of $1.26e-03$ Kg/(ms) at the nozzle to $4.07e-03$ Kg/(ms).

At an injection velocity of 100m/s, the internal resistance to the flow of eddies in the combustion chamber was $1.76e-4$ Kg/(ms) for single GDI engine as compared to a higher $1.82e-04$ Kg/(ms) for dual GDI. The turbulence viscosity decreases with increasing injection velocities in the single GDI engine to about $3.94e-4$ Kg/(ms). The turbulent viscosity in the dual GDI engine also decreases right from $1.82e-04$ Kg/(ms) at the nozzle to $4.82e-04$ Kg/(ms).

6. The peak flame temperature of the mixture under temperature and composition dependent heat capacity was high when the engine was running on early injection mode. At 2430K flame temperature, dissociation of combustion products; CO, HC, NO_x, O, C may commence to produce harmful exhaust pollutant. The opposite was also true for the late injection mode under the same conditions.

The peak flame temperature of the dual DI at early injection mode operated at 698K. Mixture was burnt at a low temperature that makes it almost impossible for dissociation of combustion products to occur. The late injection mode

under the same conditions threatened the release of high pollutant number when the flame temperature was as high as 3500K.

7. The peak specific heat capacity of the mixture in the single GDI injected early had a higher specific heat capacity of $1.40e+03$ as compared to the specific heat capacity of $1.17e+03$ of same engine when operated at late injection mode. Increased heat capacity substantially increased the peak flame temperature, and consequently threatened cylinder misfire and the dissociation of combustion products to form harmful exhaust pollutants like CO, HC and NO_x

The peak specific heat capacity of the mixture in the dual GDI injected late had a higher specific heat capacity of $1.43e+03$ as compared to the specific heat capacity of $1.17e+03$ of same engine when operated at early injection mode. Increased heat capacity increased the peak flame temperature, and consequently cylinder misfire and the dissociation of combustion products to form harmful exhaust pollutants like CO, HC and NO_x.

8. The peak burning velocity of the engine operated at late injection mode was 324m/s while that of the same engine operated at early injection mode was 263m/s.

The peak burning velocity of the dual GDI engine operated at late injection mode was 2290 m/s against 379 m/s of the same engine operated at early injection mode. The late injected fuel burnt at a higher velocity resulting in faster combustion.

9. At early injection mode, the peak mass fraction of octane in the single GDI engine that mixed with the air was $9.96e-01$ as against $5.40e-01$ around the spark plug at the start of combustion. At early injection mode, the peak mass fraction of octane that mixes with the air was $1.00e+00$ as against $9.90e-01$ as around the spark plug at the start of combustion in the dual GDI engine.

10. At the commencement of the combustion in the early injection mode of the single GDI engine, the mass fraction of oxygen in the combustion chamber was $2.34e-01$ as against $2.30e-01$ when fuel was injected late. Whereas at the commencement of the combustion in both early and late injection mode of the dual GDI engine, the mass fraction of oxygen in the combustion chambers were $2.30e-01$.

11. At the end of the combustion in the early injection mode of the single GDI, the peak mass fraction of nitrogen in the combustion chamber was $3.09e-03$ as against $3.21e-01$ in the case of late injection. At the end of the combustion in the early injection mode of the dual GDI, the mass fraction of nitrogen in the combustion chamber was $0.00e+00$ as against $7.21e-03$ in the late injection.

12. The mass fraction of CO_2 in the combustion chamber at the end of the combustion in the early injection mode was $1.93e-01$ as against $2.05e-01$ in the case of late injection. At the end of the combustion in the early injection mode, the mass fraction of CO_2 in the combustion chamber was $2.08e-01$ while the mass fraction at late injection $2.13e-01$.

13. At the end of the combustion in the early injection mode, the mass fraction of H₂O in the combustion chamber was 7.16e-02 as against 8.22e-02 in the case of late injection mode. At the end of the combustion in the late injection mode, the mass fraction of H₂O in the combustion chamber was 9.33e-02 as against 8.29e-02 in the case of early injection.
14. The mass fraction of NO_x in the single GDI engine that injected fuel early was as high as 2.98e-28. On the other hand, the formation of NO_x when the fuel was injected late in the single DI engine was 7.66e-34 which is far lower. The mass fraction of NO_x in the dual GDI engine that injected fuel late was 7.48e-28. On the other hand, NO_x formed when the fuel was injected early in the dual DI engine was 2.84e-34 which is far lower.

5.3 Conclusion

Based on the research findings following the aim of modelling a new fuel injection system to help curb the issues emissions of the gasoline direct injection engine, the following conclusions were drawn;

1. The dual direct GDI engine at early injection mode promises a better fuel diffusion, lower turbulent viscosity than the single GDI at the same condition. In the same vein, single GDI engine at late injection condition also gives a better fuel diffusion in than that of the dual GDI engine.
2. Dual direct GDI engine operating at late injection and single GDI at early injection modes have tendencies for dissociation to produce high amounts of HC, CO, CO₂, C and O and exhibit engine knock in its operation as Chen et al. (2019) also found in their work.

3. The heat capacity of the late injected fuel in single GDI and early injected fuel in dual direct GDI engines are low with lower flame temperatures and results in lower NO_x formation.
4. In both dual direct GDI and single GDI engines, fuel that is injected late burns at a higher velocity resulting in faster combustion than how the fuel burns when the same engine injects the fuel early.
5. Late injection of fuel in both single GDI and Dual GDI engines creates a lean mixture much better than when fuel is injected in the early injection mode. Thus, engines operating at late injection mode are prone to cylinder misfires.
6. More O₂ is used in combustion when the engine operates at early injection mode than in the late injection modes of the single GDI engine.
7. CO₂ production in the dual direct injection engine is higher showing a better combustion than in the single direct injection.
8. NO_x production in single GDI engine is about 10 times high when fuel-air mixture is injected early as compared to late injection of fuel. When fuel is injected late into the dual DI engine, NO_x production is 10x higher in late injection mode than in the early fuel injection mode.

5.4 Recommendation

Based on the research findings the following recommendation are made;

1. Investors should come in to invest in projects to realize and commercialize the production of the dual direct GDI engine for the general masses to popularize the new and efficient technology for job creation and the support of Ghana's industrialization drive.
2. The automotive companies in Ghana should consider the efficiency of the dual direct GDI engine for emission control and fuel economy potential for the

Ghanaian people and incorporate them into the Ghana -made vehicles for the Ghanaian market and the world at large.

3. Automotive companies worldwide may adopt the research findings for engine development for efficient engine output, emission control and fuel economy.

5.5 Suggestions for Further Research

1. Hydrocarbons (HC) and nitrogen oxides (NO_x) are the main problems associated with GDI. However, my work could not cover the production of HC. Studies into HC, CO and NO_x formation in dual direct gasoline direct injection engine should be pursued.
2. Researchers may also look at the effect of injector angle on combustion characteristic of the dual direct GDI engine.



REFERENCES

- Ahn, K. H., Stefanopoulou, A., Jiang, L., & Yilmaz, H. (2010). Ethanol content estimation in flex fuel direct injection engines with fault detection under fuel injector drifts. *IFAC Proceedings Volumes (IFAC-PapersOnline)*, 43(7), 123–130. <https://doi.org/10.3182/20100712-3-DE-2013.00095>
- Alvarez, C. E. C., Couto, G. E., Roso, V. R., Thiriet, A. B., & Valle, R. M. (2018). A review of prechamber ignition systems as lean combustion technology for SI engines. *Applied Thermal Engineering*, 128, 107–120. <https://doi.org/10.1016/j.applthermaleng.2017.08.118>
- Anbari Attar, M., Herfatmanesh, M. R., Zhao, H., & Cairns, A. (2014). Experimental investigation of direct injection charge cooling in optical GDI engine using tracer-based PLIF technique. *Experimental Thermal and Fluid Science*, 59, 96–108. <https://doi.org/10.1016/j.expthermflusci.2014.07.020>
- Anenberg, S., Miller, J., Henze, D., & Minjares, R. (2019). A global snapshot of the air pollution-related health impacts of transportation sector emissions in 2010 and 2015. *International Council on Clean Transportation*, 55. https://www.theicct.org/sites/default/files/publications/Global_health_impacts_transport_emissions_2010-2015_20190226.pdf
- Awad, O. I., Ma, X., Kamil, M., Ali, O. M., Zhang, Z., & Shuai, S. (2020). Particulate emissions from gasoline direct injection engines: A review of how current emission regulations are being met by automobile manufacturers. *Science of the Total Environment*, 718, 137302. <https://doi.org/10.1016/j.scitotenv.2020.137302>
- Ayeter, G. K., Quansah, D. A., & Adjei, E. A. (2020). Towards zero vehicle emissions in Africa: A case study of Ghana. *Energy Policy*, 143(August 2019), 111606. <https://doi.org/10.1016/j.enpol.2020.111606>
- Carroll, P. L., & Blanquart, G. (2014). *A proposed modification to Lundgren 's*

physical space velocity forcing method for isotropic turbulence A proposed modification to Lundgren ' s physical space. 105114(2013), 0–9.

<https://doi.org/10.1063/1.4826315>

Chen, W., Xia, C., Zhu, L., Mao, K., Tao, J., Fang, J., & Huang, Z. (2019). An experimental study on combustion and particulate emissions characteristics on a dual-injection gasoline engine. *Applied Thermal Engineering, 156*(February), 722–729. <https://doi.org/10.1016/j.applthermaleng.2019.04.069>

Chintala, V., & Subramanian, K. A. (2017). A comprehensive review on utilization of hydrogen in a compression ignition engine under dual fuel mode. *Renewable and Sustainable Energy Reviews, 70*(December 2015), 472–491.

<https://doi.org/10.1016/j.rser.2016.11.247>

Cho, H. M., & He, B. Q. (2007). Spark ignition natural gas engines-A review. *Energy Conversion and Management, 48*(2), 608–618.

<https://doi.org/10.1016/j.enconman.2006.05.023>

Cole, R. L., Poola, R. B., & Sekar, R. (1998). Exhaust emissions of a vehicle with a gasoline direct-injection engine. *SAE Technical Papers, 724*.

<https://doi.org/10.4271/982605>

Cracknell, R., Head, B., Remmert, S., Wu, Y., & Solutions, S. G. (2013). *Laminar burning velocity as a fuel characteristic : Impact on vehicle performance. 149–156.* <https://doi.org/10.1533/9781782421849.4.149>

Cui, Y., Zheng, Z., Wen, M., Tang, Q., Geng, C., Wang, Q., Liu, H., & Yao, M. (2021). Optical diagnostics on the effects of reverse reactivity stratification on the flame development in dual-fuel combustion. *Fuel, 287*(October), 119500.

<https://doi.org/10.1016/j.fuel.2020.119500>

Daniel, R., Xu, H., Wang, C., Richardson, D., & Shuai, S. (2013). Gaseous and

particulate matter emissions of biofuel blends in dual-injection compared to direct-injection and port injection. *Applied Energy*, 105, 252–261.

<https://doi.org/10.1016/j.apenergy.2012.11.020>

Du, Y., Yu, X., Wang, J., Wu, H., Dong, W., & Gu, J. (2016). Research on combustion and emission characteristics of a lean burn gasoline engine with hydrogen direct-injection. *International Journal of Hydrogen Energy*, 41(4), 3240–3248. <https://doi.org/10.1016/j.ijhydene.2015.12.025>

Feng, D., Wei, H., Pan, M., Zhou, L., & Hua, J. (2018). Combustion performance of dual-injection using n-butanol direct-injection and gasoline port fuel-injection in a SI engine. *Energy*, 160, 573–581. <https://doi.org/10.1016/j.energy.2018.07.042>

Fontaras, G., Zacharof, N. G., & Ciuffo, B. (2017). Fuel consumption and CO₂ emissions from passenger cars in Europe – Laboratory versus real-world emissions. *Progress in Energy and Combustion Science*, 60, 97–131. <https://doi.org/10.1016/j.pecs.2016.12.004>

Franchini, M., & Mannucci, P. M. (2015). Impact on human health of climate changes. *European Journal of Internal Medicine*, 26(1), 1–5. <https://doi.org/10.1016/j.ejim.2014.12.008>

Fraser, N., Blaxill, H., Lumsden, G., & Bassett, M. (2009). Challenges for increased efficiency through gasoline engine downsizing. *SAE Technical Papers*, 2(1), 991–1008. <https://doi.org/10.4271/2009-01-1053>

Gheorghiu, V. (2015). Ultra-Downsizing of Internal Combustion Engines. *SAE Technical Papers*, 2015-April(April). <https://doi.org/10.4271/2015-01-1252>

Gong, C., Li, Z., Yi, L., & Liu, F. (2020). Experimental investigation of equivalence ratio effects on combustion and emissions characteristics of an H₂/methanol dual-injection engine under different spark timings. *Fuel*, 262(August 2019),

116463. <https://doi.org/10.1016/j.fuel.2019.116463>

Gummesson, H., & Becquin, G. (n.d.). *MVK135 – Turbulent combustion Project – Diesel engines*.

Huang, Y., Hong, G., Cheng, X., & Huang, R. (2013). Investigation to charge cooling effect of evaporation of ethanol fuel directly injected in a gasoline port injection engine. *SAE Technical Papers*, 11. <https://doi.org/10.4271/2013-01-2610>

Huang, Y., Hong, G., & Huang, R. (2015a). Investigation to charge cooling effect and combustion characteristics of ethanol direct injection in a gasoline port injection engine. *Applied Energy*, 160, 244–254.

<https://doi.org/10.1016/j.apenergy.2015.09.059>

Huang, Y., Hong, G., & Huang, R. (2015b). Numerical investigation to the dual-fuel spray combustion process in an ethanol direct injection plus gasoline port injection (EDI + GPI) engine. *Energy Conversion and Management*, 92, 275–286. <https://doi.org/10.1016/j.enconman.2014.12.064>

Huang, Y., Ng, E. C. Y., Zhou, J. L., Surawski, N. C., & Chan, E. F. C. (2018). Eco-driving technology for sustainable road transport : A review. *Renewable and Sustainable Energy Reviews*, 93(April), 596–609.

<https://doi.org/10.1016/j.rser.2018.05.030>

Huang, Y., Surawski, N. C., Organ, B., Zhou, J. L., Tang, O. H. H., & Chan, E. F. C. (2019). Fuel consumption and emissions performance under real driving:

Comparison between hybrid and conventional vehicles. *Science of the Total Environment*, 659, 275–282. <https://doi.org/10.1016/j.scitotenv.2018.12.349>

Huang, Z., Wang, J., Liu, B., Zeng, K., Yu, J., & Jiang, D. (2007). Combustion characteristics of a direct-injection engine fueled with natural gas-hydrogen blends under different ignition timings. *Fuel*, 86(3), 381–387.

<https://doi.org/10.1016/j.fuel.2006.07.007>

James Gunasekaran, E., & Dhandapani, S. (2012). A comparison of two injectors in mixture preparation for a high tumble GDI engine-A CFD study. *SAE Technical Papers*. <https://doi.org/10.4271/2012-01-0398>

Jiang, C., Ma, X., Xu, H., & Richardson, S. (2012). An optical study of DMF and ethanol combustion under dual-injection strategy. *SAE Technical Papers*. <https://doi.org/10.4271/2012-01-1237>

Journal, I. (2019). *IJER editorial : The future of the internal combustion engine*. <https://doi.org/10.1177/1468087419877990>

Kalghatgi, G. (2019). Development of Fuel / Engine Systems — The Way Forward to Sustainable Transport. *Engineering*, 5(3), 510–518.

<https://doi.org/10.1016/j.eng.2019.01.009>

Kasseris, E., & Heywood, J. B. (2012). Charge Cooling Effects on Knock Limits in SI DI Engines Using Gasoline/Ethanol Blends: Part 2-Effective Octane Numbers. *SAE International Journal of Fuels and Lubricants*, 5(2), 844–854.

<https://doi.org/10.4271/2012-01-1284>

Kim, N., Cho, S., & Min, K. (2015). A study on the combustion and emission characteristics of an SI engine under full load conditions with ethanol port injection and gasoline direct injection. *Fuel*, 158(2015), 725–732.

<https://doi.org/10.1016/j.fuel.2015.06.025>

Kim, T., Song, J., & Park, S. (2015). Effects of turbulence enhancement on combustion process using a double injection strategy in direct-injection spark-ignition (DISI) gasoline engines. *International Journal of Heat and Fluid Flow*, 56, 124–136. <https://doi.org/10.1016/j.ijheatfluidflow.2015.07.013>

Lee, Y., Oh, S., Kim, C., Lee, J., Lee, K., & Kim, J. (2018). The dual-port fuel

- injection system for fuel economy improvement in an automotive spark-ignition gasoline engine. *Applied Thermal Engineering*, 138(February), 300–306.
<https://doi.org/10.1016/j.applthermaleng.2018.04.027>
- Lee, Z., Kim, T., Park, S., & Park, S. (2020). Review on spray, combustion, and emission characteristics of recent developed direct-injection spark ignition (DISI) engine system with multi-hole type injector. *Fuel*, 259(September 2019), 116209. <https://doi.org/10.1016/j.fuel.2019.116209>
- Liang, B., Ge, Y., Tan, J., Han, X., Gao, L., Hao, L., Ye, W., & Dai, P. (2013). Comparison of PM emissions from a gasoline direct injected (GDI) vehicle and a port fuel injected (PFI) vehicle measured by electrical low pressure impactor (ELPI) with two fuels: Gasoline and M15 methanol gasoline. *Journal of Aerosol Science*, 57, 22–31. <https://doi.org/10.1016/j.jaerosci.2012.11.008>
- Liu, Haifeng, Ma, G., Ma, N., Zheng, Z., Huang, H., & Yao, M. (2018). Effects of charge concentration and reactivity stratification on combustion and emission characteristics of a PFI-DI dual injection engine under low load condition. *Fuel*, 231(March), 26–36. <https://doi.org/10.1016/j.fuel.2018.05.027>
- Liu, Hui, Wang, Z., & Wang, J. (2014). Methanol-gasoline DFSI (dual-fuel spark ignition) combustion with dual-injection for engine knock suppression. *Energy*, 73, 686–693. <https://doi.org/10.1016/j.energy.2014.06.072>
- Liu, Y., Ersson, M., Liu, H., Jönsson, P., & Gan, Y. (2019). Comparison of Euler-Euler Approach and Euler–Lagrange Approach to Model Gas Injection in a Ladle. *Steel Research International*, 90(5), 1–13.
<https://doi.org/10.1002/srin.201800494>
- López, J. J., Salvador, F. J., De, O. A., & Arrègle, J. (2012). *A comprehensive study on the effect of cavitation on injection velocity in diesel nozzles*. 64, 415–423.

<https://doi.org/10.1016/j.enconman.2012.03.032>

Milpied, J., Jeuland, N., Plassat, G., Guichaous, S., Dioc, N., Marchal, A., &

Schmelzle, P. (2009). Impact of fuel properties on the performances and knock behaviour of a downsized turbocharged di SI engine - Focus on octane numbers and latent heat of vaporization. *SAE Technical Papers*, 2(1), 118–126.

<https://doi.org/10.4271/2009-01-0324>

Niu, R., Yu, X., Du, Y., Xie, H., Wu, H., & Sun, Y. (2016). Effect of hydrogen

proportion on lean burn performance of a dual fuel SI engine using hydrogen direct-injection. *Fuel*, 186, 792–799. <https://doi.org/10.1016/j.fuel.2016.09.021>

Ozsezen, A. N., & Canakci, M. (2011). Performance and combustion characteristics

of alcohol-gasoline blends at wide-open throttle. *Energy*, 36(5), 2747–2752.

<https://doi.org/10.1016/j.energy.2011.02.014>

Park, C., Kim, S., Kim, H., & Moriyoshi, Y. (2012). Stratified lean combustion

characteristics of a spray-guided combustion system in a gasoline direct injection engine. *Energy*, 41(1), 401–407. <https://doi.org/10.1016/j.energy.2012.02.060>

Pedrozo, V. B., May, I., Lanzasova, T. D. M., & Zhao, H. (2016). Potential of internal

EGR and throttled operation for low load extension of ethanol-diesel dual-fuel reactivity controlled compression ignition combustion on a heavy-duty engine.

Fuel, 179(April), 391–405. <https://doi.org/10.1016/j.fuel.2016.03.090>

Perry, R., & Gee, I. L. (1995). Vehicle emissions in relation to fuel composition.

Science of the Total Environment, 169(1–3), 149–156.

[https://doi.org/10.1016/0048-9697\(95\)04643-F](https://doi.org/10.1016/0048-9697(95)04643-F)

Phuangwongtrakul, S., Wechsathol, W., Sethaput, T., Suktang, K., & Wongwises, S.

(2016). Experimental study on sparking ignition engine performance for optimal mixing ratio of ethanol-gasoline blended fuels. *Applied Thermal Engineering*,

100, 869–879. <https://doi.org/10.1016/j.applthermaleng.2016.02.084>

Pontoppidan, M., & Gaviani, G. (2018). *Experimental and Numerical Approach to Injection and Ignition Optimization of Lean GDI-Combustion Behavior*.

1999(724).

Price, P., Twiney, B., Stone, R., Kar, K., & Walmsley, H. (2007). Particulate and hydrocarbon emissions from a spray guided direct injection spark ignition engine with oxygenate fuel blends. *SAE Technical Papers*, 724, 776–790.

<https://doi.org/10.4271/2007-01-0472>

Prockop, L. D., & Chichkova, R. I. (2007). *Carbon monoxide intoxication : An updated review*. 262, 122–130. <https://doi.org/10.1016/j.jns.2007.06.037>

Qian, Y., Liu, G., Guo, J., Zhang, Y., Zhu, L., & Lu, X. (2019). Engine performance and octane on demand studies of a dual fuel spark ignition engine with ethanol/gasoline surrogates as fuel. *Energy Conversion and Management*, 183(June 2018), 296–306. <https://doi.org/10.1016/j.enconman.2019.01.011>

Qian, Y., Zhou, Q., Wang, X., Zhu, L., & Lu, X. (2016). Enabling dual fuel sequential combustion using port fuel injection of high reactivity fuel combined with direct injection of low reactivity fuels. *Applied Thermal Engineering*, 103, 399–410.

<https://doi.org/10.1016/j.applthermaleng.2016.04.122>

Reitz, R. D., & Duraisamy, G. (2015). Review of high efficiency and clean reactivity controlled compression ignition (RCCI) combustion in internal combustion engines. *Progress in Energy and Combustion Science*, 46, 12–71.

<https://doi.org/10.1016/j.pecs.2014.05.003>

Saliba, G., Saleh, R., Zhao, Y., Presto, A. A., Lambe, A. T., Frodin, B., Sardar, S., Maldonado, H., Maddox, C., May, A. A., Drozd, G. T., Goldstein, A. H., Russell, L. M., Hagen, F., & Robinson, A. L. (2017). Comparison of Gasoline

- Direct-Injection (GDI) and Port Fuel Injection (PFI) Vehicle Emissions: Emission Certification Standards, Cold-Start, Secondary Organic Aerosol Formation Potential, and Potential Climate Impacts. *Environmental Science and Technology*, 51(11), 6542–6552. <https://doi.org/10.1021/acs.est.6b06509>
- Shi, L., Ji, C., Wang, S., Cong, X., Su, T., & Shi, C. (2019). Impacts of dimethyl ether enrichment and various injection strategies on combustion and emissions of direct injection gasoline engines in the lean-burn condition. *Fuel*, 254(March), 115636. <https://doi.org/10.1016/j.fuel.2019.115636>
- Shirvani, S., Shirvani, S., Shamekhi, A. H., & Reitz, R. D. (2020). A study of using E10 and E85 under direct dual fuel stratification (DDFS) strategy: Exploring the effects of the reactivity-stratification and diffusion-limited injection on emissions and performance in an E10/diesel DDFS engine. *Fuel*, 275(April), 117870. <https://doi.org/10.1016/j.fuel.2020.117870>
- Shuai, S., Ma, X., Li, Y., Qi, Y., & Xu, H. (2018). Recent Progress in Automotive Gasoline Direct Injection Engine Technology. *Automotive Innovation*, 1(2), 95–113. <https://doi.org/10.1007/s42154-018-0020-1>
- Solaka, H., Aronsson, U., Tuner, M., & Johansson, B. (2012). Investigation of partially premixed combustion characteristics in low load range with regards to fuel octane number in a light-duty diesel engine. *SAE Technical Papers*, x. <https://doi.org/10.4271/2012-01-0684>
- Sravan Kumar, P., & Rao, P. P. (2013). Design and Analysis of Gas Turbine Combustion Chamber. *International Journal Of Computational Engineering Research (Ijceronline.Com)*, 03(1), 444–447.
- Stanglmaier, R. H., Hall, M. J., & Matthews, R. D. (1998). Fuel-spray/charge-motion interaction within the cylinder of a direct-injected, 4-valve, si engine. *SAE*

Technical Papers, 724. <https://doi.org/10.4271/980155>

Stein, R. A., Polovina, D., Roth, K., Foster, M., Lynskey, M., Whiting, T., Anderson, J. E., Shelby, M. H., Leone, T. G., & VanderGriend, S. (2012). Effect of Heat of Vaporization, Chemical Octane, and Sensitivity on Knock Limit for Ethanol - Gasoline Blends. *SAE International Journal of Fuels and Lubricants*, 5(2), 823–843. <https://doi.org/10.4271/2012-01-1277>

Stovell, C., Matthews, R., Johnson, B. E., Ng, H., & Larsen, B. (1999). Emissions and fuel economy of a 1998 toyota with a direct injection spark ignition engine. *SAE Technical Papers*, 724. <https://doi.org/10.4271/1999-01-1527>

Thakur, A. K., Kaviti, A. K., Mehra, R., & Mer, K. K. S. (2017). Progress in performance analysis of ethanol-gasoline blends on SI engine. *Renewable and Sustainable Energy Reviews*, 69(July 2016), 324–340. <https://doi.org/10.1016/j.rser.2016.11.056>

Thangavelu, S. K., Ahmed, A. S., & Ani, F. N. (2016). Review on bioethanol as alternative fuel for spark ignition engines. *Renewable and Sustainable Energy Reviews*, 56, 820–835. <https://doi.org/10.1016/j.rser.2015.11.089>

Tsokolis, D., Tsiakmakis, S., Dimaratos, A., Fontaras, G., Pistikopoulos, P., Ciuffo, B., & Samaras, Z. (2016). Fuel consumption and CO₂ emissions of passenger cars over the New Worldwide Harmonized Test Protocol. *Applied Energy*, 179(443), 1152–1165. <https://doi.org/10.1016/j.apenergy.2016.07.091>

Turner, J. W. G., Popplewell, A., Patel, R., Johnson, T. R., Darnton, N. J., Richardson, S., Bredda, S. W., Tudor, R. J., Bithell, C. I., Jackson, R., Remmert, S. M., Cracknell, R. F., Fernandes, J. X., Lewis, A. G. J., Akehurst, S., Brace, C. J., Copeland, C., Martinez-Botas, R., Romagnoli, A., & Burluka, A. A. (2014). Ultra Boost for Economy: Extending the Limits of Extreme Engine Downsizing.

SAE International Journal of Engines, 7(1), 387–417.

<https://doi.org/10.4271/2014-01-1185>

Venugopal, T., & Ramesh, A. (2014). Experimental studies on the effect of injection timing in a SI engine using dual injection of n-butanol and gasoline in the intake port. *Fuel*, 115, 295–305. <https://doi.org/10.1016/j.fuel.2013.07.013>

Wang, J., Huang, Z., Fang, Y., Liu, B., Zeng, K., Miao, H., & Jiang, D. (2007). Combustion behaviors of a direct-injection engine operating on various fractions of natural gas-hydrogen blends. *International Journal of Hydrogen Energy*, 32(15 SPEC. ISS.), 3555–3564. <https://doi.org/10.1016/j.ijhydene.2007.03.011>

Wei, L., & Geng, P. (2016). A review on natural gas/diesel dual fuel combustion, emissions and performance. *Fuel Processing Technology*, 142, 264–278. <https://doi.org/10.1016/j.fuproc.2015.09.018>

Wen, M., Zhang, C., Yue, Z., Liu, X., Yang, Y., Dong, F., Liu, H., & Yao, M. (2020). Effects of Gasoline Octane Number on Fuel Consumption and Emissions in Two Vehicles Equipped with GDI and PFI Spark-Ignition Engine. *Journal of Energy Engineering*, 146(6), 04020069. [https://doi.org/10.1061/\(asce\)ey.1943-7897.0000722](https://doi.org/10.1061/(asce)ey.1943-7897.0000722)

White, C. M., Steeper, R. R., & Lutz, A. E. (2006). The hydrogen-fueled internal combustion engine: a technical review. *International Journal of Hydrogen Energy*, 31(10), 1292–1305. <https://doi.org/10.1016/j.ijhydene.2005.12.001>

Wu, X., Daniel, R., Tian, G., Xu, H., Huang, Z., & Richardson, D. (2011). Dual-injection: The flexible, bi-fuel concept for spark-ignition engines fuelled with various gasoline and biofuel blends. *Applied Energy*, 88(7), 2305–2314. <https://doi.org/10.1016/j.apenergy.2011.01.025>

Wyszynski, L. P., Stone, C. R., & Kalghatgi, G. T. (2002). The volumetric efficiency

- of direct and port injection gasoline engines with different fuels. *SAE Technical Papers*, 2002(724). <https://doi.org/10.4271/2002-01-0839>
- Yang, Z., & Bandivadekar, A. (2017). 2017 Global update: Light-duty vehicle greenhouse gas and fuel economy standards. *International Council on Clean Transportation (ICCT)*, 36. <https://theicct.org/publications/2017-global-update-LDV-GHG-FE-standards>
- Yu, X., Guo, Z., He, L., Dong, W., Sun, P., Du, Y., Li, Z., Yang, H., Wang, S., & Wu, H. (2019). Experimental study on lean-burn characteristics of an SI engine with hydrogen/gasoline combined injection and EGR. *International Journal of Hydrogen Energy*, 44(26), 13988–13998. <https://doi.org/10.1016/j.ijhydene.2019.03.236>
- Zhao, F, Lai, M., & Harrington, D. L. (1999). *Automotive spark-ignited direct-injection gasoline engines*. 25, 437–562.
- Zhao, Fu-quan, Lai, M., & Harrington, D. L. (2018). *A Review of Mixture Preparation and Combustion Control Strategies for Spark-Ignited Direct-Injection Gasoline Engines* c *KDetro MJ7chi9oon7 February 24-27 , 1997*. 412.
- Zhao, W., Li, Z., Huang, G., Zhang, Y., Qian, Y., & Lu, X. (2020). Experimental investigation of direct injection dual fuel of n-butanol and biodiesel on Intelligent Charge Compression Ignition (ICCI) Combustion mode. *Applied Energy*, 266(March), 114884. <https://doi.org/10.1016/j.apenergy.2020.114884>
- Zheng, M., Tan, Y., Mulenga, M. C., & Wang, M. (2007). Thermal efficiency analyses of diesel low temperature combustion cycles. *SAE Technical Papers*, 724. <https://doi.org/10.4271/2007-01-4019>
- Zhu, R., Hu, J., Bao, X., He, L., Lai, Y., Zu, L., Li, Y., & Su, S. (2016). Tailpipe emissions from gasoline direct injection (GDI) and port fuel injection (PFI)

vehicles at both low and high ambient temperatures. *Environmental Pollution*, 216, 223–234. <https://doi.org/10.1016/j.envpol.2016.05.066>

Zhuang, Y., & Hong, G. (2013). Primary investigation to leveraging effect of using ethanol fuel on reducing gasoline fuel consumption. *Fuel*, 105, 425–431. <https://doi.org/10.1016/j.fuel.2012.09.013>

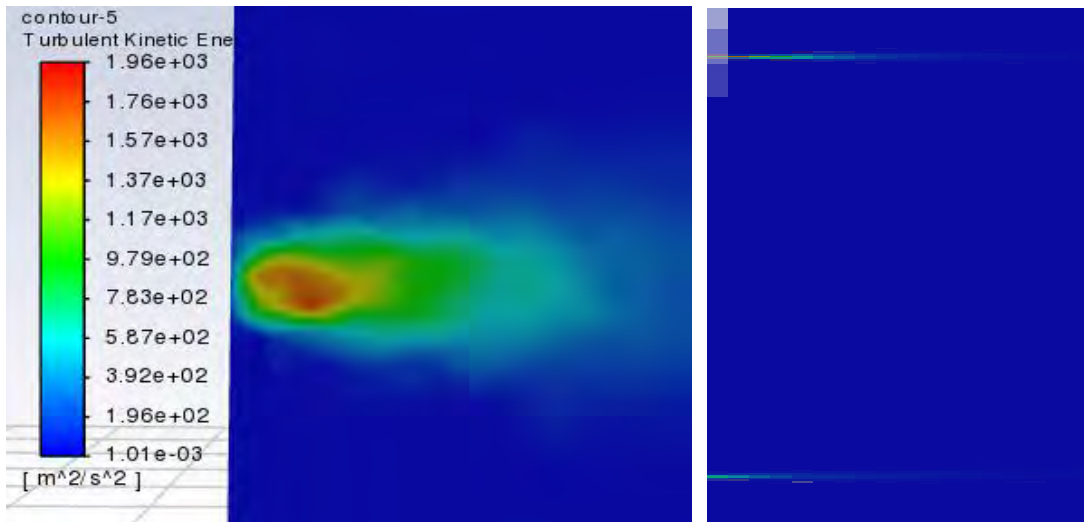
Zhuang, Y., Qian, Y., & Hong, G. (2017). The effect of ethanol direct injection on knock mitigation in a gasoline port injection engine. *Fuel*, 210(April), 187–197. <https://doi.org/10.1016/j.fuel.2017.08.060>

Zhuang, Y., Qian, Y., & Hong, G. (2018). Lean Burn Performance of a Spark Ignition Engine with an Ethanol-Gasoline Dual Injection System. *Energy and Fuels*, 32(3), 2855–2868. <https://doi.org/10.1021/acs.energyfuels.7b03028>



APPENDICES

Turbulent Kinetic Energy (TKE)

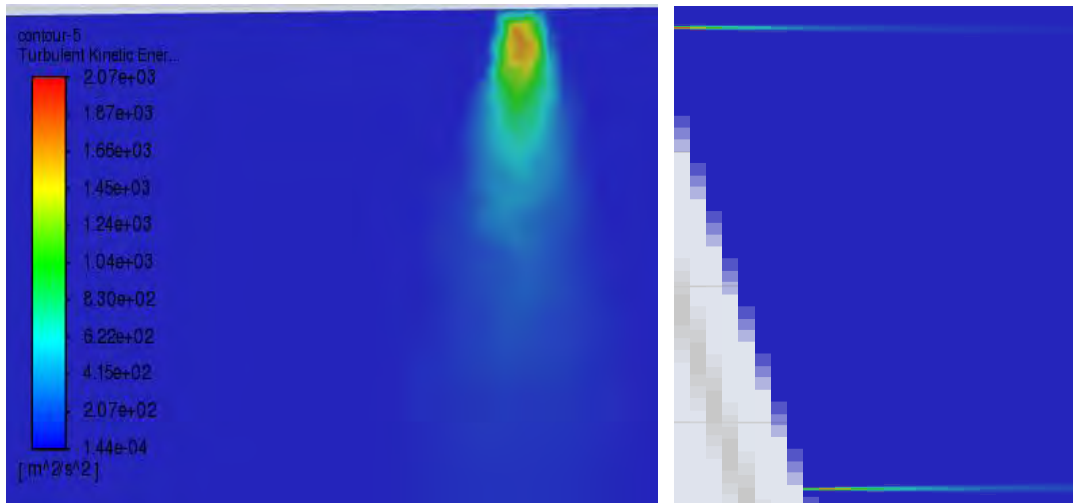


(a)



(b)

Contour plot of Turbulent Kinetic Energy (TKE) for (a) Dual GDI, (b) single GDI at BDC



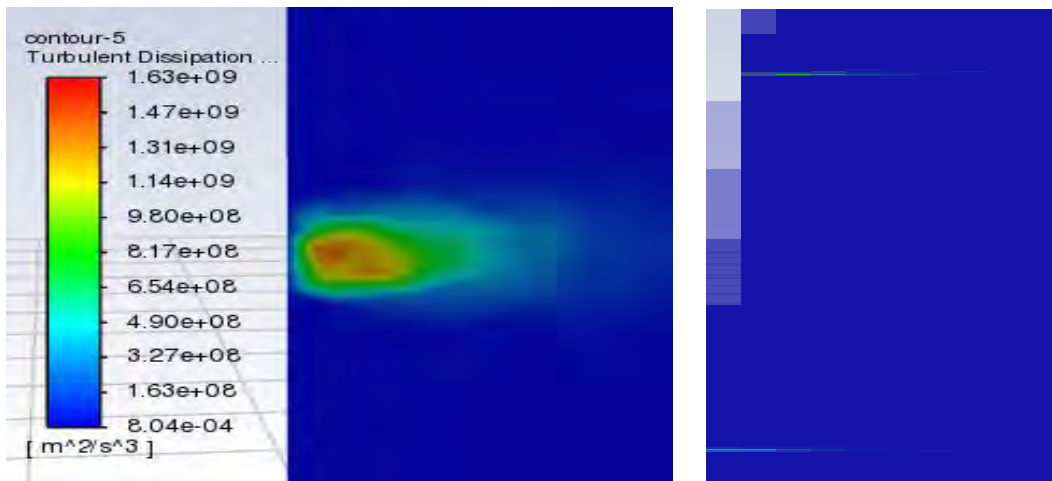
(a)



(b)

Contour plot of Turbulent Kinetic Energy (TKE) for (a) Dual GDI, (b) single GDI at BDC

Turbulent Dissipation Rate

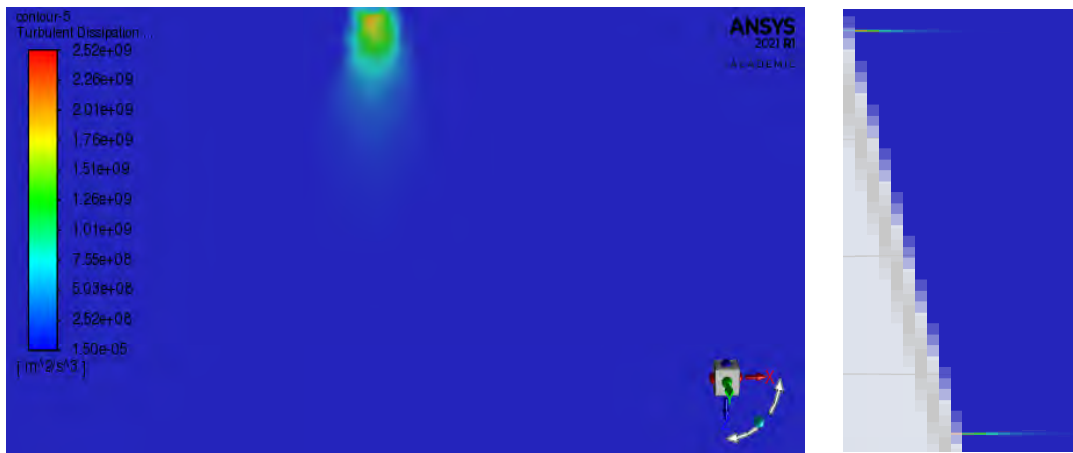


(a)



(b)

Contour plot of Turbulent Dissipation Rate for (a) Dual GDI , (b) single GDI at BDC



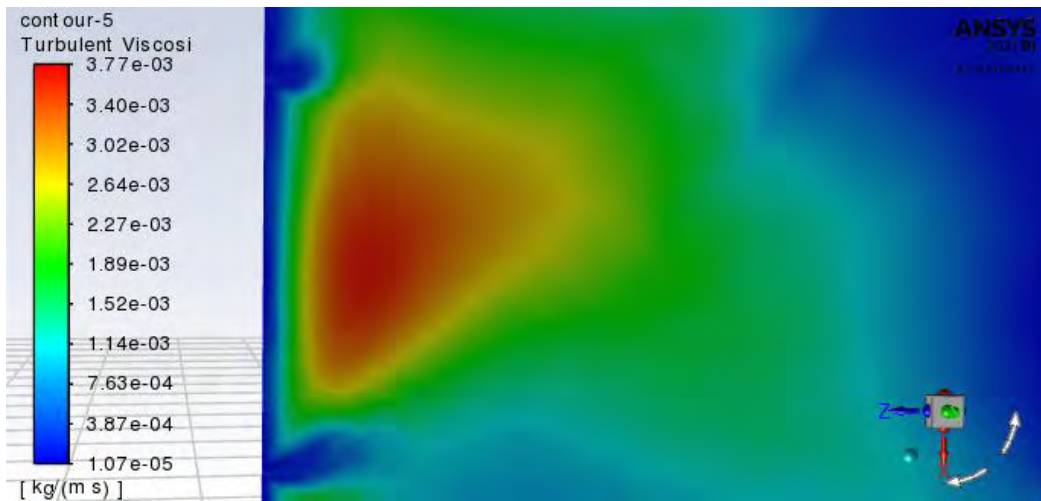
(a)



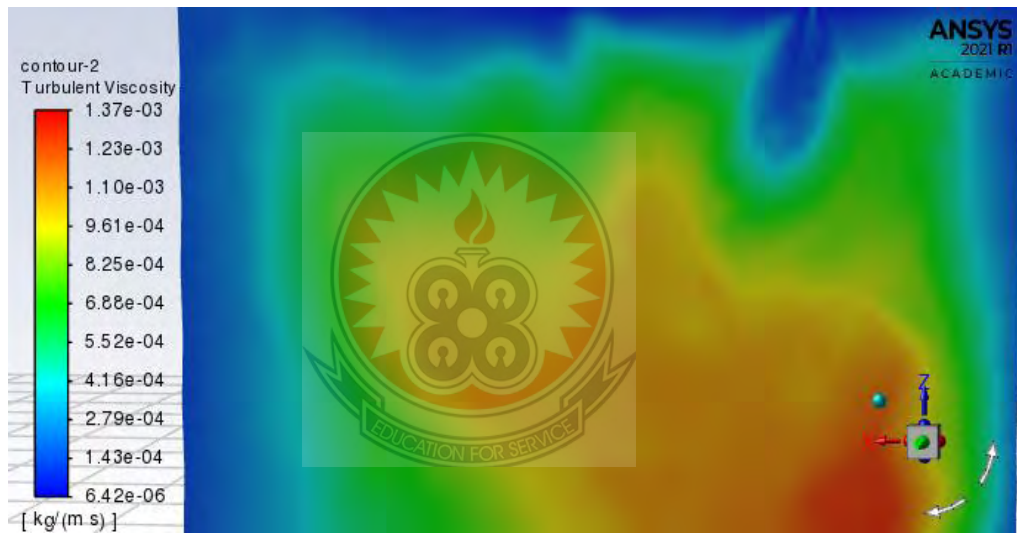
(b)

Contour plot of Turbulent Dissipation Rate for (a) Dual GDI, (b) single GDI at TDC

Turbulent viscosity

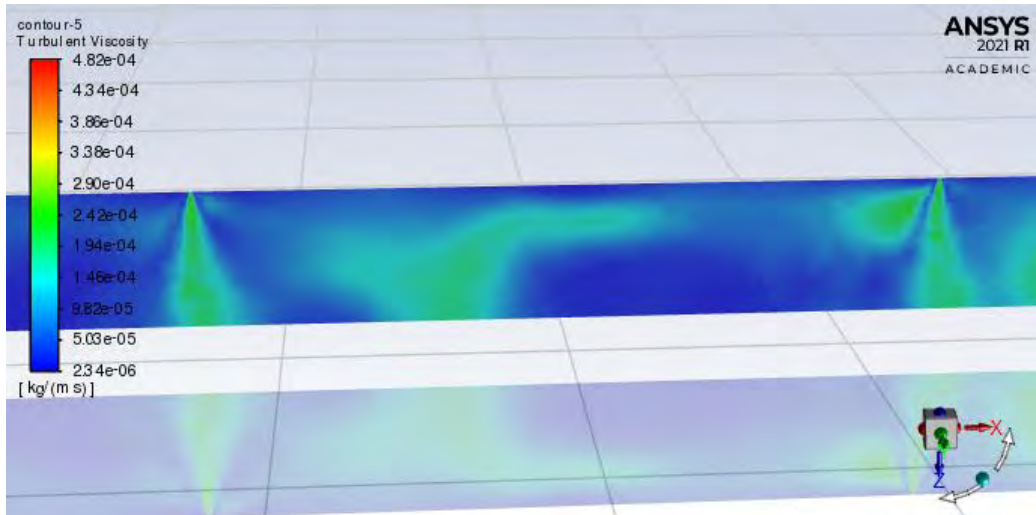


(a)



(b)

Contour plot of Turbulent Viscosity for(a) Dual GDI, (b) single GDI at BDC



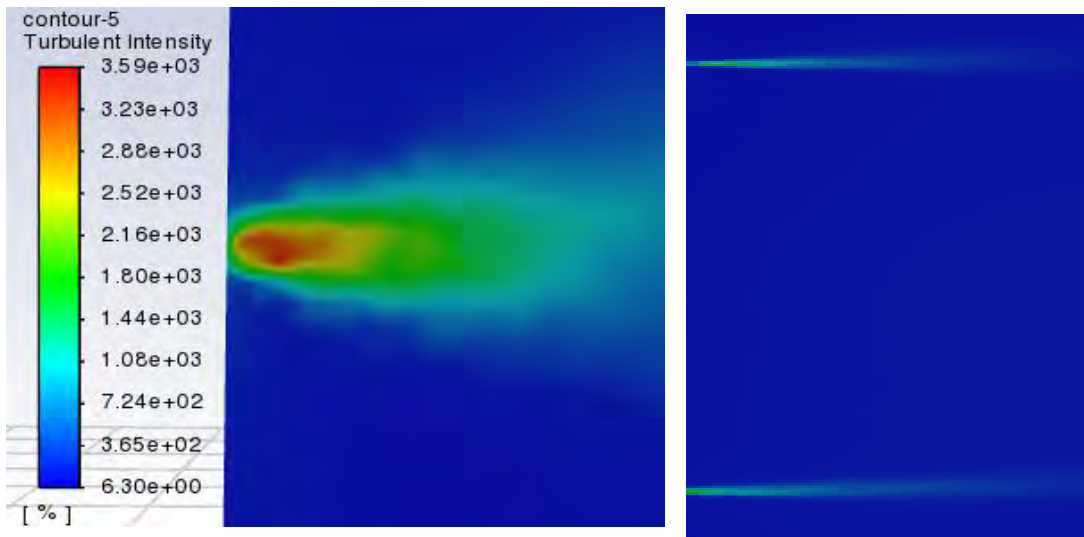
(a)



(b)

Contour plot of Turbulent Viscosity for (a) Dual GDI, (b) single GDI at TDC

Turbulent Intensity

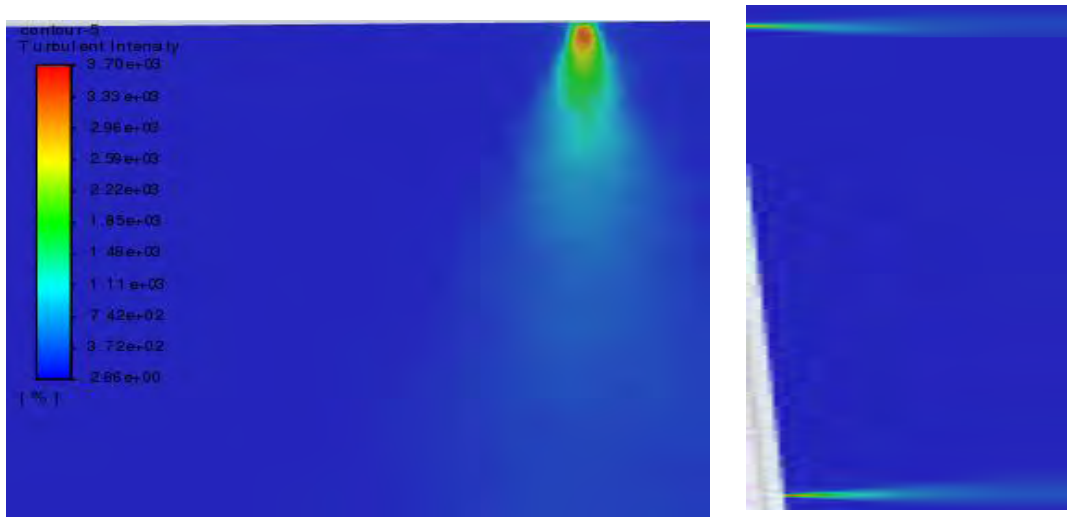


(a)



(b)

Contour plot of Turbulent Intensity for (a) Dual GDI, (b) single GDI at BDC



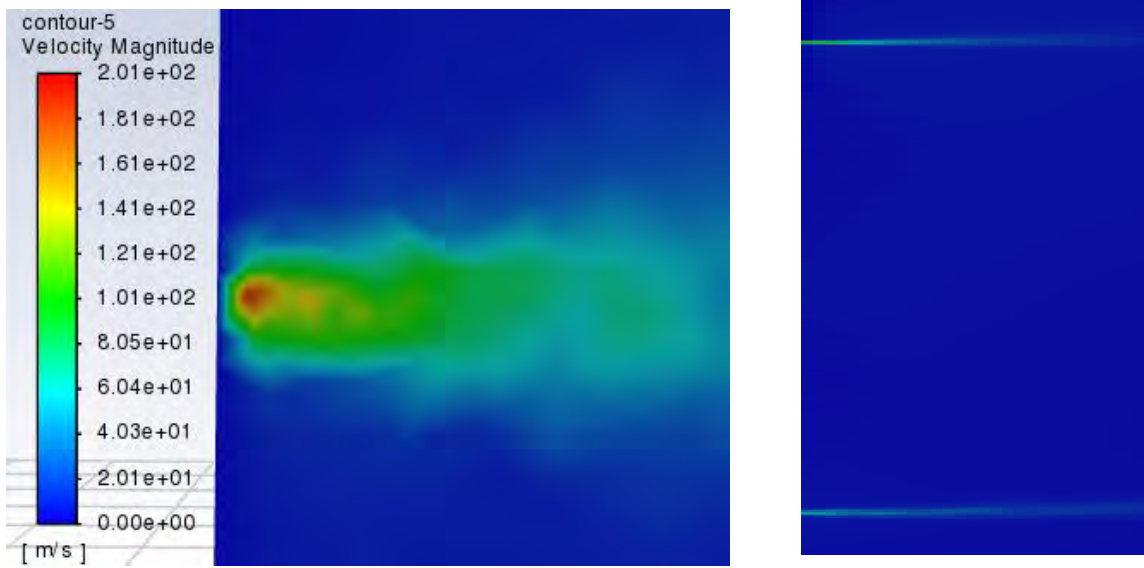
(a)



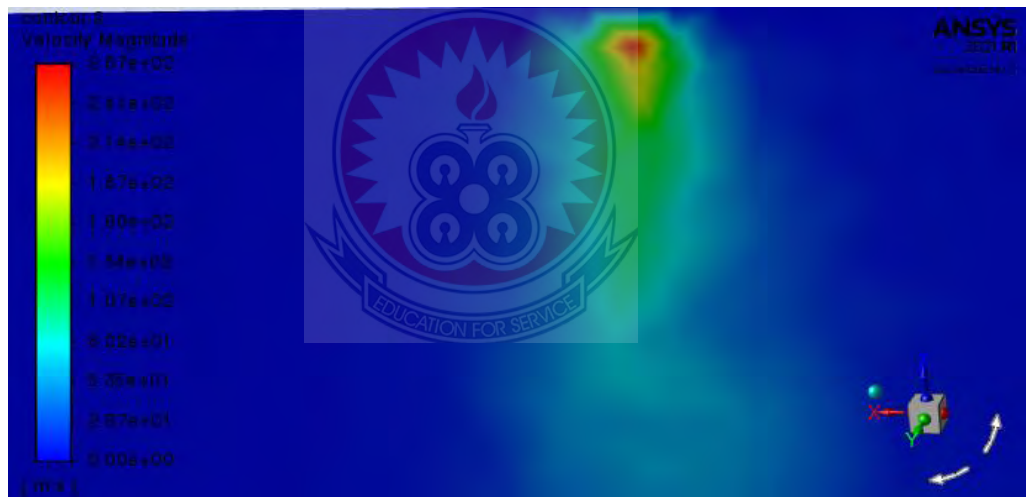
(b)

Contour plot of Turbulent Intensity for (a) Dual GDI, (b) single GDI at TDC

Velocity Magnitude

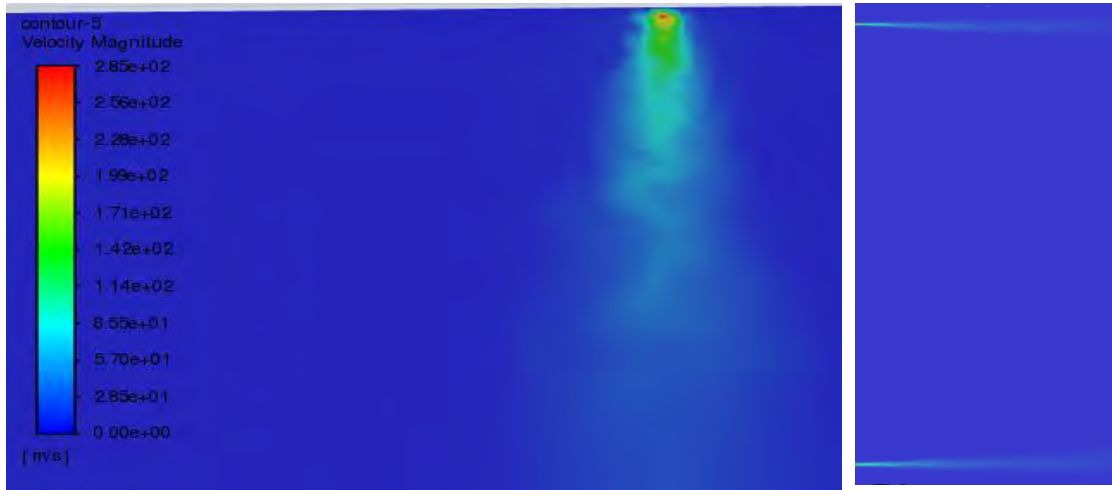


(a)



(b)

Contour plot of Velocity Magnitude for (a) Dual GDI, (b) single GDI at BDC



(a)



(b)

Contour plot of Velocity Magnitude for (a) Dual GDI, (b) single GDI at TDC